



HUNGARIAN UNIVERSITY OF AGRICULTURE AND LIFE SCIENCES

Influence of moisture content on soil bearing capacity and spectral reflectance

PhD Dissertation

by

Ahmed Elawad Eltayeb Ahmed

Gödöllő
2025

Doctoral school

Denomination: Doctoral School of Mechanical Engineering

Science: Mechanical Engineering

Leader: Prof. Dr. Gábor Kalácska, DSc
Institute of Technology
Hungarian University of Agriculture and Life Sciences, Szent István
Campus, Gödöllő, Hungary

Supervisor: Prof. Dr. Péter Kiss, PhD
Institute of Technology
Hungarian University of Agriculture and Life Sciences, Szent István
Campus, Gödöllő, Hungary

Co-Supervisor: Dr. György Pillinger, PhD
Institute of Technology
Hungarian University of Agriculture and Life Sciences, Szent István
Campus, Gödöllő, Hungary

.....
Affirmation of supervisor

.....
Affirmation of head of school

CONTENTS

| | |
|---|----|
| NOMENCLATURE AND ABBREVIATIONS | 6 |
| 1. INTRODUCTION, OBJECTIVES | 8 |
| 1.1 Introduction | 8 |
| 1.2 Objectives | 9 |
| 2. LITERATURE REVIEW | 10 |
| 2.1 Soil structure and its strength | 10 |
| 2.2 Soil shearing strength and characteristics..... | 11 |
| 2.2.1 <i>Elastic Medium</i> | 13 |
| 2.2.2 <i>Plastic Region</i> | 14 |
| 2.3 Soil load-bearing capacity | 14 |
| 2.4 Soil colour and spectral behaviour in property characterization | 16 |
| 2.5 Soil moisture content..... | 17 |
| 2.5.1 <i>The influence of soil moisture content on off-road vehicle performance</i> | 17 |
| 2.5.2 <i>The moisture content relationship with soil spectral reflectance</i> | 18 |
| 2.6 Measurement of terrain properties and soil colour | 18 |
| 2.6.1 <i>Cone penetrometer</i> | 18 |
| 2.6.2 <i>Bevometer technique</i> | 19 |
| 2.6.3 <i>Spectrophotometers</i> | 21 |
| 2.6.4 <i>Colourimeters</i> | 22 |
| 2.6.5 <i>Traditional soil moisture measurement methods</i> | 22 |
| 2.7 Bearing capacity (pressure-sinkage relationship)..... | 23 |
| 2.7.1 <i>Effect of plate size and shape</i> | 28 |
| 2.7.2 <i>Effect of load direction, plate inclination and soil deformation</i> | 30 |
| 2.8 Summary..... | 30 |
| 3. MATERIALS AND METHODS | 32 |
| 3.1 Soil types | 32 |
| 3.2 Soil preparation..... | 33 |
| 3.3 Experimental procedure..... | 33 |
| 3.3.1 <i>Load-bearing capacity measurement (bevometer test)</i> | 33 |
| 3.3.2 <i>Determining the moisture content of the soil</i> | 36 |
| 3.3.3 <i>Spectral behaviour measurements (colour test)</i> | 36 |
| 3.3.4 <i>Cone penetrometer technique with colour measurement (field measurements)</i> | 37 |
| 3.4 Extra measurement | 38 |
| 2.4.1 <i>Soil reflectance at zero moisture content (close to zero)</i> | 38 |
| 2.4.2 <i>The effect of the plate size on the sinkage</i> | 38 |
| 2.4.3 <i>The effect of the load speed on the sinkage</i> | 38 |
| 4. RESULTS | 39 |
| 4.1 Bevometer results (pressure-sinkage relationship)..... | 39 |
| 4.2 The impact of moisture content | 41 |
| 4.2.1 <i>On the soil density</i> | 41 |
| 4.2.2 <i>On the soil relative sinkage</i> | 41 |
| 4.3 Spectral behaviour (Spectrophotometer)..... | 43 |
| 4.3.1 <i>Spectral reflectance affected by moisture contents</i> | 45 |
| 4.4 Soil properties underload and the spectral reflectance at 700 nm | 48 |
| 4.4.1 <i>Relative density ratio – spectral reflectance at 700 nm relationship</i> | 48 |
| 4.4.2 <i>Relative sinkage – spectral reflectance at 700 nm relationship</i> | 49 |
| 4.5 Estimation of soil-specific constants and moisture content calculations | 50 |
| 4.6 Soil load-bearing capacity – optical reflectance relationship..... | 52 |
| 4.7 Soil saturation- spectral reflectance relationship..... | 54 |
| 4.8 The effect of the plate size on the sinkage..... | 54 |

| | | |
|------|---|----|
| 4.9 | The effect of the load velocity on the soil sinkage..... | 55 |
| 4.10 | Cone penetrometer technique with colour measurement (field measurements)..... | 56 |
| 5. | NEW SCIENTIFIC RESULTS..... | 58 |
| 6. | CONCLUSION AND SUGGESTIONS..... | 63 |
| 7. | SUMMARY..... | 65 |
| 8. | ÖSSZEFOGLALÁS (SUMMARY IN HUNGARIAN)..... | 67 |
| 9. | APPENDICES..... | 69 |
| A1. | Bibliography..... | 69 |
| A2. | Publications related to the dissertation..... | 79 |
| A3. | Pressure-sinkage curves..... | 81 |
| A4. | Influence of moisture content on soil relative sinkage and relative density ratio curves..... | 82 |
| A5. | Soil spectral behaviour curves..... | 84 |
| A6. | Influence of moisture content on spectral reflectance curves..... | 86 |
| A7. | Soil relative density ratio – spectral reflectance at 700 nm relationship curves..... | 87 |
| A8. | Soil relative sinkage – spectral reflectance at 700 nm relationship curves..... | 89 |
| A9. | Influence of moisture content on spectral reflectance curves..... | 91 |
| 10. | ACKNOWLEDGEMENT..... | 93 |

NOMENCLATURE AND ABBREVIATIONS

Symbols

| | |
|----------------------------|---|
| \hat{A} | Constant of soil parameters (-) |
| $A_1, A_2, B_1,$ and B_2 | Constants depend on soil texture (-) |
| D | Diameter of the loading area (m) |
| F | Rolling resistance coefficient (-) |
| H | Soil depth or soil thickness (m) |
| K_r | The ratio of the residual shear stress (-) |
| K_w | Modulus of soil shear displacement (kPa) |
| MC | Moisture content (%) |
| $N_c, N_\gamma,$ and N_q | Bearing capacity factors (-) |
| R_i | Soil reflectance wavelength (%) |
| W | Normal load (N) |
| b | Smaller dimension of the contact patch (m) |
| c | Cohesion (kPa) |
| f | Rolling resistance coefficient (-) |
| j | Shear displacement (m) |
| k | Load carrying capacity factor (bar) |
| k_c | Sinkage modulus influenced by soil cohesion (bar) |
| k_{eq} | Equivalent sinkage influenced by k_c and k_ϕ (bar) |
| k_ϕ | Sinkage modulus influenced by soil friction angle (bar) |
| m | Mass (kg) |
| n | An exponent of deformation (-) |
| \hat{n} | Constant of soil parameters (-) |
| p | Pressure or stress (bar) |
| u | The sinkage velocity (m/s) |
| u_0 | The plate sinkage velocity (m/s) |
| z | Sinkage of the flat plate (m) |
| z/D | Relative sinkage (-) |

Greek symbols

| | |
|--|--|
| β | Geometric constant (-) |
| γ | Unit weight of the soil (N/m ³) |
| $\Delta\rho$ | Soil relative density ratio (-) |
| ε | Soil saturation level (-) |
| ϕ | The angle of internal friction (°) |
| $\lambda_c, \lambda_\gamma,$ and λ_q | Shape coefficients of the plate (-) |
| λ_N | The dimensionless function of plate or running gear parameters (-) |
| ρ | Soil density (kg/m ³) |
| σ | Normal stress (kPa) |
| τ | Shear stress (kPa) |
| Φ | Angle of internal shearing resistance (°) |

Abbreviations

| | |
|------|--|
| ASAE | American Society of Agricultural Engineering |
| CEC | Cation Exchange Capacity |

| | |
|------|--|
| CI | Cone Index |
| NASA | The National American Aeronautics and Space Administration |
| NIR | Near-Infrared |
| ORN | Off-Road Vehicles |
| RCI | Rating Cone Index |
| RI | Remoulding Index |
| SWIR | Shortwave Infrared |
| VCI | Vehicle Cone Index |
| VIS | Visible Spectrum |
| WES | Waterways Experimental |

1. INTRODUCTION, OBJECTIVES

In this chapter, the background and importance of the current research are presented, along with the objectives of this research.

1.1 Introduction

Despite the importance of transporting passengers and goods on paved roads, many activities in agriculture, logging, construction, mining, exploration, recreation, and military operations require movement over unprepared terrain using specialized off-road vehicles. The systematic study of principles for the rational development and design of these vehicles has attracted significant interest, especially since World War II (Pytko, 2016).

"Terramechanics" refers to the study of off-road vehicle performance on various terrains. It is crucial for developing and assessing off-road equipment for specific terrains (Wong, 2010; Ahmed et al., 2021). In land locomotion studies, the material on which a vehicle moves must be considered, analyzing this material's strength is vital for evaluating vehicle performance on that terrain. Understanding the soil's mechanical properties is essential to predict its behaviour under the loads generated by vehicle movement (Ahmed and Siddiqua, 2016; Alamanis, 2021; Mašin, 2019).

The primary mechanical properties indicating soil strength are load-bearing capacity and shear strength (Bekker, 1969; Ding et al., 2014). When the wheel's normal pressure exceeds the soil's load-bearing capacity, the wheel compacts and sinks into the soil (Ahmed et al., 2021). Conversely, if the pressure is below the bearing capacity, the wheel remains on the surface, and vehicle movement is unaffected. Shear strength prevents internal shearing failure under applied shearing forces, ensuring the wheel does not slip as long as the shear stress remains below the soil's shear strength (Yong et al., 1984). Experimentally studying a soil's load-bearing capacity is crucial for understanding its vertical deformation under normal pressure from wheels or tracks and for selecting appropriate vehicles based on wheel design and vehicle mass. If unsuitable machinery is chosen, it is essential to avoid areas with weak bearing capacity. Researchers in terramechanics have long utilized the bevometer technique to measure soil bearing capacity (pressure-sinkage relationship) as it simulates the normal pressure exerted by a wheel. Developed by Bekker, the bevometer technique provides relevant terrain properties for off-road studies (Wong, 2010).

The bevometer, a Terramechanics measuring technique developed by Bekker, assesses soil's load-bearing capacity, strength, and sinkage parameters under a running wheel. The wheel connected to the vehicle applies both vertical (normal) and tangential (shear) stresses on the terrain, transferring power from the transmission to the wheels as tractive forces, thus enabling vehicle movement. The bevometer technique is superior for simulating real wheel-terrain contact by studying these loads (Wong, 2010; Wong, 2001).

Soil deformation due to vehicle passage is influenced by its physical composition, moisture content, density, and initial compression. Increased moisture compacts the soil further (Pillinger et al., 2018). Variations in soil moisture content alter its mechanical properties, affecting load-bearing capacity (Ahmed et al., 2023a; Ahmed et al., 2023b). Soil spectral behaviour, reflecting its absorption and reflection of light wavelengths, helps to determine physical and chemical properties (Chen and Chen, 2015). Higher moisture content alters soil's spectral characteristics

compared to dry soil (Li and Su, 2011). This moisture-induced colour change is crucial for linking soil's mechanical properties (Mouazen et al., 2007). Various methods measure soil colour, including the Munsell soil colour charts (1975), a qualitative method (Nickerson, 1975; Rabenhorst et al., 2015), and spectrophotometry, a precise quantitative approach (Aitkenhead et al., 2013; Bloch et al., 2021; Viscarra Rossel, 2006). Scientists agree that the reflected spectrum describes visible color, despite individual vision differences. Thus, it is preferable to rely on a method that measures spectral reflectance (Csanády et al., 2015; Csanády et al., 2019; Sitkei, 2020). Orna (1978) described how an observable property is linked to an underlying theory through colour. Soil components like organic matter, iron oxides, and carbonates have been qualitatively assessed using soil colour in remote sensing and soil science for many years (Escadafal, 1993).

Soil colour generally darkens with increased moisture. The spectrophotometer emits electromagnetic waves in the visible spectrum that reach the soil; some wavelengths are absorbed, and the rest are reflected, determining the soil's colour (William and Chancellor, 1994).

This study investigates the load-bearing capacity and spectral characteristics of soil as a homogeneous material. Parameters of the pressure-sinkage relationship and soil reflectance wavelength will be examined for eight soil types. Additionally, the effects of plate size and loading speed will be analyzed. The study will include measurements of plate size and loading speed, as well as field measurements for the cone index (CI) and the analysis of one soil type.

1.2 Objectives

This study aims to investigate the load-bearing capacity and spectral behaviour of eight soil types and correlate these factors based on moisture content. The research could benefit off-road engineering vehicles, especially autonomous ones operating on soil terrains. Additionally, the study will examine the effects of plate size and loading speed on the pressure-sinkage relationship and conduct field measurements for the cone index (CI) of sandy loam. The specific research objectives are:

- Investigate to examine the load-bearing capacity of eight varieties of soil with diverse moisture content.
- Additionally, the soil colour (spectral behaviour) for the above-mentioned types of soil with the same diverse moisture content must be identified.
- Determine the relationship between the soil load-bearing capacity and its relative sinkage and relative density ratio and ascertain which one is more suitable.
- Identify the soil colour (spectral behaviour) at various moisture content ranges to determine which range should be considered to evaluate the reflectance behaviour.
- Establish the connection between the soil properties (load-bearing capacity, soil colour) to determine their relationship between them.
- Investigate the spectral reflectance of eight types of soil at zero moisture content (MC = 0.00%) to determine which ones have the highest and lowest reflectance.
- Moreover, investigate the influence of plate size and loading speed on the pressure-sinkage relationship of sandy loam soil.
- Conduct measurements using the cone index (CI) to determine the penetration resistance - depth relationship, as well as the spectral behaviour of the sandy loam soil (field measurement).

2. LITERATURE REVIEW

This chapter investigates the obstacles, gaps, and findings in the extant literature within the field, considering recommendations for addressing such obstacles and previously encountered issues. One of the objectives of this study is to bridge the gaps in existing literature.

2.1 Soil structure and its strength

Soil structure refers to the arrangement of solid particles and voids at different scales, excluding the chemical variations of the solid phase. The solid phase and pore space are complementary components and can be analyzed from both angles (Rabota et al., 2018). This arrangement results in a complex network of pores, crucial for physical, chemical, and biological processes in both natural and human-modified soils, such as liquid, gas, and heat movement and storage; root growth; microbial activity; and organic matter breakdown and storage.

Soil structure is complex due to varying particle sizes, shapes, chemical traits, and bonding mechanisms. It is hierarchically organized: small primary particles form secondary particles, which then create larger aggregates. It is dynamic, changing over time due to moisture, temperature, biological activity, and human actions, and applies to various scales, from tiny clay particles to large clods and earthworm tunnels (Dexter, 1988).

Soil structure comprises three phases: gas (air and water vapour), solid (rock minerals, clay, organic matter), and liquid (water and dissolved salts) (Scott, 1994). These factors influence soil strength. Soils are generally classified into cohesive and frictional types, though most soils are a mix of both (Inns and Kilgour, 1978).

Cohesion refers to particle or aggregate bonding due to particle properties (such as mineral type and shape) and water tension (affected by void ratio). Water adheres to soil particles, and cohesion occurs between adjacent water molecules, related to soil water suction rather than moisture content (Earl, 1996).

Friction refers to the resistance experienced when soil particles slide past each other. It increases with the irregularity of grain shape and the number of particle contacts. Higher soil bulk density typically results in increased friction (Godwin et al., 1991). Soil types are categorized by particle size, including coarse, fine, and organic types. Classification groups particles into stone, gravel, sand, silt, and clay, from largest to smallest. Soil strength is heavily influenced by particle size distribution. Soil properties such as plasticity, compressibility, particle shape, void ratio, and grain size impact its strength and stability (Whitlow, 1995).

Understanding vehicle-terrain interaction is crucial for analyzing terrain behaviour under vehicle loads. Traditionally, the terrain has been modelled either as an elastic medium or a rigid-perfectly plastic material. Elastic models are useful for studying soil compaction and damage from vehicular traffic, while rigid-perfectly plastic models predict maximum traction from off-road vehicles and the thrust generated by vehicle lugs (Wong, 2010). Various terrain modelling approaches include treating terrain as elastic or as a rigid material when it reaches an irreversible state. Elasticity theory underpins many studies on dense soils, but it is limited when soil-bearing capacity is exceeded. In such cases, plasticity theory explains soil failure, setting the maximum vehicle traction limit. The stress-strain relationship in both elastic and plastic regions is depicted in Figure 2.1 (Taghavifar

and Mardani, 2017).

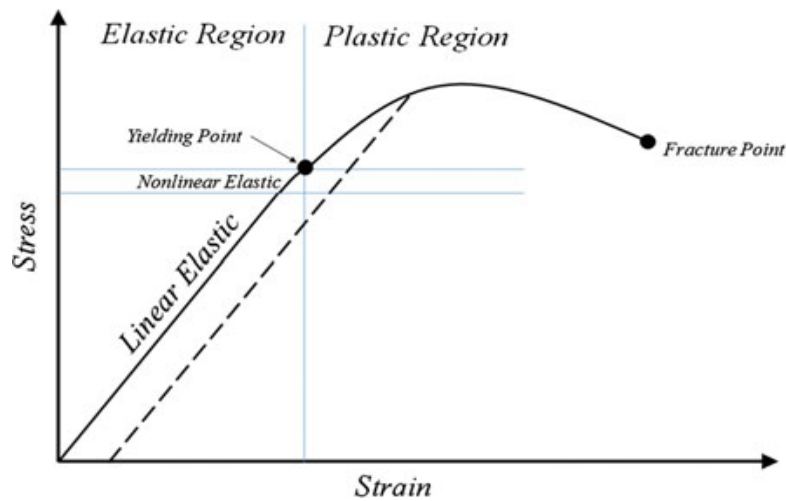


Figure 2.1. Typical soil stress-strain curve for elastic and plastic regions (Taghavifar & Mardani, 2017).

2.2 Soil shearing strength and characteristics

Micklethwaite achieved a significant advancement in terramechanics by modifying Coulomb's established equation for predicting a vehicle's maximum tractive effort. The general definition of Coulomb's equation for shear stress is as follows (Micklethwait, 1944),

$$\tau_{max} = c + \sigma \tan \phi \quad (2.1)$$

Where c and ϕ represent the cohesion and friction angle of the soil, respectively, and σ denotes the normal stress or ground pressure under the loaded area.

Freitag emphasizes considering traction performance for cohesive, frictional, and cohesive-frictional soils (Freitag, 1966). The Mohr-Coulomb diagrams of the three different soil classes are depicted in Figure 2.2.

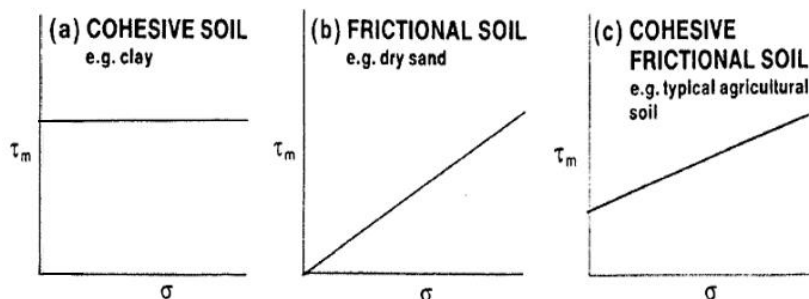


Figure 2.2. Soil strength graphs (Inns & Kilgour, 1978).

Where:

- Pure cohesive soil, which has only cohesive (non-frictional) strength. Water-saturated clay is an example.
- Pure frictional soil, which has only frictional strength (no cohesion). Dry sand represents this type.

- c) Cohesive-frictional soil, which combines both cohesive and frictional strength. Examples include saturated clays, loams, and sands. (Ahmed et al, 2021)

For soils exhibiting brittle behaviour, which demonstrate a peak in maximum shear stress, Bekker proposed the following equation to describe the shear stress–displacement relationship (Bekker, 1956):

$$\tau = \tau_{max} \frac{\left(\exp\left[(-K_2 + \sqrt{K_2^2 - 1})K_1 j\right] - \exp\left[(-K_2 - \sqrt{K_2^2 - 1})K_1 j\right] \right)}{\left(\exp\left[(-K_2 + \sqrt{K_2^2 - 1})K_1 j_0\right] - \exp\left[(-K_2 - \sqrt{K_2^2 - 1})K_1 j_0\right] \right)} \quad (2.2)$$

where τ and τ_{max} represent the shear stress and the maximum shear stress, respectively; j and j_0 denote the shear and shear displacement at τ_{max} , respectively; K_1 and K_2 are empirical constants.

For plastic soils which do not exhibit a 'hump' of maximum shear stress, a modified version of Bekker's equation containing only one constant was proposed by Janosi and Hanamoto and is widely utilized in practice (Janosi and Hanamoto, 1961):

$$\tau = \tau_{max} \left(1 - \exp\left(\frac{-j}{K}\right) \right) \quad (2.3)$$

K , often called the shear deformation parameter, measures magnitude. For internal shearing of the muskeg mat, shear curves show a peak in maximum shear stress, followed by a steady decrease in shear stress with increased shear displacement. Studies indicate that the following equation accurately fits this shear curve (Wong, 1979; Wong and Preston-Thomas, 1983):

$$\frac{\tau}{\tau_{max}} = \left(\frac{-j}{K_w}\right) \left(1 - \exp\left(\frac{-j}{K_w}\right) \right) \quad (2.4)$$

where K_w is a constant. In physical terms, K_w is equal to the shear displacement j where the shear stress peaks.

Wong proposed an alternative equation for shear stress to predict the thrust–slip relationship of a vehicle running gear. This equation is (Wong, 1983):

$$\frac{\tau}{\tau_{max}} = K_r \left[1 + \left[\frac{1}{\left(K_r \left(1 - \frac{1}{e}\right)\right)} - 1 \right] \exp\left(1 - \frac{j}{K_w}\right) \right] \left[1 - \exp\left(\frac{-j}{K_w}\right) \right] \quad (2.5)$$

where K_r is the ratio of the residual shear stress τ_r to the maximum shear stress τ_{max} , and K_w is the shear displacement where τ_{max} occurs.

Soils were studied as elastic and plastic mediums. The considerations in the two mediums are explained in the below subsections.

2.2.1 Elastic Medium

Stress in terrain concentrates along the central axis of the load area, increasing with higher soil moisture content. Boussinesq (1885) developed a solution for elastic stress distribution from a point load on a semi-infinite mass. Froehlich (1934) introduced a concentration factor to adjust Boussinesq's distribution based on soil strength (Gill and Berg, 1967).

In hard, dry soil, tyre pressure without lugs is uniform across the contact area. In soft soils, pressure distribution changes with rut depth, decreasing at the edges and concentrating in the centre. Figure 2.3 illustrates typical pressure distributions for tyres without lugs under various soil conditions (Sohen, 1958)

Hallonborg (1996) studied stress distribution in elastic mediums under loads in elliptic or super-elliptic areas like a tyre's contact patch. Figure 2.4 shows vertical stress patterns beneath a vehicle with two tracks, modelled as rigid footings. At a depth equal to the track width, vertical stress beneath the load area centre is about 50% of the surface pressure, P_0 , applied by the track. Vertical stress boundaries slope at a 45° angle from the horizontal, as depicted in Figure 2.4 (Bekker, 1956).

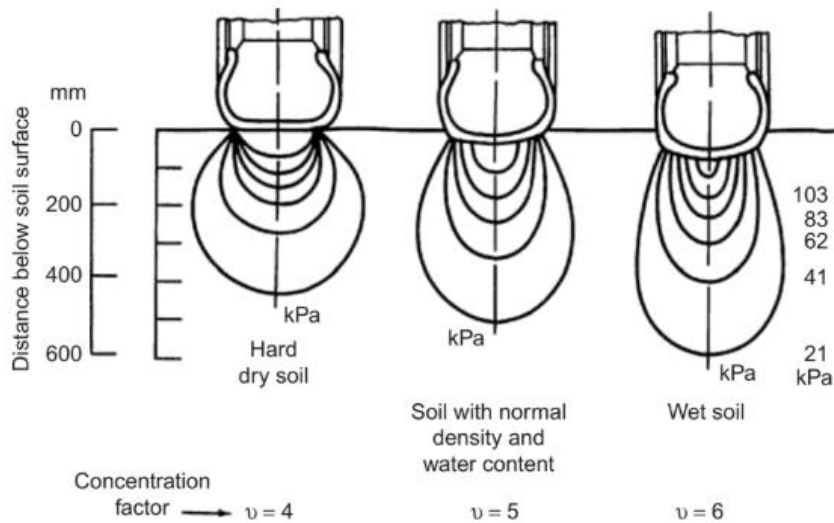


Figure 2.3. Distributions of major principal stress under a tyre for different soil conditions (Tyre size 11-28, load = 7.4 kN, inflation pressure = 83 kPa) (Sohen, 1958)

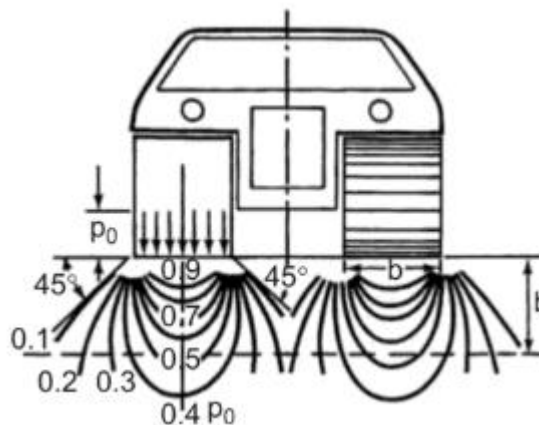


Figure 2.4. Distribution of vertical stresses in a semi-infinite elastic medium under a tracked vehicle (Bekker, 1956)

2.2.2 Plastic Region

In the plasticity region, various methods have been devised to define terrain failure, with the Mohr-Coulomb failure criterion being predominant. This criterion states that soil failure happens when the shear stress at a point meets equation 2.1:

The Mohr circle of stress elucidates the Mohr-Coulomb failure criterion. Drawing a Mohr circle for various stress states in a terrain material at multiple failure points, as shown in Figure 2.5, allows for the determination of the terrain's cohesion by the line's intercept with the shear stress axis and the internal shearing resistance by the line's slope. The Mohr-Coulomb failure criterion indicates failure when a Mohr circle representing the terrain's stress state contacts the enclosing line (Wong, 2010).

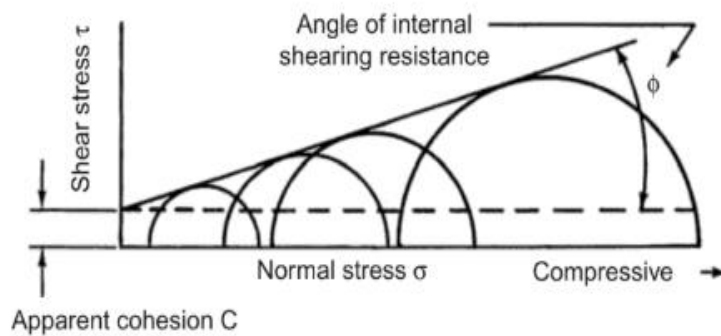


Figure 2.5. Mohr-Coulomb failure criterion in plastic region (Taghavifar and Mardani, 2017).

The thrust (or tractive effort) produced by a vehicle's running gear, such as a tyre or track, results from its shearing action on the terrain, as shown in Figure 2.6. Equation 2.6 estimates the maximum thrust generated by the vehicle's running gear (Wong, 2001).

$$F_{max} = \tau A = (c + \sigma \tan \phi)A = cA + W \tan \phi \quad (2.6)$$

Where A represents the contact area, and the product of the contact pressure and the contact area equals the normal load on the tyre or track, denoted as W .

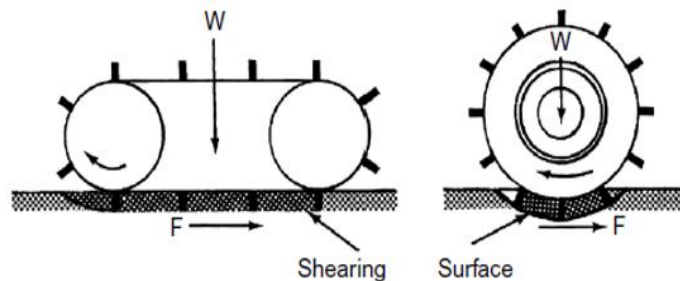


Figure 2.6. The shearing action of a track and a wheel (Wong, 2001).

2.3 Soil load-bearing capacity

Bearing capacity pertains to the soil's ability to sustain applied loads, defined as the maximum average contact pressure between the foundation and soil without causing shear failure. Ultimate

bearing capacity indicates the theoretical maximum pressure the soil can support without failure (Terzaghi, 1943). Terzaghi developed a comprehensive theory to determine the ultimate bearing capacity of a shallow, rough, rigid, continuous (strip) footing on a homogeneous soil layer of significant depth. He defined a shallow foundation as one with width B equal to or less than its depth D . The failure surface in the soil at ultimate load, as Terzaghi proposed, is depicted in Figure 2.7 (Das, 2017).

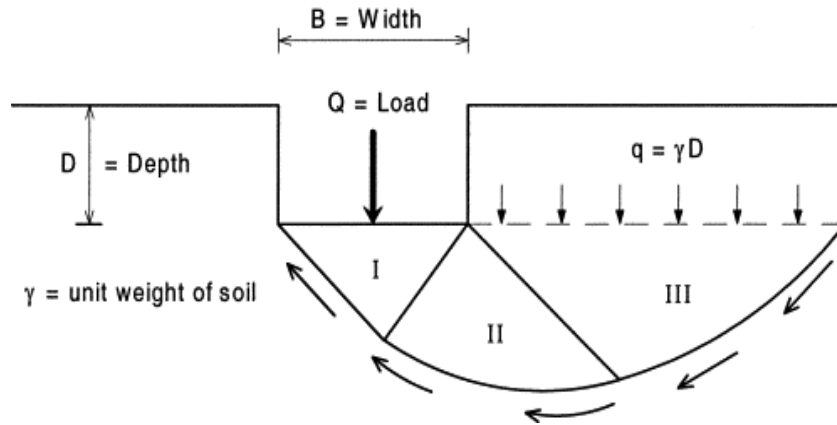


Figure 2.7. General description of bearing capacity (Kulhawy and Hirany, 2003).

The ultimate bearing capacity for the general shear mode is calculated using the shear surface depicted in Figure 2.7, assuming an infinitely long foundation. The soil within the shear surface is treated as a rigid-plastic medium and divided into three zones: an active Rankine zone (I) directly beneath the footing, a radial Prandtl zone (II), and a passive Rankine zone (III) (Kulhawy and Hirany, 2003). Terzaghi's bearing capacity is presented in Equation 2.7:

$$p = cN_c\lambda_c + \frac{B}{2}\gamma N_\gamma\lambda_\gamma + \gamma N_q\lambda_q z \quad (2.7)$$

where z is the vertical distance between the soil's top surface and the place where the plate rests (depth of footing), c is the cohesion of the soil, γ is the unit weight of the soil, λ_c , λ_γ , and λ_q are the shape coefficients of the plate, and N_c , N_γ , and N_q are the bearing capacity factors that are functions of soil friction angle ϕ and the shape coefficient's λ_c , λ_γ , λ_q (Das, 2017; He et al., 2019).

Various parameters have been employed to assess soil-bearing capacity and susceptibility to plastic deformation. Constitutive soil properties such as texture, organic matter, structure, bulk density, and soil moisture status, indirectly related to soil strength, have been used to qualitatively predict soil stability (Alakukku et al., 2003). Traditional theories for the ultimate capacity of shallow foundations assume an infinite bearing stratum thickness. However, a hard layer at a certain depth below the foundation can significantly affect the unit load supported by the soil. Thus, original bearing capacity equations should be adjusted to account for this in determining the ultimate bearing capacity (Cerato and Lutenege, 2006). Egorov (1961) proposed a model for stress and displacement in finite-thickness foundations of homogeneous soil, highlighting stress distribution under a circular plate due to a rigid layer at a specific depth (see Figure 2.8).

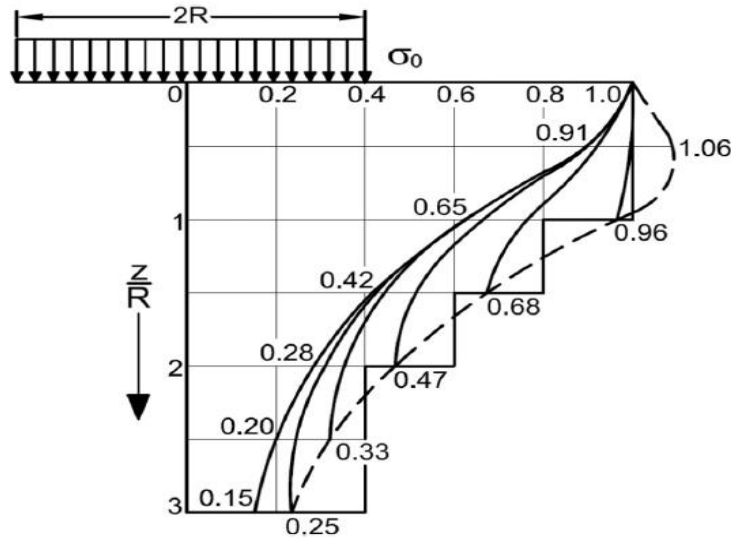


Figure 2.8. Distortion of stress distribution under a circular plate caused by a rigid layer at a certain depth (Sitkei et al., 2019).

This model is mainly used to study soil layer deformation over a rigid stratum without compaction. It showed that deformations beneath foundations, even without a rigid layer below, are concentrated in the upper soil mass and do not extend deeply. This creates an active zone, where the foundation experiences significant deformation. The core depth issue is crucial for calculating finite-thickness foundations and can only be resolved empirically through measurements of layer-by-layer soil deformations.

2.4 Soil colour and spectral behaviour in property characterization

Soil consists of solid particles surrounded by water and/or air and light interaction with these particles generates specular and diffuse reflections. Specular reflection occurs similarly to light reflecting off a mirror, while diffusing reflection results from light scattering. These scattering shapes the soil's colour, an additive mix of individual particle colours, proportionally weighted (Sánchez-Marañón et al., 2004). Soil colour, a prominent characteristic, is often used to indicate organic matter and other vital soil properties and can be mapped via remote sensing (Phinzi and Ngetar, 2019). Although soil colour does not directly affect soil behaviour, except for albedo and heat absorption, it indicates soil processes and conditions. Early soil scientists like Dokuchaiev, Sibirtsev, and Hilgard suggested that soil colour was primarily determined by humus and ferric oxide content and that black, red, and white colours indicated soil productivity, age, and drainage (Bigham and Ciolkosz, 1993). Since the 1940s, the Munsell soil colour chart has been used to assess soil colour visually, validated by the 1980s through experimental measurements and uniform colour-space models (Sánchez-Marañón, 2011).

Soil spectral behaviour is crucial for soil identification and characterization. It refers to soils' reflection of electromagnetic energy, especially in the visible (VIS), near-infrared (NIR), and shortwave infrared (SWIR) regions, closely linked to soil colour and vital for remote and proximal sensing techniques (Sahar et al., 2022; Rizzo et al., 2021). Reflectance spectroscopy in the VIS-NIR-SWIR range is a valuable tool for analyzing soil properties, revealing physical, chemical, and mineralogical attributes (Dwivedi, 2017; José et al., 2012). Different soil types have distinct spectral signatures, with sandy soils showing higher reflectance and clayey soils with lower

reflectance (Muraru, 2021). Spectral data can estimate key soil properties like organic carbon, clay content, cation exchange capacity (CEC), and iron forms, and identify specific minerals such as kaolinite, gibbsite, hematite, and goethite (Soydan, 2014; Basarygina et al., 2022). Spectral reflectance also helps predict soil salinity levels, with certain bands negatively correlating with electrical conductivity (Cierniewski, 2020). Thus, soil spectral behaviour is essential for agricultural and environmental research, enabling cost-effective and efficient soil monitoring to enhance management decisions (Mauli et al., 2022).

2.5 Soil moisture content

Soil moisture, a vital aspect of the soil's three-phase system (solids, moisture, and air), is crucial for understanding soil behaviour in engineering, agriculture, geology, and ecology. It affects properties like consistency, swelling, shrinking, and density. Variables such as topography, vegetation, and soil structure influence moisture distribution, which ranges from dry to saturated based on climatic conditions. Measuring soil moisture is crucial in agriculture and engineering due to its significant impact on soil's physical and mechanical traits. Susha mentioned Briggs categorized soil moisture into gravity, capillary, and hygroscopic (Susha Lekshmi et al., 2014).

2.5.1 The influence of soil moisture content on off-road vehicle performance

Soil moisture content significantly influences the performance and impact of off-road vehicles (ORVs) on terrain. Understanding this relationship is crucial for managing soil health and vehicle efficiency in off-road conditions.

2.5.1.1 Effects of soil moisture on infiltration and sediment production

- ORV traffic reduces soil infiltration rates, particularly in dry conditions. For instance, infiltration rates on disturbed interspace soils can decrease to as low as 1.39×10^{-6} cm/sec after vehicular impact, compared to 8.33×10^{-4} cm/sec on undisturbed soils (Eckert et al., 1979).
- Sediment production increases substantially with vehicular disturbance, with rates reaching 1,338 kg/ha under certain conditions (Eckert et al., 1979).

2.5.1.2 Soil compaction and moisture interaction

- Soil moisture content directly affects compaction levels. Higher moisture levels can lead to increased soil density under ORV traffic, which can impede water infiltration (Raghavan et al., 1976; Webb, 1982).
- A study demonstrated that soil density increased from 1.53 to 1.77 metric tons/cubic metre after multiple motorcycle passes, indicating significant compaction effects influenced by moisture levels (Webb, 1982).

2.5.1.3 Terrain variability and moisture content

- The variability of soil parameters, including moisture content, complicates predictions of vehicle performance on off-road terrains. Stochastic modelling can help capture this variability, allowing for a better understanding and management of ORV impacts (Sandu et al., 2005).

While the detrimental effects of ORVs on soil moisture and structure are well-documented, some

researchers posit that controlled ORV use can be managed to minimize environmental impact, suggesting a need for balanced recreational policies.

2.5.2 The moisture content relationship with soil spectral reflectance

The relationship between soil moisture content and spectral reflectance is of paramount importance for accurate soil water assessment. Numerous studies have demonstrated that specific wavelengths in the near-infrared spectrum can effectively indicate moisture levels in soil.

2.5.2.1 Reflectance measurements and soil moisture

- Reflectance at 1.94 microns exhibits a log-linear relationship with soil water content, demonstrating particular efficacy in assessing surface moisture (Skidmore et al., 1975).
- A study utilising soil-methanol extracts identified a linear correlation between absorbance at 1.94 microns and soil water content across diverse soil types, indicating the potential for reflectance-based moisture determination (Bowers and Smith, 1972).
- An apparatus employing fibre optics to measure reflectance at multiple infrared wavelengths has been developed, facilitating moisture content calculations at various soil depths (Auer, 1978).

2.5.2.2 Practical applications

- A hand-held near-infrared reflectance moisture meter has been designed, achieving a standard error of $\pm 1.9\%$ moisture units, thus demonstrating its reliability for field measurements (Kano et al., 1985).
- Advancements in electromagnetic methods, including time domain reflectometry and ground penetrating radar, have enhanced the capacity to measure soil moisture non-invasively, further corroborating the utilization of spectral reflectance techniques (Topp and Ferré, 2006).

While spectral reflectance presents a promising approach for measuring soil moisture, it is imperative to consider the influence of soil texture and composition, which may affect reflectance readings.

2.6 Measurement of terrain properties and soil colour

2.6.1 Cone penetrometer

The cone penetrometer, initially employed by the U.S. Army Engineer Waterways Experimental Station (WES) for soil strength evaluations in trafficability studies (Freitag, 1966), is standardized for agricultural applications as ASAE S313.2. This standard facilitates result interpretation and comparison by specifying the index application range, penetration speed, and depth increments for various penetrometer types. The penetrometer comprises a 30° circular stainless-steel cone connected to a circular stainless-steel shaft (Figure 2.9).

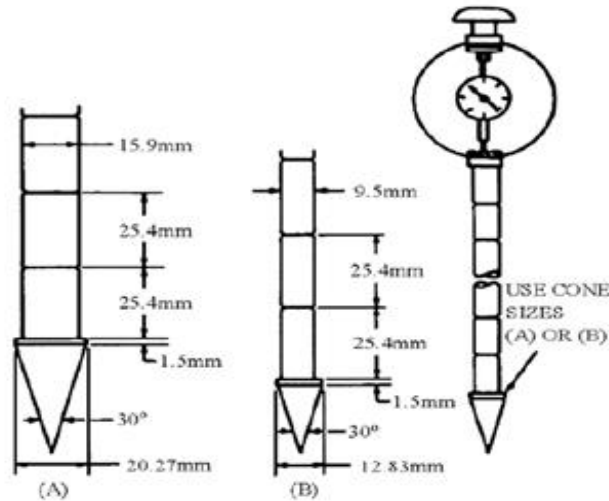


Figure 2.9. Cone penetrometer standardized by the ASAE S313.2 (Wong, 2010).

The "Cone Index (CI)" measures the average force per unit projected cone base area exerted by soil against a conical head at a penetration rate of about 3 cm/s, according to the American Society of Agriculture Engineering (ASAE) standard S313.2. This index combines shear, compression, and soil-metal friction factors (ASAE, 1988). CI values can vary with depth, so the average CI at the depth of maximum tyre or track sinkage is often used for traction prediction (Wismer and Luth, 1973).

A remoulding index (RI) quantifies terrain strength changes due to repeated vehicular activity, calculated as the ratio of the cone index after remoulding to before. Fine-grained soils are remoulded with 100 blows of a 1.135 kg hammer dropped from 30.5 cm, while coarse-grained soils with fines are remoulded by dropping the cylinder and base 25 times from a height of 15.2 cm (SAE, 1967).

The rating cone index (RCI), the product of RI and pre-remoulding CI, indicates terrain strength under repeated vehicular activity. The vehicle cone index (VCI) measures terrain trafficability, defined as the minimum CI in the critical layer for multiple vehicle passes without immobilization, with critical layer depth varying by vehicle type and weight (Wong, 2010).

Rohani and Baladi (1981) calculated the CI using the terrain's internal shearing resistance, cohesion, density, and apparent shear modulus, considering the cone shape and penetration depth, and idealizing the terrain as a rigid, fully plastic material.

Hettiaratchi and Liang (1987) developed a formula for the load on a conical or wedge-shaped indenter based on its geometry, penetration depth, internal shearing resistance angle, and terrain cohesion.

Key characteristics associated with the cone penetrometer include CI, RI, RCI, VCI, and Slope Index (Taghavifar and Mardani, 2017).

2.6.2 *Bevometer technique*

The bevometer method, introduced by Bekker, assesses soil strength and sinkage parameters

LITERATURE REVIEW

crucial for traction performance. Since traction devices exert contact pressure and tangential stresses on the terrain to generate tractive effort, simulating this by applying loads in both directions are logical. The bevameter approach seeks to more accurately replicate this scenario than existing methods (Wong, 2010; Wong, 2001). The bevameter technique includes:

1. A plate sinkage test determines the pressure-sinkage relationships of the soil.

and

2. A shear test determines the in-situ shear strength parameters of the soil. A schematic illustration of a complete bevameter is presented in Figure 2.10.

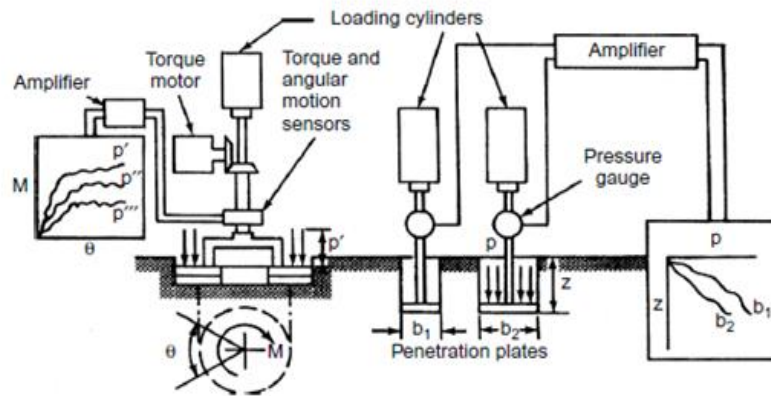


Figure 2.10. Schematic diagram of a bevameter (Bekker, 1969).

The shear device comprises a grousers annular ring attached to a shaft's end. Shear measurements are conducted by applying constant vertical loads to the ring, which is then rotated at a consistent speed. Torque and angular displacement records determine shear strength. The bearing capacity device, a plate penetrometer, measures bearing capacity by forcing flat plates of various sizes into the soil and using penetration force and sinkage data. The bevameter measures cohesion (c), angle of internal friction (ϕ), sinkage moduli (k , k_c , k_ϕ), and sinkage exponent (n) (Taghavifar and Mardani, 2017). Michael B. Edwards et al. (2017) used a custom-built bevameter at the National Aeronautics and Space Administration (NASA) Glenn Research Center, illustrated in Figure 2.11., to measure pressure sinkage. This instrument performs normal and shear tests for soil-wheel interactions. In a normal test, the instrument employs a piston to press a plate into the soil specimen, a load cell to measure resistance force, and laser range finders to continuously measure vertical displacement.

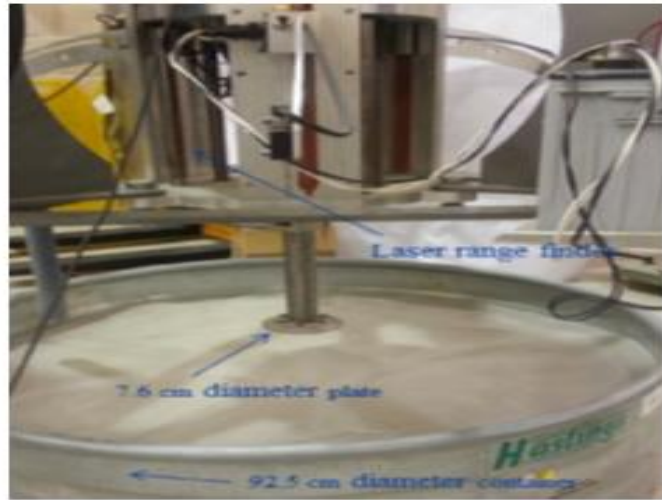


Figure 2.11. Normal bevameter test set up (Michael B. Edwards et al., 2017).

The shear bevameter tests employed the same equipment as the normal bevameter test, supplemented with torque and angular motion sensors to measure rotational resistance under a constant normal load.

2.6.3 Spectrophotometers

The spectrophotometer, a common analytical device, determines analyte concentrations by assessing light absorption at specific wavelengths. However, its high cost, limited portability, and need for a constant power supply can restrict its widespread use and sometimes affect accuracy in urgent field testing (Jun-Jie et al., 2021). A spectrophotometer comprises a spectrometer, generating monochromatic light from a diffraction grating to illuminate the sample, and a photometer, measuring the light reflected or transmitted at distinct wavelengths, providing a voltage signal to a display device. This signal varies based on the light absorbed by the sample. Instrument accuracy depends on several factors, particularly the spectral bandpass, which is the range of wavelengths measured at each spectrum point (Roy-Choudhury, 2014). Figure 2.12 illustrates the basic structure of spectrophotometers, including a light source, collimator, monochromator, wavelength selector, sample solution cuvette, photoelectric detector, and a digital display or meter.

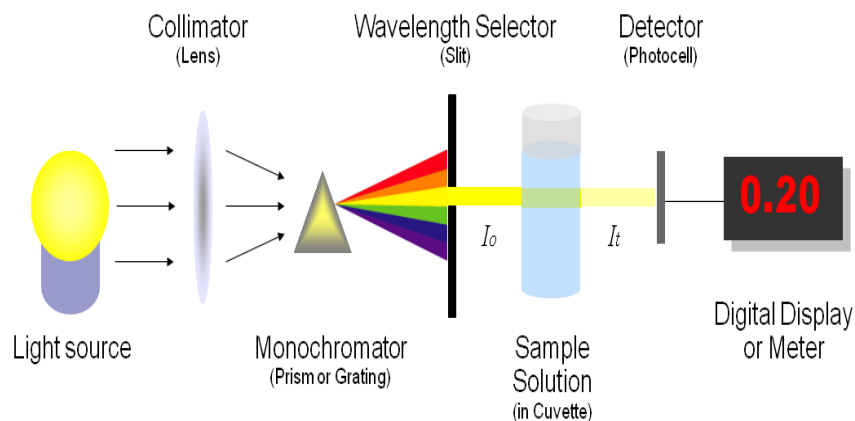


Figure 2.12. The basic structure of spectrophotometers (Skoog et al. 2007; Pavia et al., 2001)

2.6.4 Colourimeters

A colourimeter measures light absorption by assessing changes in visible electromagnetic radiation intensity upon transmission or reflection by an object or solution. The photocell within the colourimeter detects transmitted light, generating a current proportional to the light intensity after passing through the sample. Higher colourant concentrations lead to greater absorption, reducing transmission and lowering the generated current. Colourimeters estimate colour using three wideband measurements across the visible spectrum, typically employing filters to mimic human vision. Colourimeters are classified as visual or photoelectric. The Nessler tube, the earliest colour comparator, evolved into the Duboscq colourimeter, which compares the optical properties of samples with specific colourants, sufficient for many colour-assessment tests. The instrument's construction is illustrated in Figure 2.13. (Roy-Choudhury, 2014).

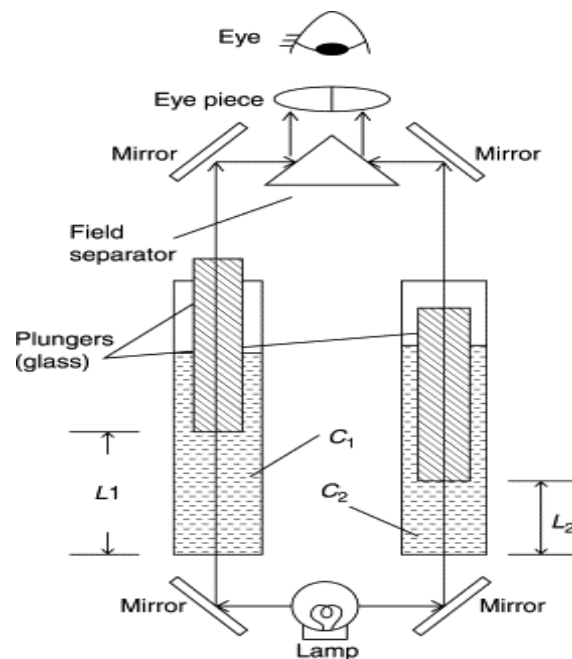


Figure 2.13. Duboscq colourimeter (Roy-Choudhury, 2014)

2.6.5 Traditional soil moisture measurement methods

The assessment of soil moisture content has long been a pivotal element in both agricultural and environmental research. Traditional methodologies have been developed to measure this parameter, each presenting distinct advantages and limitations.

2.6.5.1 Gravimetric method

One of the most established and rigorous techniques is the gravimetric method. This approach entails weighing a soil sample prior to and following its drying at a specified temperature, typically 105°C, to eliminate all water content. The resultant weight difference facilitates the calculation of moisture content as a percentage of the dry soil weight. Despite its recognised accuracy and widespread acceptance, the gravimetric method is labour-intensive, time-consuming, and necessitates meticulous handling to prevent errors (Hillel, 1998; Campbell and Norman, 1998).

2.6.5.2 Oven-drying method

Closely related to the gravimetric approach is the oven-drying method, which employs a laboratory

oven to accelerate the drying process. This technique remains a standard reference for evaluating other methods due to its precision. Nonetheless, it shares similar limitations, including being time-consuming and requiring the collection and transportation of samples (Rawls et al., 2003; Rawls et al., 1989).

2.6.5.3 Ring infiltrometer

Indirect measurement techniques, such as the ring infiltrometer, have been developed. This method assesses the rate at which water infiltrates the soil, which can be correlated with soil moisture levels under specific conditions. However, the efficacy of this approach is significantly influenced by soil texture and structure, rendering it less reliable in heterogeneous soils (Bouyoucos, 1962).

2.6.5.4 Tensiometers

A more sophisticated traditional method involves the utilization of tensiometers. These devices measure soil water potential by monitoring the tension exerted on a porous ceramic cup inserted into the soil. Tensiometers provide continuous data and are valuable for understanding plant-available water. However, they are limited to particular moisture ranges and require regular calibration and maintenance (Cresswell and Hamilton, 2002).

2.7 Bearing capacity (pressure-sinkage relationship)

In 1959, Saakyan proposed a pressure–sinkage equation based on the Boussinesq theory concerning the elastic half-space, as indicated in Equation 2.8 (Salman et al., 2021).

$$p = k \left(\frac{Z}{D} \right)^n \quad (2.8)$$

where p is the average pressure under an indenter, D is the diameter of the indenter, Z is the vertical soil deformation (sinkage), and k is the sinkage modulus (load-carrying capacity factor).

Bernstein, whose primary area of expertise was agricultural engineering, empirically demonstrated that if a plate penetrates the soil to a depth z under a certain pressure p , then the resultant experimental pressure-sinkage curve can be approximate utilising the following equation:

$$p \cong kz^{0.5} \quad (2.9)$$

where k is a modulus of inelastic deformation, and 0.5 is the exponent of sinkage (Bernstein, 1913).

Russian investigators subsequently refined this equation, concluding that the formula could potentially be reduced to the following form:

$$p = kz^n \quad (2.10)$$

The pressure-sinkage relationship for a flat plate follows a power function with curve-fitting parameters k and n derived from empirical soil data, where n ranges from 0 to 1 (Figure 2.13). Despite the limitation of assuming constant k and n for a given soil, which varies with surface loading and load range (Ageykin, 1973), this formula laid the foundation for more advanced models. Bekker discovered that the plate's width or radius influences the parameters and proposed the renowned Bekker model in 1956, simplifying the average pressure and plate sinkage

relationship for homogeneous terrain (Bekker, 1956).

$$p = \left(\frac{k_c}{b} + k_\phi \right) z^n \quad (2.11)$$

The penetration test parameters include plate width (b), pressure-sinkage effect due to cohesion (k_c) and friction (k_ϕ), plate sinkage (z), and deformation exponent (n). The dimensions of k_c and k_ϕ rely on n , limiting the model. Equation 2.11 accurately assesses soil resistance to penetration across various soil types and effectively predicts trends without direct experimental data. Experimental data is fitted to Equation 2.9 to determine k_c , k_ϕ , and n , while p and z are measured (Wong, 2001).

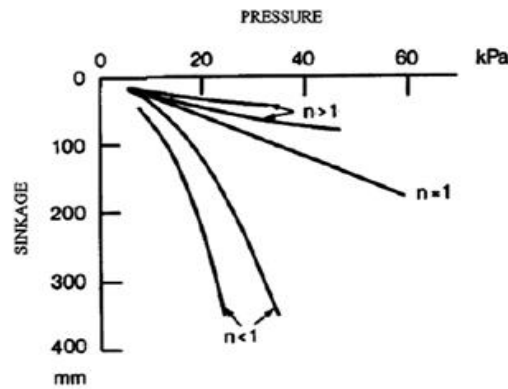


Figure 2.13. Typical pressure-sinkage curves (Bekker, 1969)

Bekker further modified Equation 2.11 to determine the wheel sinkage of a vehicle,

$$z = \frac{3W}{\left((3-n)(K_c + bK_\phi) d^{\frac{1}{2}} \right)^{\frac{2}{2n+1}}} \quad (2.12)$$

where (W) is the wheel load and (d) and (b) are the tyre diameter and tyre width, respectively (Bekker, 1960).

Onafeko and Reece (1967) noted that the pressure-sinkage relationship in Equation 2.11 is insufficient because the dimensions of soil parameters k and n depend on n , complicating derived relationships. Therefore, Equation 2.11 was revised to be

$$p = (c\hat{k}_c + \gamma b\hat{k}_\phi) \left(\frac{z}{b} \right)^n \quad (2.13)$$

where \hat{k}_c , \hat{k}_ϕ , and n are new dimensionless pressure-sinkage parameters, and γ is the specific weight of the terrain.

Reece constructed the instrument shown in Figure 2.14 to measure soil shear strength parameters. A key advantage of Reece's methodology and apparatus was the inclusion of slip-sinkage, the sinkage caused by shear.

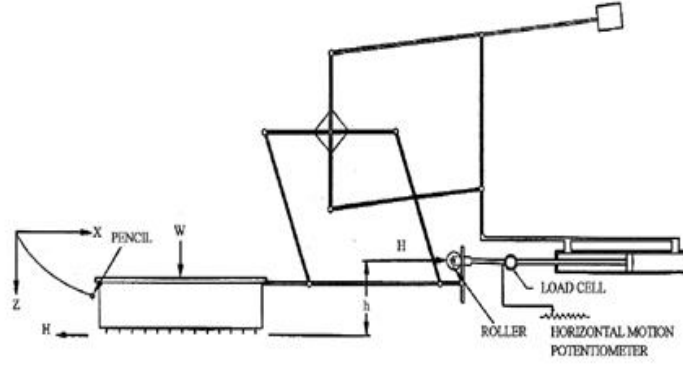


Figure 2.14. Reece's linear shear apparatus to measure soil shear strength and sinkage (Reece,1965).

To obtain the values of n , k_c , k_ϕ , \hat{k}_c and \hat{k}_ϕ , Wong proposed a weighted least squares method to derive unique parameter values (Wong, 2010). Wong's method for data processing determines the optimal values of the pressure-sinkage terrain parameters by minimising the following function using a weighting factor p^2 ,

$$F = \sum p^2 [\ln p - \ln k_{eq} - n \ln z]^2 \quad (2.14)$$

Where: $k_{eq} = \frac{k_c}{b} + k_\phi$

Take two partial derivatives of F , one with respect n and the other with k_{eq} , to minimize the value of function F . The following two equations appears:

$$\ln k_{eq} \sum p^2 \ln z + n \sum p^2 (\ln z)^2 = \sum p^2 \ln p \ln z \quad (2.15)$$

$$\ln k_{eq} \sum p^2 + n \sum p^2 \ln z = \sum p^2 \ln p \quad (2.16)$$

By solving these equations, the value of n and $\ln k_{eq}$ can obtain

$$n = \frac{\sum p^2 \sum p^2 \ln p \ln z - \sum p^2 \ln p \sum p^2 \ln z}{\sum p^2 \sum p^2 (\ln z)^2 - (\sum p^2 \ln z)^2} \quad (2.17)$$

$$\ln k_{eq} = \frac{\sum p^2 \ln p - n \sum p^2 \ln z}{\sum p^2} \quad (2.18)$$

When using two different plate sizes a unique n is usually obtained for each. Therefore, it is required to use the average n -value resulting from the two different plates when calculating the natural logarithm of k_{eq} in Equation 2.18. However, since there will be two resulting k_{eq} values: one for plate size b_1 and another for plate size b_2 . Accordingly, the values of k_c and k_ϕ can be determined using the subsequent equations (Dewhirst, 1964).

LITERATURE REVIEW

$$k_c = \frac{(k_{eq})_{b_1} - (k_{eq})_{b_2}}{b_2 - b_1} b_1 b_2 \quad (2.19)$$

$$k_\phi = (k_{eq})_{b_1} - \frac{(k_{eq})_{b_1} - (k_{eq})_{b_2}}{b_2 - b_1} b_2 \quad (2.20)$$

Wong also developed a method for defining the error between the experimental and theoretical data. He referred to this as the “goodness-of-fit” equation which defines the ratio of the root mean square error to the mean value of pressure as follows,

$$\varepsilon = 1 - \frac{\sqrt{\frac{\sum (p_m - p_{lc})^2}{N - 2}}}{\frac{\sum p_m}{N}} \quad (2.21)$$

where p_m is the measured pressure, p_{lc} is the calculated pressure using the procedures described above, and N is the number of data points used for the curve fitting. If ε is 1, that mean the fit is perfect. This technique can also be applied to Reece’s equation.

Table 2.1: Mean values of the parameters characterizing the pressure–sinkage relations of various mineral terrains (Wong, 2010). Table 2.1 summarizes the mean values of k_c , k_ϕ , k_c'' , k_ϕ'' and n for the various mineral terrains tested and the goodness-of-fit of the Bekker and Reece Eqs. to the measured data.

| Terrain type | Constants for Bekker's equation | | | Constants for Reece's equation | | | Goodness-of-fit % | Wet density (kg/m ³) | Moisture content % |
|-------------------------|---------------------------------|------------------------------|---------------------------------|--------------------------------|------------------------------|---------------------------------|-------------------|----------------------------------|--------------------|
| | n | k_c (kN/m ⁿ⁺¹) | k_ϕ (kN/m ⁿ⁺²) | n | k_c'' (kN/m ²) | k_ϕ'' (kN/m ³) | | | |
| LETE sand | 0.705 | 6.94 | 505.8 | 0.705 | 39.1 | 779.8 | 95.3 | ~1600 | |
| | 0.611 | 1.16 | 475.0 | 0.611 | 28.2 | 1066 | 94.5 | | |
| | 0.804 | 3.93 | 599.5 | 0.804 | 16.9 | 879.6 | 93.8 | | |
| | 0.728 | | 1348 | 0.728 | 18.3 | 2393 | 88.8 | | |
| | 0.578 | 9.08 | 2166 | 0.578 | 197 | 4365 | 89.2 | | |
| | 0.781 | 47.8 | 6076 | 0.781 | 229.7 | 8940 | 89.8 | | |
| | 0.806 | 155.9 | 4526 | 0.806 | 413.5 | 5420 | 88.1 | | |
| Upland sandy loam | 1.10 | 74.6 | 2080 | 1.10 | 42.0 | 1833 | 87.7 | 1557 | 51.6 |
| | 0.97 | 65.5 | 1418 | 0.97 | 77.4 | 1464 | 92.0 | 1542 | 49.2 |
| | 1.00 | 5.7 | 2293 | 1.00 | 5.3 | 2283 | 94.8 | 1570 | 49.1 |
| | 0.74 | 26.8 | 1522 | 0.74 | 121.7 | 2092 | 95.1 | 1519 | 44.3 |
| | 1.74 | 259.0 | 1643 | 1.74 | -0.9 | 763 | 86.0 | 1696 | 50.0 |
| | 0.85 | 3.3 | 2529 | 0.85 | 42.4 | 3270 | 87.5 | 1471 | 28.6 |
| | 0.72 | 59.1 | 1856 | 0.72 | 231.4 | 2323 | 84.2 | 1592 | 34.3 |
| | 0.77 | 58.4 | 2761 | 0.77 | 214.1 | 3626 | 86.6 | 1559 | 35.1 |
| | 1.09 | 24.9 | 3573 | 1.09 | 6.7 | 2982 | 91.9 | 1716 | 31.2 |
| | 0.70 | 70.6 | 1426 | 0.70 | 279.3 | 1317 | 94.3 | 1470 | 27.3 |
| 0.75 | 55.7 | 2464 | 0.75 | 213.6 | 3244 | 89.4 | 1526 | 32.6 | |
| Rubicon sandy loam | 0.66 | 6.9 | 752 | 0.66 | 63.3 | 1176 | 92.6 | 1561 | 43.3 |
| | 0.65 | 10.5 | 880 | 0.65 | 88.2 | 1358 | 97.0 | 1588 | 44.2 |
| North Gower clayey loam | 0.73 | 41.6 | 2471 | 0.73 | 121.2 | -4.2 | 88.8 | 1681 | 45.8 |
| | 0.85 | 6.8 | 1134 | 0.85 | 27.0 | 1430 | 90.0 | 1597 | 52.0 |
| Grenville loam | 1.01 | 0.06 | 5880 | 1.01 | -1.3 | 5814 | 87.4 | 1326 | 24.1 |
| | 1.02 | 66.0 | 4486 | 1.02 | 55.3 | 4292 | 89.1 | 1339 | 18.2 |

Upadhyaya et al. (1993) developed a fully instrumented device (Figure 2.15) to measure soil sinkage parameters, shear parameters, and cone index. The device's effectiveness was confirmed through field tests using rectangular plates in firm and tilled Yolo loam soil.

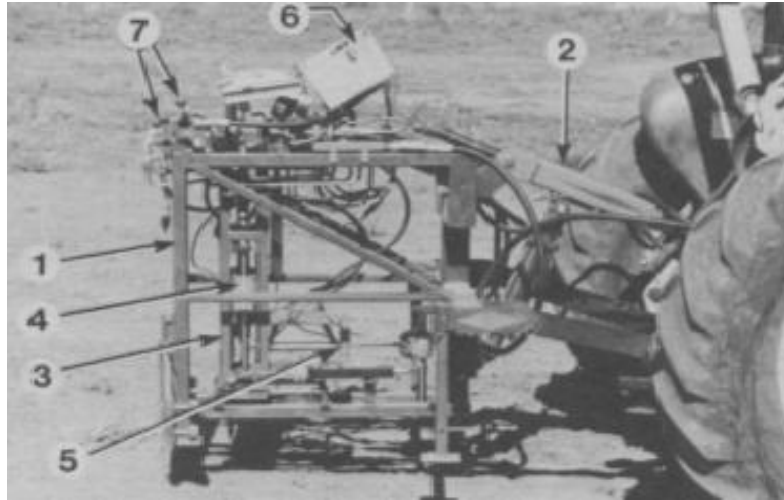


Figure 2.15. The fully instrument soil test device.

(1-main frame, 2-hydraulic cylinder, 3- secondary frame, 4- load cells and a displacement transducer, 5- arm) (Upadhyaya et al., 1993).

Kougre et al. (1983) demonstrated that a hyperbola better reflects the load-sinkage relationship, where higher pressure results in increased soil resistance. At greater depths, additional pressure minimally affects sinkage. Therefore, semi-empirical methods are superior to extending elasticity and plasticity theories for this description.

Emori and Schuring proposed that the force required to push a plate was a function of penetration depth (Z^*), plate velocity (\dot{Z}) and plate acceleration (\ddot{Z}) as shown in Equation 2.22.

$$F_s = f_1(Z^*) + f_2(Z^*, \dot{Z}) + f_3(Z^*, \ddot{Z}) \quad (2.22)$$

Where (F_s) is the soil force acting on the plate. The first term in Equation 2.22 represents the static force; the second symbolizes the force due to lateral acceleration of soil particles and soil viscosity; and the third shows the inertia force vertically accelerated soil particles (Emori and Schuring, 1966).

Grahn (1991) expresses that under a constant load, the soil surface sinkage was smaller at higher penetration velocities and the modulus of soil deformation in Bekker's equation was equal to ($K_0 \dot{Z}^m$) where (\dot{Z}) is the vertical velocity, (K_0) is the static modulus of soil deformation, and (m) is the exponent of the penetration velocity.

$$p = K_0 \dot{Z}^m Z^n \quad (2.23)$$

Figure 2.16 represents the data for different load speeds. This dynamic relation is not valid for penetration velocities below 10 mm/min, which are defined as a static condition.

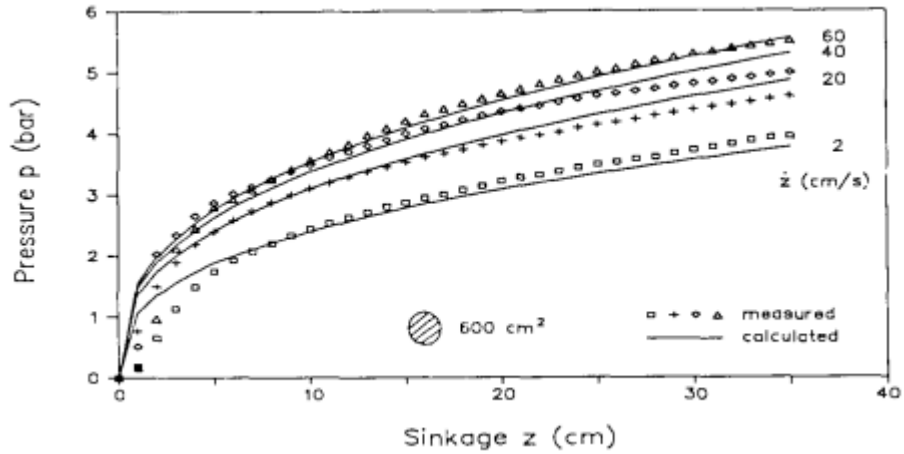


Figure 2.16. Correlation of measured and calculated pressure-sinkage curves for different penetration velocities (Grahn, 1991).



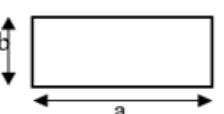

2.7.1 Effect of plate size and shape

Youssef and Ali (1982) determined that plate sinkage study accuracy depended on the plate's dimensions, configuration, and soil strength parameters. They concluded that consistent and uniform plate penetration rates, mimicking conditions under a track or wheel, would yield more representative outcomes. However, achieving the necessary high loading rate to simulate traffic conditions was impractical. They found comparable results using circular and rectangular sinkage plates and proposed Equation 2.24 by modifying the Bekker and Reece models.

$$p = (K_1 + 0.5bK_2)\beta^n Z^n \tag{2.24}$$

where β is a geometric constant depending on the shape of the loading surface as in Table 2.2.

Table 2.2 Plate geometric constants, β vs. A/S (Youssef and Ali, 1982)

| Plate shape | A/S | β_0 |
|--|--|--|
| Circular  | $d/4$ | 4 |
| Square  | $a/4$ | 4 |
| Rectangular  | $\frac{a \cdot b}{2(a + b)}$ | $\frac{2}{a}(a + b)$ |
| Ellipse  | $\frac{a \cdot b}{2(a + b)}$ Min. $\frac{a \cdot b}{4\sqrt{\frac{1}{2}(a^2 + b^2)}}$ Max. | $\frac{2}{a}(a + b)$ Max. $\frac{4\sqrt{\frac{1}{2}(a^2 + b^2)}}{a}$ Min. |

Modifying the plate size to match the wheel-soil contact patch would necessitate numerous plates to represent the area increase with sinkage. This implies conducting plate tests for each sinkage level and new wheel diameter. Meirion-Griffith and Spenko (2011) studied the impact of wheel diameter on soil pressure-sinkage and adjusted the Bekker model accordingly, as shown in Equation 2.25:

$$p = \hat{K} z^{\hat{n}} D^{\hat{m}} \quad (2.25)$$

Where D is the wheel diameter and \hat{m} is the diameter exponent. Similar to the Bernstein–Goriatchkin expression, the proposed model describes a power function, for which \hat{K} , $z^{\hat{n}}$ and $D^{\hat{m}}$ are fitting constants.

This modification is validated by results from 160 experiments using five-wheel diameters and three soil types. The proposed model's improvement stems from incorporating, which makes the curvature of the pressure-sinkage relationship dependent on both sinkage and diameter. The researchers used the vehicle-terrain testbed shown in Figure 2.17 for validation.

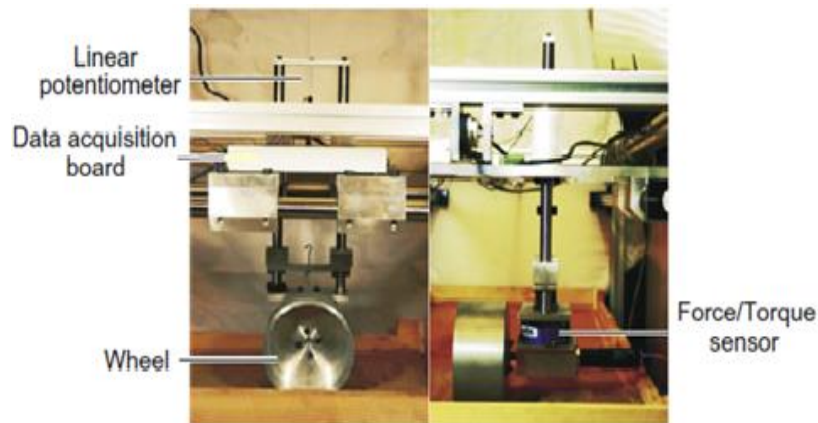


Figure 2.17. Single-wheel vehicle-terrain testbed (Meirion-Griffith and Spenko, 2011).

In 2013, Meirion-Griffith and Spenko (2013) modified the new pressure-sinkage model to consider the effect of wheel width on sinkage, in addition to the effect of the diameter.

The form of 2.25 allows the pressure at the wheel-soil interface to be a function of both b and D ; the model yields the sinkage equation:

$$z_0 = \frac{3W}{b(3 - \hat{n})\hat{k} \left(b\sqrt{Dz_0 - z_0^2} \right)^{m+0.5}} \quad (2.26)$$

Where W is the normal load on the wheel, z_0 is now a function of itself and cannot be separated, leading to an equation without a closed-form solution. However, plotting every possible value of z_0 within the length function against the solution for z_0 shows convergence only once for sinkages less than the wheel radius, providing the correct solution (Meirion-Griffith and Spenko, 2013).

Despite the semiempirical method's reliance on two simple relations and the observed variations in the pressure–sinkage relationship from experiments, the analysis of traction performance for off-road wheels using this method has been refined for practical applications in terramechanics (Wong and Asnani, 2008).

Thomas Keller and M. Lamande examined predicting the contact area and vertical stress distribution beneath tyres, identifying these as the upper boundary conditions for soil compaction models. Accurate stress prediction at the contact patch is therefore essential. Their model incorporated wheel load, tyre inflation pressure, recommended tyre inflation pressure, tyre width, and tyre diameter as key inputs. The study highlighted how wheel load and tyre inflation pressure affect contact pressure distribution, significantly enhancing input data for soil compaction models and improving the accuracy of soil stress and compaction predictions (Keller, 2005).

The rate of sinkage is a crucial factor in pressure-sinkage relationships. R. G. Pope investigated the effect of sinkage rate. He postulated that the pressure-sinkage rate relationship conforms to a power law of the form (Pope, 1969):

$$p = p_0 \left(\frac{u}{u_0} \right)^m \quad (2.27)$$

Upon submission of the Reece model, the new model shall be represented by the following equation:

$$p = (ck_c + \gamma bk_\phi) \left(\frac{z}{b} \right)^n \left(\frac{u}{u_0} \right)^m \quad (2.28)$$

Where u represents sinkage velocity, u_0 represents plate sinkage velocity, and m and n are sinkage exponents.

2.7.2 Effect of load direction, plate inclination and soil deformation

Xu et al. (1996) proposed a pressure-sinkage relation under a horizontal plate-inclined load, observing that (k) decreased as angles α and β increased, resulting in greater sinkage under an inclined load compared to a vertical load. Wood and Wells (1985) characterized soil deformation by measuring grid point displacement and converting these to volumetric strain, with results comparable to gamma-ray density gauge readings. Ohtomo and Andy (2001) assessed vertical soil displacement under an axial compressive load, finding that displacement was dependent on initial penetration depth, with maximum deformation unaffected by initial compressive load and soil density remaining stable beyond 270 mm. Lyasko (2010) developed the load-sinkage analytical (LSA) model to predict sinkage and penetration force based on soil parameters and plate or traction device characteristics, reducing the need for extensive testing.

2.8 Summary

The performance of off-road vehicles is influenced by vehicle-terrain interaction. Comprehending this interaction is crucial for selecting appropriate vehicle configurations and design parameters to meet operational requirements. Terramechanics aims to establish a quantifiable relationship between an off-road vehicle's performance and design for a particular unpaved terrain environment. This literature review examines terramechanics simulation models that investigate wheeled vehicle performance over deformable terrains, as well as load-bearing capacity and soil spectral behaviour.

The discussion commences with an exploration of soil structure and strength, delineating the fundamental properties that determine soil stability and mechanical performance. It then extends

LITERATURE REVIEW

to soil shearing strength and its characteristics, which are crucial in understanding how soil resists deformation under stress. The analysis distinguishes between the stress distribution in elastic and plastic regions, defining soil deformation characteristics under applied forces and their implications for vehicle mobility.

A key focus is placed on soil load-bearing capacity, which is crucial in off-road engineering and terrain interaction. Concurrently, soil colour and spectral behaviour are examined, analyzing their role in property characterization and assessing variations in soil composition. The influence of moisture content is also investigated, particularly in relation to off-road vehicle performance and its effect on soil spectral reflectance, demonstrating the correlation between moisture levels and spectral responses.

Additionally, methodologies for measuring terrain properties and soil colour are examined, elucidating key techniques such as cone penetrometers, bevameter techniques, spectrophotometers, and colorimeters. Furthermore, traditional soil moisture measurement methods are discussed, providing fundamental benchmarks for modern moisture measurement technologies and offering critical insights into soil-water interactions and their implications for terrain assessment.

Furthermore, the bearing capacity of soil is investigated through the pressure-sinkage relationship, emphasizing the effects of plate size, shape, load direction, plate inclination, and soil deformation. This section is particularly pertinent to understanding soil behaviour under varying loading conditions, contributing to enhanced predictive models for terrain performance.

By synthesizing mechanical and spectral perspectives, this study advances the understanding of soil behaviour, with significant implications for off-road engineering, geotechnical applications, and remote sensing-based soil assessment.

3. MATERIALS AND METHODS

This chapter presents the experimental methodology, materials, instrumentation, procedures, and processes used in the research, including the scientific methods involved in the experimental measurements and the description of the test systems to obtain the set research objectives.

3.1 Soil types

Eight different types of soil were collected from various regions in Hungary, as listed in Table 3.1 and depicted in the triangle-textured diagram (Figure 4.1).

Table 3.1. Shows eight soil textures from different regions in Hungary.

| Soil no. | Soil type | Sand (%) | Silt (%) | Clay (%) | Location | Coordinates |
|----------|------------|----------|----------|----------|-----------------------|------------------------|
| 1 | Sandy loam | 90.50 | 3.20 | 6.30 | Gödöllő, Hungary | 47.5816264, 19.3984064 |
| 2 | Silty loam | 11.64 | 62.18 | 26.18 | Karcag, Hungary | 47.2884618, 20.9213624 |
| 3 | Clay | 13.16 | 31.28 | 55.56 | Karcag, Hungary | 47.235285, 20.7345042 |
| 4 | Sand | 95.68 | 2.12 | 2.21 | Csölyospálos, Hungary | 46.3954473, 19.8210738 |
| 5 | Silty clay | 3.34 | 52.05 | 44.61 | Karcag, Hungary | 47.2829123, 20.8821998 |
| 6 | Clay loam | 30.77 | 40.70 | 28.53 | Sopron, Hungary | 47.6924941, 16.635592 |
| 7 | Loam | 31.29 | 49.67 | 19.03 | Sopron, Hungary | 47.6709397, 16.5644485 |
| 8 | Loamy sand | 82.13 | 12.10 | 5.77 | Órbottyán, Hungary | 47.6743804, 19.2466272 |

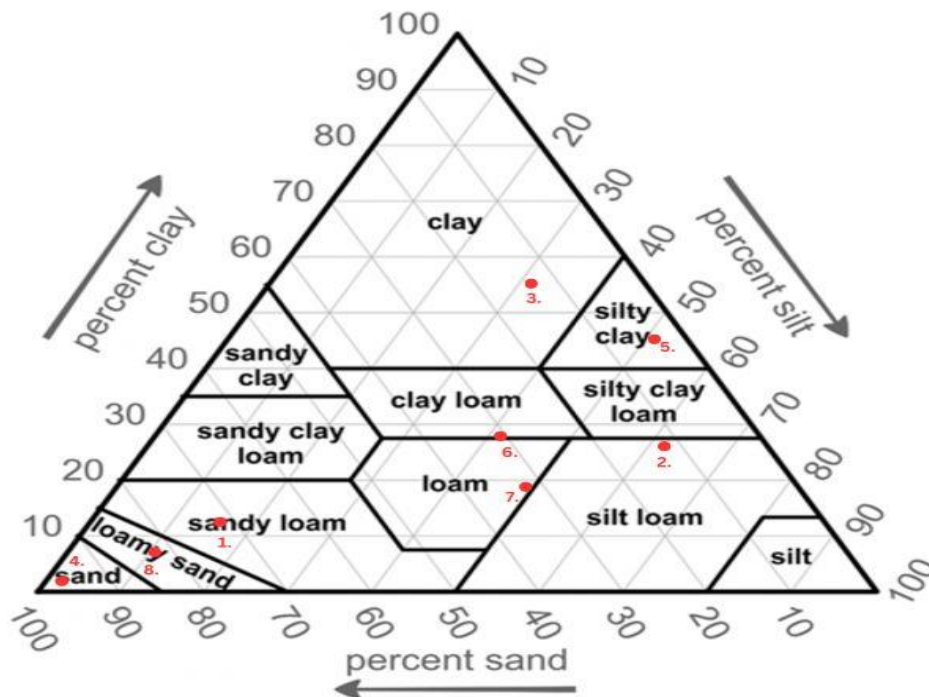


Figure 3.1. Shows the eight soil textures as mentioned in Table 3.1.

3.2 Soil preparation

Since the soil infield is inhomogeneous and anisotropic, it is complicated to study the soil (Pillinger, 2016, Salman. et al., 2022). To simplify this engineering case (studying the soil’s mechanical properties), the soil was sieved using a 5 mm mesh to eliminate the coarse parts and plant roots for studying it as a homogeneous material.

3.3 Experimental procedure

3.3.1 Load-bearing capacity measurement (bevameter test)

In the bevameter experiment (see Figure 3.2a), plate penetration is utilized to measure pressure–sinkage parameters (such as force and displacement, shown in Figure 3.2d) that influence motion resistance. The bevameter is connected to a computer using Catman 4.5 software via a Spider8 data logger (Figure 3.2c) to collect data (Time Device No., Displacement, and Force), as illustrated in Figure 3.2d.

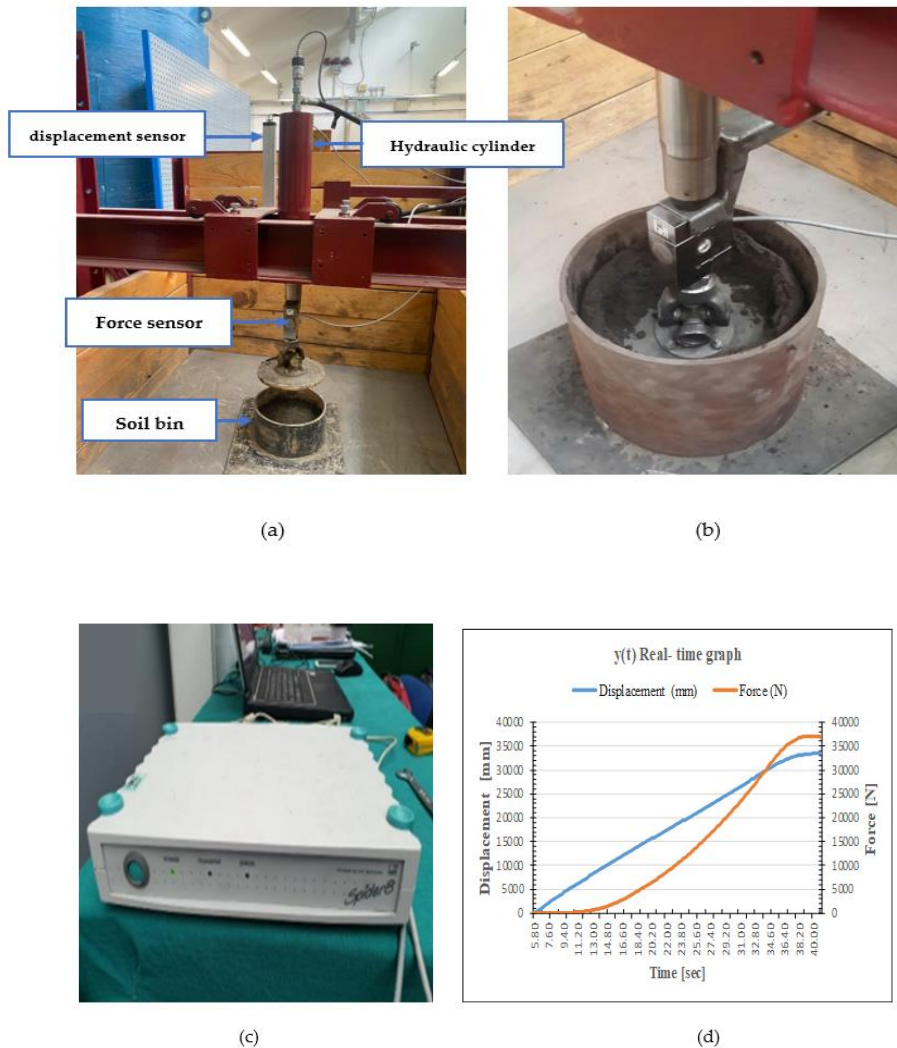


Figure 3.2. Shows (a) the main structure of the bevameter equipment, (b) the plate size (diameter = 20 cm), the soil bin (height = 12 cm, inner diameter = 22 cm), and the soil sample, (c) the data logger (Spider8), and (d) the CATMAN 4.5 software recording the data (force and Displacement as a function of time).

MATERIALS AND METHODS

The experiments were conducted at Hungarian University of Agriculture and Life Sciences. The soil, initially at ambient conditions with moisture due to surrounding humidity, was sieved (section 3.2) and prepared in the bevameter bin with a height of $H_1 = 12$ cm and an inner diameter of $D_1 = 22$ cm. The soil was filled to a height of $H_2 = 10$ cm and centred under the bevameter pressing plate, which had a diameter of $D_2 = 20$ cm (Figure 3.2b).

Two sensors were mounted on the top of the bevameter plate—one for measuring vertical displacement (mm) and the other for measuring applied load (force in Newtons) (Salman et al., 2020). Data were transmitted to a computer via a Spider8 data logger and displayed through CATMAN 4.5 software, with the force-displacement graph plotted as a function of time (Figures 3.2c and 3.2d).

The initial test was conducted with the soil at ambient conditions. It was subsequently repeated on the same soil sample after increasing the moisture content. Following each measurement, the soil was removed from the bin, and placed in a bucket, and water was added to increase the moisture content. The soil's mass at each moisture level and the final height (after compression by the plate, H_3) were recorded. These values, along with the initial height (H_2), were utilized to calculate soil density before and after load application.

The properties and measurement parameters for the eight soil textures are presented in Table 3.1. Each soil sample was tested at the same density but with six different moisture contents (MC%). The soil height before and after testing was $H_2 = 10$ cm and $H_3 =$ Height of the soil layer after pressing the soil, respectively. The mass of the soil (m) was measured to determine density across varying moisture contents. The initial soil density, ρ_1 , and post-compression density, ρ_2 , were calculated using Equation 3.1. Testing soil filled in the bin at $H_2/D_2 \leq 0.5$ demonstrated similar behaviour to testing it in infinite space (Salman et al, 2022). By maintaining a fixed H_2/D_2 ratio of 0.5 at different moisture levels, any excess soil (after stirring with water) was removed. The mass of the soil at different moisture contents used for filling the bin to the required height (keeping the H_2/D_2 value equal to 0.5) was recorded, and density was calculated based on mass and height.

$$\rho_{1,2} = \frac{m}{\pi \cdot r^2 \cdot H_{2,3}} \quad (3.1)$$

Table 3.1. Eight samples of soil with the same density but different moisture content.

| Soil type | Sample no. | H_2/D_2 | MC [%] | Mass [kg] | Height [cm] | Density [g/cm ³] | $\Delta\rho$ [-] |
|------------|------------|-----------|--------|-----------|---------------------|-------------------------------|------------------|
| Sandy loam | 1 | 0.5 | 01.12 | 4.75 | $H_2= 10, H_3= 9.0$ | $\rho_1 = 1.51, \rho_2= 1.68$ | 0.17 |
| | 2 | 0.5 | 04.68 | 4.75 | $H_2= 10, H_3= 8.1$ | $\rho_1 = 1.51, \rho_2= 1.87$ | 0.35 |
| | 3 | 0.5 | 08.77 | 4.75 | $H_2= 10, H_3= 7.5$ | $\rho_1 = 1.51, \rho_2= 2.02$ | 0.50 |
| | 4 | 0.5 | 12.00 | 4.75 | $H_2= 10, H_3= 7.1$ | $\rho_1 = 1.51, \rho_2= 2.13$ | 0.62 |
| | 5 | 0.5 | 15.04 | 4.75 | $H_2= 10, H_3= 6.9$ | $\rho_1 = 1.51, \rho_2= 2.19$ | 0.68 |
| | 6 | 0.5 | 17.84 | 5.57 | $H_2= 10, H_3= 8.3$ | $\rho_1 = 1.77, \rho_2= 2.14$ | 0.36 |
| Silty loam | 1 | 0.5 | 05.70 | 3.71 | $H_2= 10, H_3= 7.5$ | $\rho_1 = 1.18, \rho_2= 1.57$ | 0.39 |
| | 2 | 0.5 | 07.91 | 3.71 | $H_2= 10, H_3= 7.3$ | $\rho_1 = 1.18, \rho_2= 1.62$ | 0.44 |
| | 3 | 0.5 | 11.30 | 3.71 | $H_2= 10, H_3= 6.8$ | $\rho_1 = 1.18, \rho_2= 1.74$ | 0.56 |

MATERIALS AND METHODS

| | | | | | | | |
|------------|---|-----|-------|------|---------------------|-------------------------------|------|
| | 4 | 0.5 | 14.49 | 3.71 | $H_2= 10, H_3= 6.2$ | $\rho_1 = 1.18, \rho_2= 1.90$ | 0.72 |
| | 5 | 0.5 | 17.56 | 3.71 | $H_2= 10, H_3= 5.7$ | $\rho_1 = 1.18, \rho_2= 2.07$ | 0.89 |
| | 6 | 0.5 | 21.58 | 3.71 | $H_2= 10, H_3= 5.5$ | $\rho_1 = 1.18, \rho_2= 2.15$ | 0.97 |
| Clay | 1 | 0.5 | 10.23 | 3.56 | $H_2= 10, H_3= 7.1$ | $\rho_1 = 1.13, \rho_2= 1.60$ | 0.46 |
| | 2 | 0.5 | 14.40 | 3.56 | $H_2= 10, H_3= 6.4$ | $\rho_1 = 1.13, \rho_2= 1.77$ | 0.64 |
| | 3 | 0.5 | 17.00 | 3.56 | $H_2= 10, H_3= 5.8$ | $\rho_1 = 1.13, \rho_2= 1.95$ | 0.82 |
| | 4 | 0.5 | 21.58 | 3.56 | $H_2= 10, H_3= 5.6$ | $\rho_1 = 1.13, \rho_2= 2.02$ | 0.89 |
| | 5 | 0.5 | 24.19 | 3.56 | $H_2= 10, H_3= 5.4$ | $\rho_1 = 1.13, \rho_2= 2.10$ | 0.97 |
| | 6 | 0.5 | 26.73 | 3.56 | $H_2= 10, H_3= 5.5$ | $\rho_1 = 1.13, \rho_2= 2.08$ | 0.93 |
| Sand | 1 | 0.5 | 01.09 | 4.71 | $H_2= 10, H_3= 8.9$ | $\rho_1 = 1.50, \rho_2= 1.68$ | 0.19 |
| | 2 | 0.5 | 03.90 | 4.71 | $H_2= 10, H_3= 8.8$ | $\rho_1 = 1.50, \rho_2= 1.70$ | 0.20 |
| | 3 | 0.5 | 06.74 | 4.71 | $H_2= 10, H_3= 8.5$ | $\rho_1 = 1.50, \rho_2= 1.76$ | 0.26 |
| | 4 | 0.5 | 09.37 | 4.71 | $H_2= 10, H_3= 8.3$ | $\rho_1 = 1.50, \rho_2= 1.81$ | 0.31 |
| | 5 | 0.5 | 12.19 | 4.71 | $H_2= 10, H_3= 7.7$ | $\rho_1 = 1.50, \rho_2= 1.95$ | 0.45 |
| | 6 | 0.5 | 15.08 | 4.71 | $H_2= 10, H_3= 7.5$ | $\rho_1 = 1.50, \rho_2= 2.00$ | 0.50 |
| Silty clay | 1 | 0.5 | 04.02 | 3.00 | $H_2= 10, H_3= 7.6$ | $\rho_1 = 0.95, \rho_2= 1.26$ | 0.30 |
| | 2 | 0.5 | 10.69 | 3.00 | $H_2= 10, H_3= 6.4$ | $\rho_1 = 0.95, \rho_2= 1.49$ | 0.54 |
| | 3 | 0.5 | 14.84 | 3.00 | $H_2= 10, H_3= 5.8$ | $\rho_1= 0.95, \rho_2= 1.65$ | 0.69 |
| | 4 | 0.5 | 17.83 | 3.00 | $H_2= 10, H_3= 5.1$ | $\rho_1 = 0.95, \rho_2= 1.87$ | 0.92 |
| | 5 | 0.5 | 23.30 | 3.00 | $H_2= 10, H_3= 4.8$ | $\rho_1 = 0.95, \rho_2= 1.99$ | 1.03 |
| | 6 | 0.5 | 26.22 | 3.00 | $H_2= 10, H_3= 4.6$ | $\rho_1 = 0.95, \rho_2= 2.08$ | 1.12 |
| Clay loam | 1 | 0.5 | 04.58 | 3.14 | $H_2= 10, H_3= 7.5$ | $\rho_1 = 1.00, \rho_2= 1.33$ | 0.33 |
| | 2 | 0.5 | 08.25 | 3.14 | $H_2= 10, H_3= 6.4$ | $\rho_1 = 1.00, \rho_2= 1.56$ | 0.56 |
| | 3 | 0.5 | 12.48 | 3.14 | $H_2= 10, H_3= 5.5$ | $\rho_1 = 1.00, \rho_2= 1.82$ | 0.82 |
| | 4 | 0.5 | 16.11 | 3.14 | $H_2= 10, H_3= 4.8$ | $\rho_1 = 1.00, \rho_2= 2.08$ | 1.08 |
| | 5 | 0.5 | 20.58 | 3.14 | $H_2= 10, H_3= 4.7$ | $\rho_1 = 1.00, \rho_2= 2.13$ | 1.13 |
| | 6 | 0.5 | 22.98 | 3.14 | $H_2= 10, H_3= 4.6$ | $\rho_1 = 1.00, \rho_2= 2.17$ | 1.17 |
| Loam | 1 | 0.5 | 02.04 | 3.61 | $H_2= 10, H_3= 8.0$ | $\rho_1 = 1.15, \rho_2= 1.44$ | 0.29 |
| | 2 | 0.5 | 06.87 | 3.61 | $H_2= 10, H_3= 6.6$ | $\rho_1 = 1.15, \rho_2= 1.74$ | 0.59 |
| | 3 | 0.5 | 11.18 | 3.61 | $H_2= 10, H_3= 5.9$ | $\rho_1 = 1.15, \rho_2= 1.95$ | 0.80 |
| | 4 | 0.5 | 13.93 | 3.61 | $H_2= 10, H_3= 5.3$ | $\rho_1 = 1.15, \rho_2= 2.17$ | 1.02 |
| | 5 | 0.5 | 16.71 | 3.61 | $H_2= 10, H_3= 4.9$ | $\rho_1 = 1.15, \rho_2= 2.35$ | 1.20 |
| | 6 | 0.5 | 20.78 | 3.61 | $H_2= 10, H_3= 4.8$ | $\rho_1 = 1.15, \rho_2= 2.39$ | 1.24 |
| Loamy sand | 1 | 0.5 | 01.25 | 4.21 | $H_2= 10, H_3= 7.9$ | $\rho_1 = 1.34, \rho_2= 1.70$ | 0.36 |
| | 2 | 0.5 | 06.19 | 4.21 | $H_2= 10, H_3= 7.0$ | $\rho_1 = 1.34, \rho_2= 1.91$ | 0.57 |
| | 3 | 0.5 | 08.21 | 4.21 | $H_2= 10, H_3= 6.7$ | $\rho_1 = 1.34, \rho_2= 2.00$ | 0.66 |
| | 4 | 0.5 | 11.57 | 4.21 | $H_2= 10, H_3= 6.4$ | $\rho_1 = 1.34, \rho_2= 2.09$ | 0.75 |
| | 5 | 0.5 | 14.30 | 4.21 | $H_2= 10, H_3= 6.1$ | $\rho_1 = 1.34, \rho_2= 2.20$ | 0.86 |
| | 6 | 0.5 | 16.42 | 4.21 | $H_2= 10, H_3= 5.3$ | $\rho_1 = 1.34, \rho_2= 2.53$ | 1.19 |

3.3.2 *Determining the moisture content of the soil*

The Moisture Analyzer (HE53 230 V) was used to measure the soil's moisture content. It works based on the principle of drying. An amount of soil is placed on the tray inside the moisture analyzer and the heating plates inside the moisture analyzer start to dry the sample till reaching unchangeable soil mass (dry mass).

The analyzer calculates the moisture percentage by subtracting the remaining mass from the initial mass and the answer is divided by the initial mass (the moisture content obtained is the wet-based result). The moisture analyzer is shown in Figures 3.3a, and 3.3b.

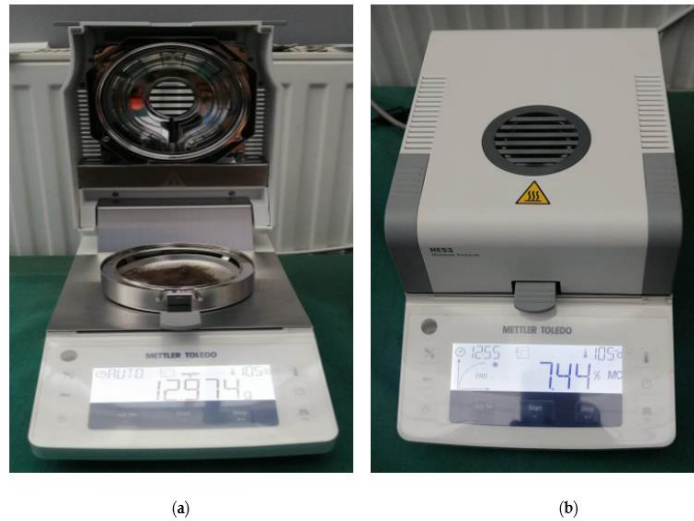


Figure 3.3. Shows the moisture analyzer (HE53 230 V), (a) the analyzer shows the mass of the sample, and (b) the analyzer shows the percentage of moisture content.

Table 3.2. Specifications of the (HE53 230V) moisture analyzer (Ahmed et al., 2022; Ahmed and Kiss, 2022).

| Specification | Moisture Analyzer (HE53 230V) |
|----------------------------|--|
| Measurement Range | Recommended for moisture content $\geq 1\%$ MC |
| Readability | 0.01% MC (1 mg) |
| Repeatability (2g sample) | $\pm 0.15\%$ |
| Repeatability (10g sample) | $\pm 0.05\%$ |
| Drying Temperature Range | 50°C – 160°C (adjustable in 1°C increments) |

3.3.3 *Spectral behaviour measurements (colour test)*

The Spectrophotometer CM-700d (see Figures 3.4a,3.4b) was used to measure the soil's colour (soil spectral behaviour). The colour of the soils was taken by the Spectrophotometer at each moisture content before the bevameter test.

The spectrophotometer sends electromagnetic waves in the visible range (400 – 700 nm; light visible band), and the colour of the soil will be determined based on the reflected wavelength (spectral reflectance %). Three records were taken by the spectrophotometer for the soil at each moisture content, and the averaging of these records was considered as the result.

The CM-700d spectrophotometer ensures high measurement accuracy, with a repeatability of $\Delta E^*_{ab} \leq 0.1$ and an inter-instrument agreement of $\Delta E^*_{ab} \leq 0.2$, based on British Ceramic Research

Association (BCRA) tile comparisons (Konica Minolta, 2024). The device utilizes a pulsed xenon lamp to minimize external light interference; however, strong ambient lighting should be avoided to ensure measurement consistency. Its integrating sphere reduces external influences, but controlled lighting conditions are recommended for optimal accuracy in spectral analyses (Konica Minolta, 2024).

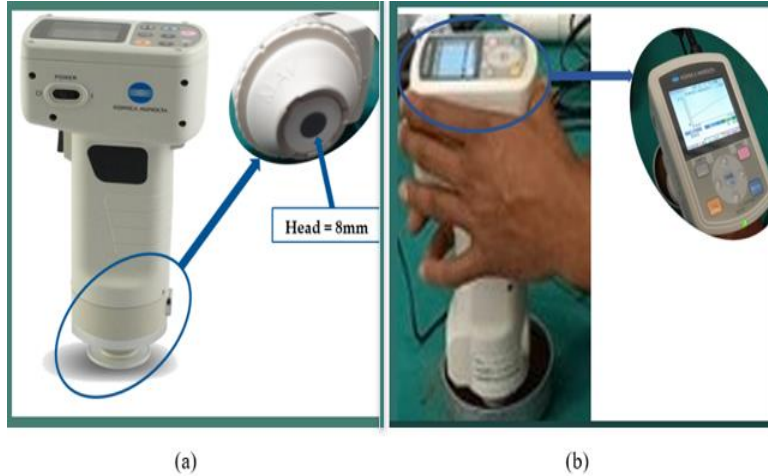


Figure 3.4. Shows (a) the Spectrophotometer (CM-700d) and the 8mm head (the electromagnetic waves pass through), and (b) the Spectrophotometer (CM-700d) while measuring and recording the data.

3.3.4 Cone penetrometer technique with colour measurement (field measurements)

Using a Cone penetrometer (06.02 Penetrograph) from Eijkelkamp company as shown in Figure 3.5 at the field to record the data (penetration resistance) on a chart as in Figure 3.6 to show the relation between the penetration resistance (MPa) and the depth (cm).

The soil, characterized as sandy loam from the campus area, underwent vegetation removal followed by a resting period of one to two days. Subsequently, soil penetration resistance and colour were measured over various days under differing moisture conditions. Before utilizing the cone penetrometer for penetration resistance measurements, spectral reflectance measurements, as outlined in Section 3.3.3, were taken to assess soil colour.



Figure 3.5. Cone penetrometer (06.02 Penetrograph) while the measurement.

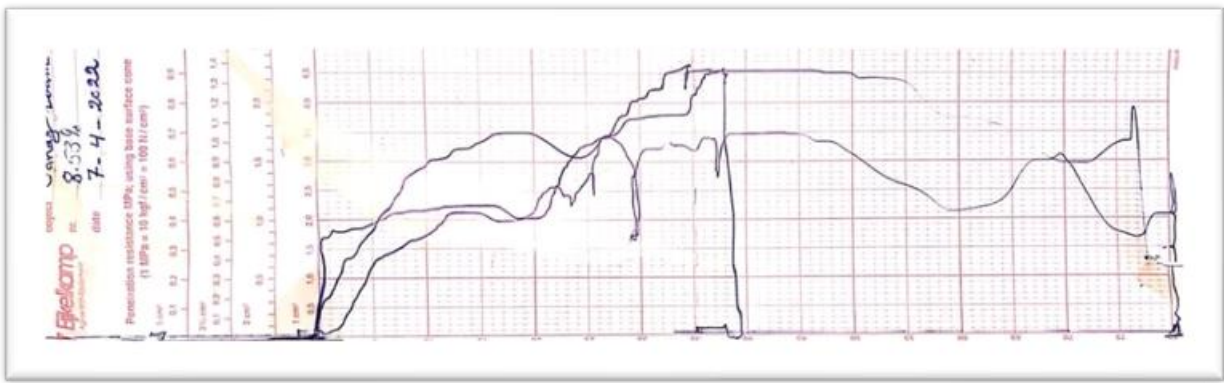


Figure 3.6. Soil resistance data recorded by penetrometer (penetration resistance (MPa) and depth (cm)).

3.4 Extra measurement

2.4.1 Soil reflectance at zero moisture content (close to zero)

The eight soil types were dried in the oven for 24 hours at 105 °C, followed by measurement of their spectral reflectance as in section (3.3.3).

2.4.2 The effect of the plate size on the sinkage

Using the bevameter test procedure (section 3.3.1) but only changing the plate size (using plate sizes 20 and 15 cm) to identify the effect of the plate size on only two soil textures (sandy loam and sand).

2.4.3 The effect of the load speed on the sinkage

Using the bevameter test procedure (section 3.3.1) but only changing the load speed by adjusting the speed through the valve, the soil used was sandy loam soil.

4. RESULTS

This chapter presents the results obtained from the experimentations and the discussions highlighting the new scientific findings. These include calculating soil density after and before compression and then calculating the relative density ratio ($\Delta\rho$). Moreover, analyzing the pressure-sinkage relationship by considering ($H/D = 0.5$) for all soil types and relating both the relative sinkage (z/D) and the relative density ratio ($\Delta\rho$) to the moisture content. In the meantime, measuring the spectral reflectance of the soil and defining its relationship with the moisture content. A bigger plate, due to its more equalizing ability, gives always more reliable results and, therefore, the results for a 20 cm plate diameter are taken as more definitive.

4.1 Bevameter results (pressure-sinkage relationship)

The pressure-sinkage curves (Figures 4.1 – 4.3) of the three soils resulting from the bevameter test were read through the CATMAN 4.5 software (see Table 3.1). The figures elucidate the correlation between applied pressure and relative sinkage in soils of initial specific densities, revealing that as moisture content escalates, relative sinkage correspondingly increases until the soil's load-bearing capacity is compromised. This phenomenon is exemplified in Figure 4.1 for sandy loam at 17.84% moisture content, and Figure 4.3 for clay at 26.73%, These observations align with established understandings that elevated moisture levels diminish soil strength, thereby reducing its capacity to support applied loads. The remaining results for the other five soil textures are presented in Appendix A3.

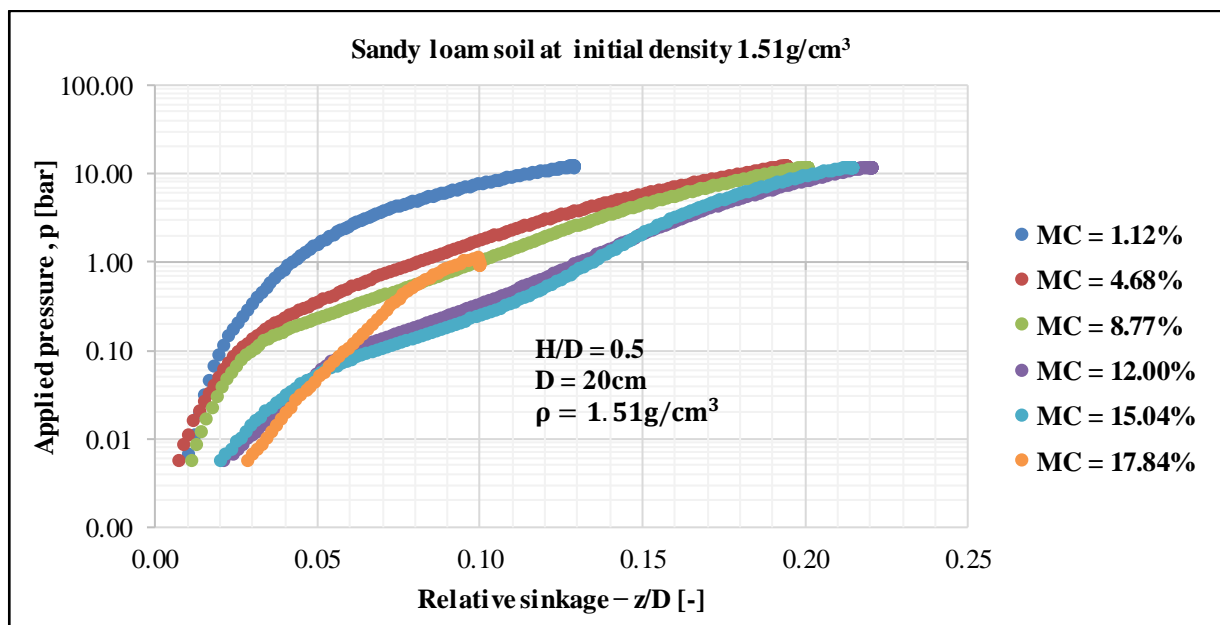


Figure 4.1. Sandy loam soil texture pressure – sinkage relationship at different moisture contents for 1.51 g/cm³ density.

RESULTS

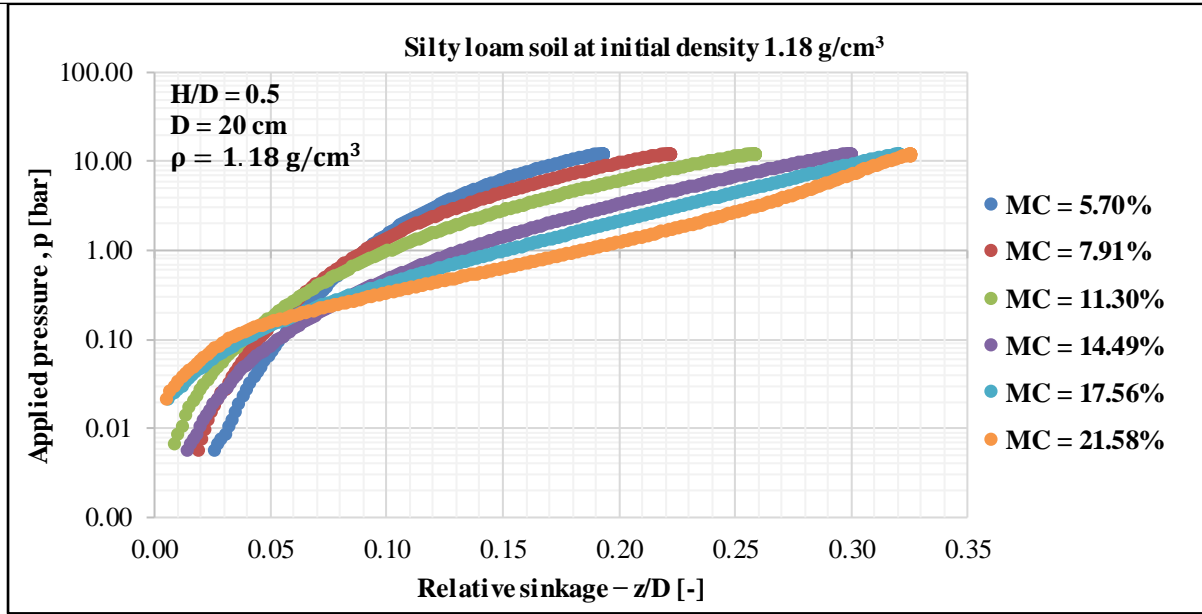


Figure 4.2. Silty loam soil texture pressure – sinkage relationship at different moisture contents for 1.18 g/cm³ density.

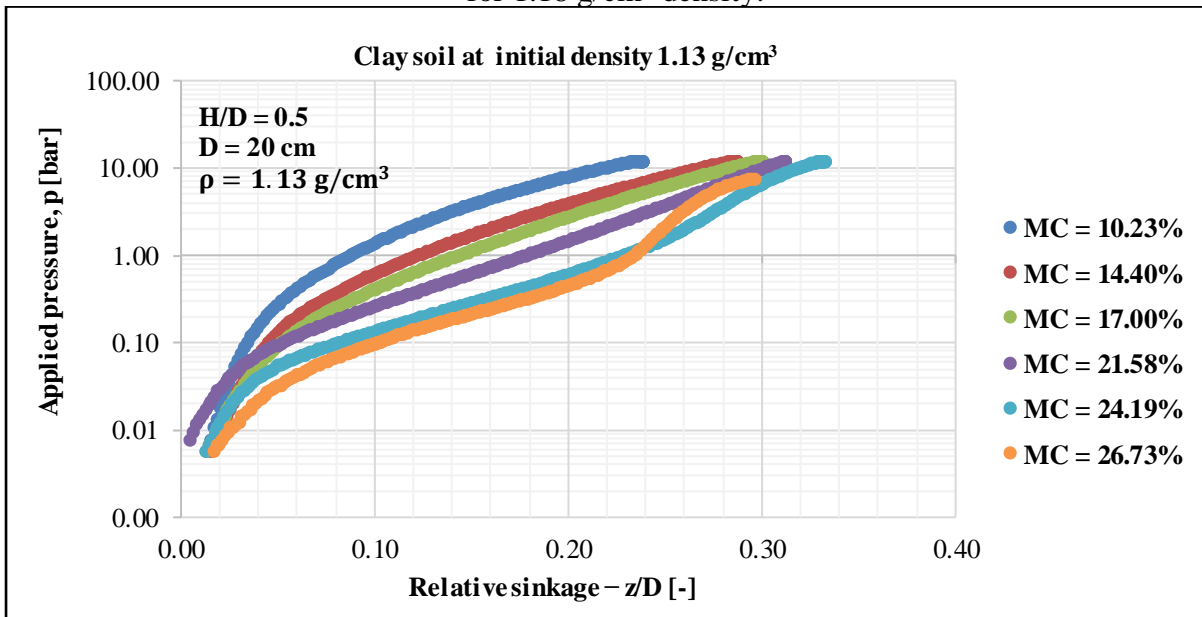


Figure 4.3. Clay soil texture pressure – sinkage relationship at different moisture contents for 1.13 g/cm³ density.

For every moisture content level, the relative sinkage (expressed as the ratio z/D) escalates with the increase in applied pressure (the force divided by the plate's area). The pressure-sinkage relationship observed at each water content is consistent with the pressure-sinkage equation proposed by Saakyan (1965), which is derived from the elastic half-space Boussinesq theory (referenced as Equation 2). (Salman et al, 2022; Saakyan, 1965; Salman et al, 2021; Sitkei, 2015; Bernstein, 1913).

$$p = k \left(\frac{z}{D} \right)^n \quad (4.1)$$

Where:

p : the applied pressure,

D : the diameter of the plate,

Z : the soil vertical deformation (sinkage),

k : the sinkage modulus.

n : exponent characterizes soil's deformation behaviour.

Equation 4.1 shows that the sinkage is directly proportional to the pressure applied, as is evident in the resulting curves.

Under a constant applied pressure, the relative sinkage is observed to increase with an increase in water level at varying moisture levels. The pressure-sinkage relationship traces a similar hyperbolic path across different moisture levels. At the peak applied pressure, approximately 12 bar, the greatest sinkage occurs at the highest moisture content, indicating that the relative sinkage escalates with moisture increase at a set pressure.

4.2 The impact of moisture content

Soil moisture content significantly influences the physical and mechanical properties of soils, affecting their compressibility, density, and load-bearing capacity. This section examines the impact of varying moisture levels on soil density and relative sinkage under the same applied pressures.

4.2.1 On the soil density

The density of moist soil increases after compaction under a consistent load. As moisture content rises, the soil becomes more compressible, resulting in reduced volume (higher sinkage after compaction at higher moisture). Consequently, the same mass over a diminishing volume leads to increased density.

Soil compressibility can be determined by plotting the relative density ratio versus moisture content for the three soil textures (see Figures 4.5 – 4.07), the remaining results for the other five soil textures are presented in Appendix A4. The density ratio, denoted by $\Delta\rho$, is derived from Equation 4.2. As the moisture content rises, there is a corresponding increase in the relative density ratio.

$$\Delta\rho = \frac{\rho_2 - \rho_1}{\rho_1} \quad (4.2)$$

4.2.2 On the soil relative sinkage

For the eight soil textures, the effect of the applied pressure exerted by the plate on the relative sinkage (z/D) was evaluated for 1.0 bar, 1.5 bar, 2.0 bar, 5.0 bar, and 12.0 bar. The effect was significant; consequently, 1.0 bar (the tyre inflation pressure commonly utilized in agricultural applications) was selected for further analysis. Figure 4.4 illustrates this effect for sandy loam soil.

RESULTS

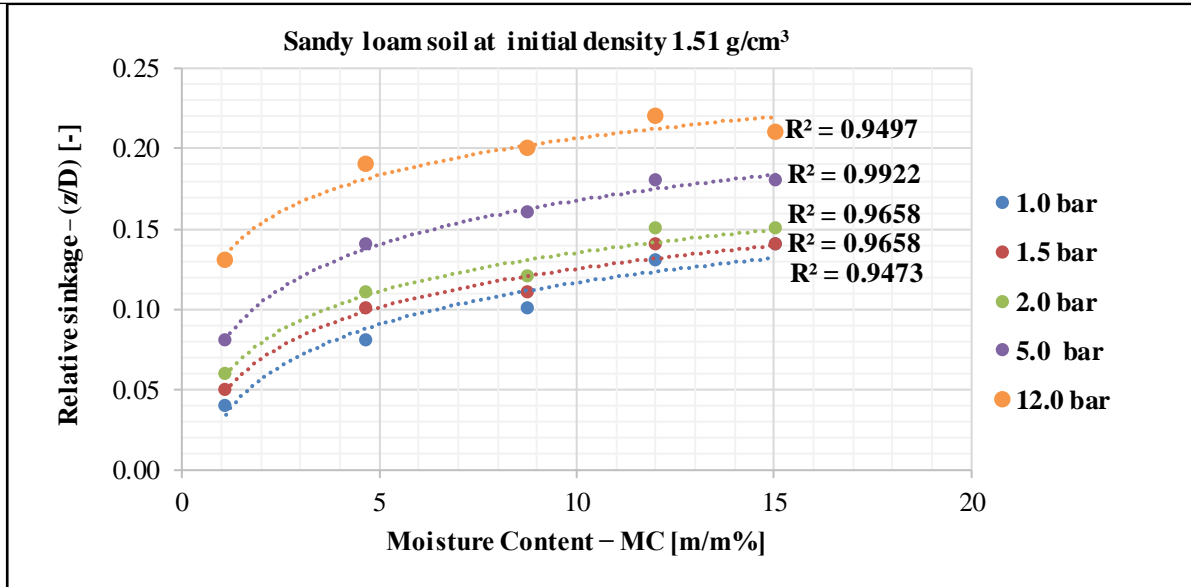


Figure 4.4. Illustrates the relative sinkage (z/D) for sandy loam soil as influenced by moisture content at varying pressures.

Figures 4.5 – 4.7 also show the relative sinkage (z/D) at applied pressure (1.0 bar) as a function of moisture content for the three clay soil textures mentioned

The results indicate that as moisture content increases, the sinkage rate also increases, demonstrating that elevated moisture levels generally lead to increased soil compaction under equivalent compressive loads. This aspect is critical in our research, as moisture significantly influences the bearing capacity of soil. The remaining results for the other five soil textures are presented in Appendix A4.

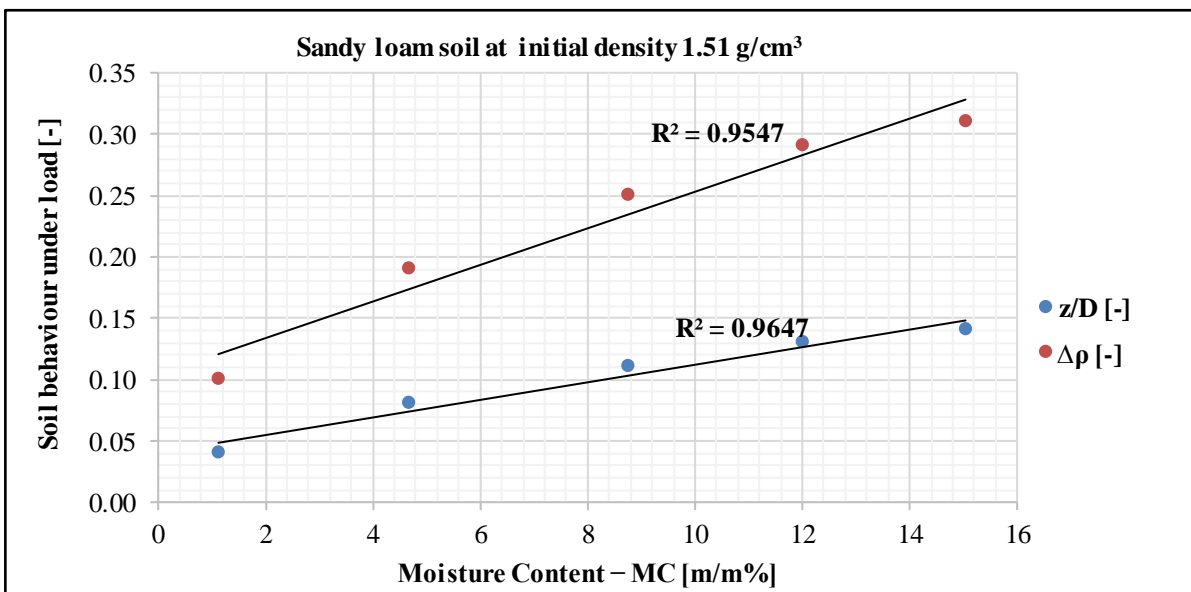


Figure 4.5. The relative sinkage and density ratio of sandy loam soil as a function of moisture content.

RESULTS

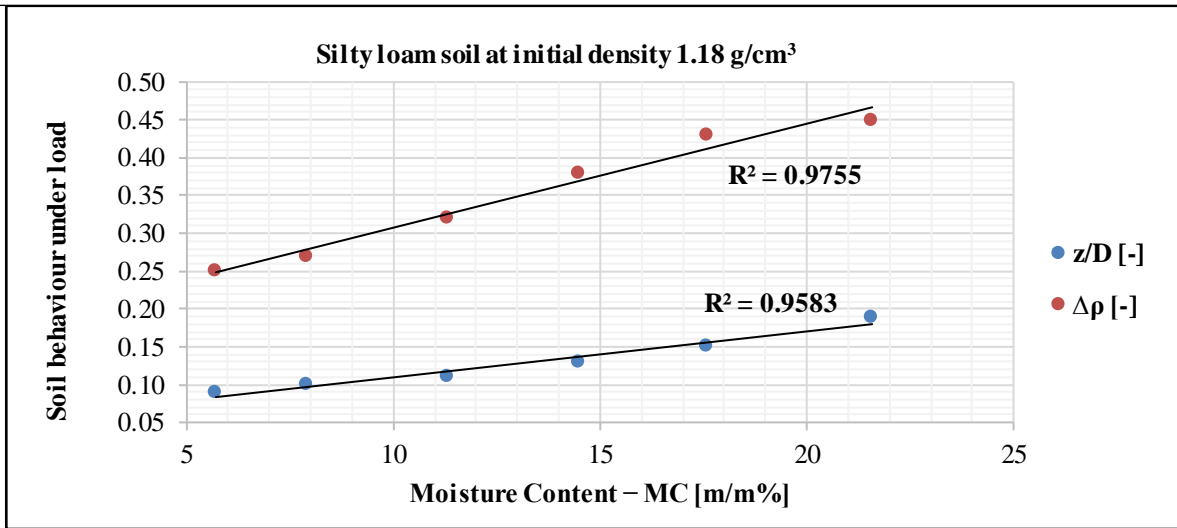


Figure 4.6. The relative sinkage and density ratio of silty loam soil as a function of moisture content.

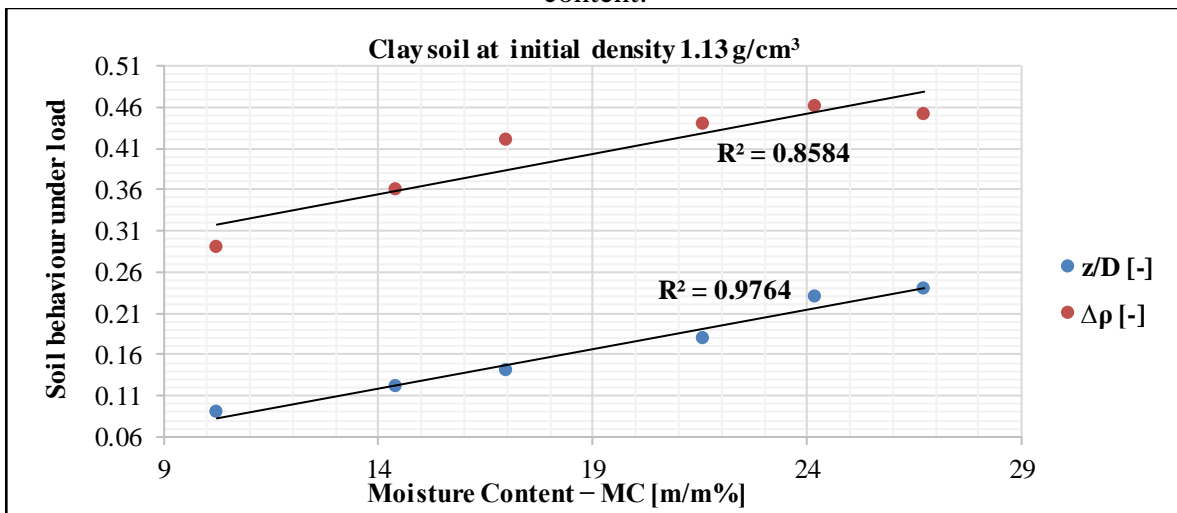


Figure 4.7. The relative sinkage and density ratio of clay soil as a function of moisture content.

4.3 Spectral behaviour (Spectrophotometer)

For the same eight soil samples mentioned (Table 4.2), the three soil spectral behaviour results were determined using the spectrophotometer as illustrated in Figures 4.8 – 4.10. The remaining results for the other five soil textures are presented in Appendix A5. The spectral reflectance of the soil at each light wavelength can be derived from the curves. The incident light wavelengths for measuring the colour of the soil at each moisture content are within the range of 400 – 700 nm. Beginning with the lowest moisture content, as the value of the incident wavelength increases, the reflected wavelength also increases. This relationship is observed for the soil at all tested moisture contents.

When comparing the soil colour behaviour at different moisture contents, the obtained results indicate that with an increase in moisture content at a fixed incident wavelength, the reflected wavelength decreases. At certain moisture content levels, the reflected wavelength begins to overlap at wavelengths (incident wavelengths) below 550 nm. This overlapping in the results demonstrates that with increasing moisture content, the reflected wavelength remains constant in the range of 400 – 550 nm, thus indicating that the determination of the reflected wavelength (soil colour) will depend on the range of 550-700 nm.

RESULTS

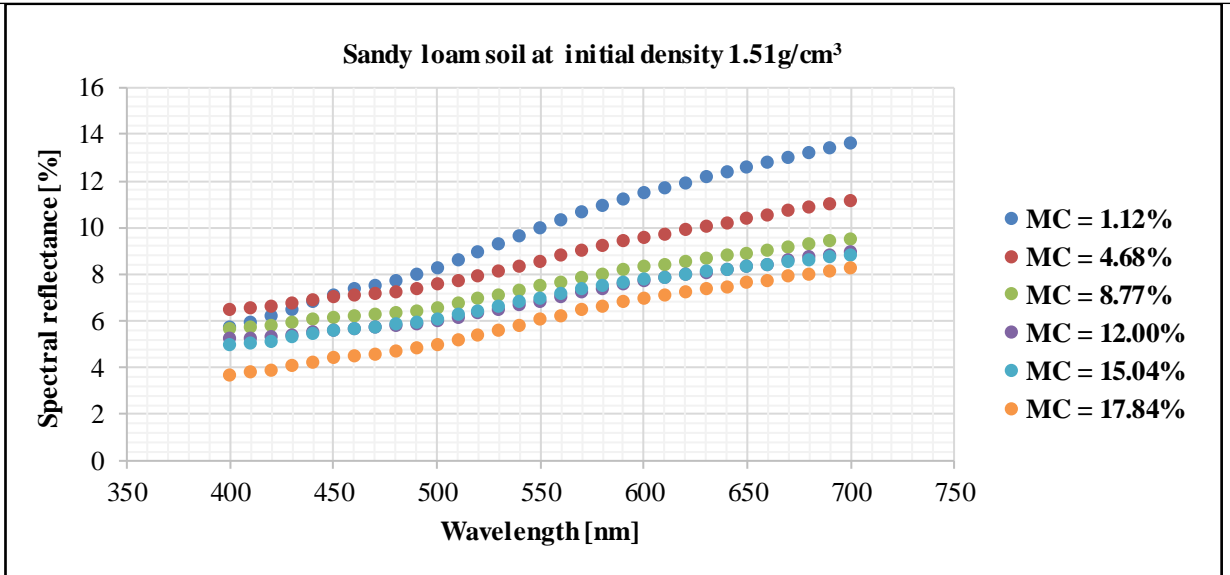


Figure 4.8. The spectral reflectance of sandy loam soil in the visible range at varying moisture content levels.

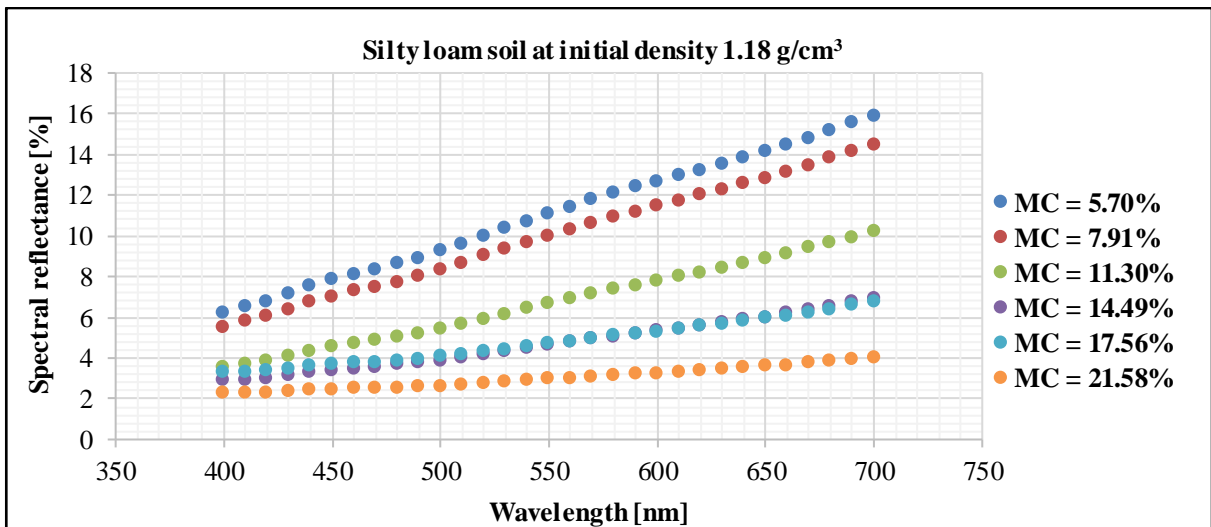


Figure 4.9. The spectral reflectance of silty loam soil in the visible range at varying moisture content levels.

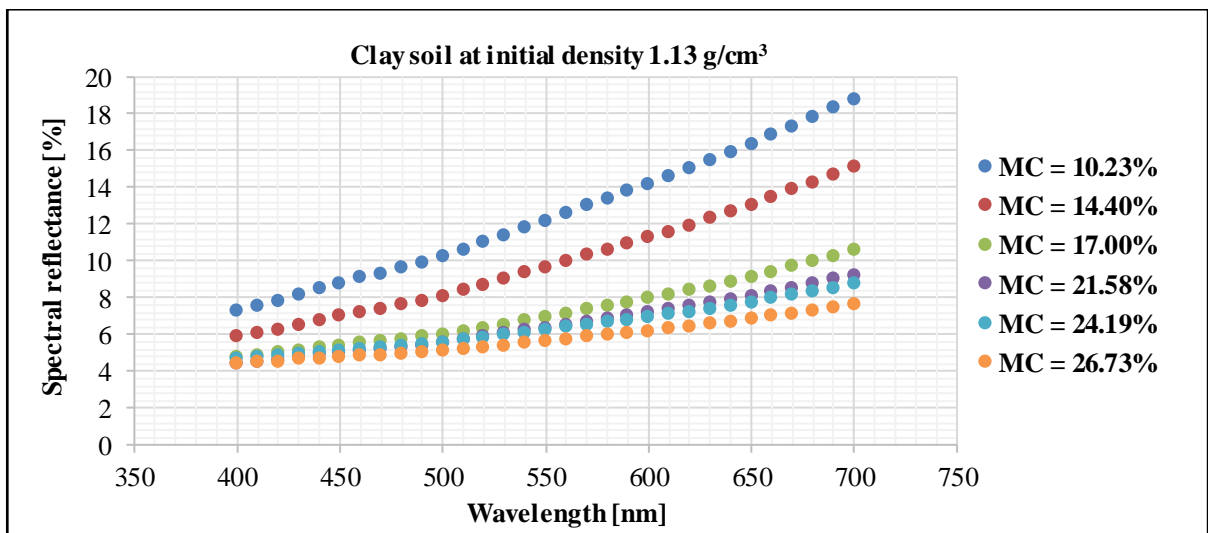


Figure 4.10. The spectral reflectance of clay soil in the visible range at varying moisture content levels

RESULTS

4.3.1 Spectral reflectance affected by moisture contents

To validate the findings presented in Figures 4.8 – 4.10, which demonstrate an inverse relationship between moisture content and soil reflectance, the reflection values were averaged across three spectral ranges: 400 – 500 nm, 400 – 700 nm, and 600-700 nm. Equations 4.3, 4.4, and 4.5 were employed to calculate the mean reflected wavelengths at varying moisture levels.

$$R_m^{4/5} = \frac{\sum_{400}^{500} R_i}{11} \quad (4.3)$$

$$R_m^{4/7} = \frac{\sum_{400}^{700} R_i}{31} \quad (4.4)$$

$$R_m^{6/7} = \frac{\sum_{600}^{700} R_i}{11} \quad (4.5)$$

Where:

R_i : The reflected wavelength at a specific spectrum of 400 – 700 nm.

$R_m^{4/5}$: The mean for wavelengths in the 400 – 500 nm range.

$R_m^{4/7}$: The mean for wavelengths in the 400 – 700 nm range.

$R_m^{6/7}$: The mean for wavelengths in the 600 – 700 nm range.

When comparing the Z (10°/D65) value, a spectrophotometer colour measuring tristimulus parameter (in the spectrophotometer system), the results indicate that with an increase in moisture, the Z parameter decreases, thus conforming to the reflectance behaviour of soil.

Furthermore, comparing the reflected wavelength at 700 nm at the maximum sent wavelength (spectrum, 700 nm), the results demonstrate a decrease in the reflected value (see Table 4.2) with an increase in moisture. Figures 4.11 – 4.13 illustrate the averaging (R_m ; Equations 4.3, 4.4, and 4.5), and the reflected wavelengths at 700 nm (Ref. at 700 nm) values serve as an indicator of moisture content for three soil textures. The remaining results for the other five soil textures are presented in Appendix A6.

Table 4.2 presents average results from measurements taken at 400 – 500 nm, 400 – 700 nm, and 600 – 700 nm, including tristimulus Z (10°/D65) values and reflectance at the peak of the visible spectrum (Ref at 700 nm). The data indicates a decrease in all measured values with increasing moisture content. This information is essential for understanding how soil moisture affects its spectral properties, which is useful for devising techniques to estimate soil moisture content using spectral data.

Table 4.2. This table shows the main spectral reflectance parameters.

| Soil texture | Sample no. | MC [%] | Z(10°/D65) | $R_m^{(4/5)}$ | $R_m^{(4/7)}$ | $R_m^{(6/7)}$ | Ref. at 700 nm |
|--------------|------------|--------|------------|---------------|---------------|---------------|----------------|
| Sandy loam | 1 | 01.12 | 07.60 | 06.98 | 09.81 | 12.54 | 13.58 |
| | 2 | 04.68 | 07.51 | 06.96 | 08.62 | 10.34 | 11.15 |
| | 3 | 08.77 | 06.55 | 06.07 | 07.47 | 08.88 | 09.49 |

RESULTS

| | | | | | | | |
|------------|---|-------|-------|-------|-------|-------|-------|
| | 4 | 12.00 | 05.96 | 05.53 | 06.89 | 08.30 | 08.94 |
| | 5 | 15.04 | 05.95 | 05.50 | 06.90 | 08.28 | 08.80 |
| | 6 | 17.84 | 04.67 | 04.30 | 05.96 | 07.59 | 08.23 |
| Silty loam | 1 | 05.70 | 08.47 | 07.78 | 11.02 | 14.23 | 15.92 |
| | 2 | 07.91 | 07.58 | 06.96 | 09.96 | 12.92 | 14.49 |
| | 3 | 11.30 | 04.90 | 04.51 | 06.72 | 08.96 | 10.24 |
| | 4 | 14.49 | 03.67 | 03.39 | 04.71 | 06.09 | 06.94 |
| | 5 | 17.56 | 03.97 | 03.68 | 04.80 | 06.00 | 06.79 |
| | 6 | 21.58 | 02.66 | 02.46 | 03.03 | 03.64 | 04.06 |
| Clay | 1 | 10.23 | 09.49 | 08.75 | 12.47 | 16.41 | 18.81 |
| | 2 | 14.40 | 07.57 | 06.99 | 09.94 | 13.12 | 15.16 |
| | 3 | 17.00 | 05.81 | 05.38 | 07.19 | 09.19 | 10.57 |
| | 4 | 21.58 | 05.41 | 05.00 | 06.52 | 08.15 | 09.20 |
| | 5 | 24.19 | 05.53 | 05.12 | 06.40 | 07.80 | 08.75 |
| | 6 | 26.73 | 05.14 | 04.77 | 05.77 | 06.87 | 07.62 |
| Sand | 1 | 01.09 | 08.67 | 07.97 | 12.26 | 16.64 | 18.97 |
| | 2 | 03.90 | 06.47 | 05.95 | 09.26 | 12.70 | 14.59 |
| | 3 | 06.74 | 05.90 | 05.43 | 08.32 | 11.32 | 12.94 |
| | 4 | 09.37 | 06.42 | 05.91 | 08.46 | 11.09 | 12.49 |
| | 5 | 12.19 | 06.08 | 05.59 | 08.21 | 10.92 | 12.39 |
| | 6 | 15.08 | 05.69 | 05.23 | 07.61 | 10.07 | 11.36 |
| Silty clay | 1 | 04.02 | 08.68 | 08.02 | 10.67 | 13.40 | 15.10 |
| | 2 | 10.69 | 07.96 | 07.36 | 09.76 | 12.24 | 13.80 |
| | 3 | 14.84 | 06.18 | 05.71 | 07.79 | 10.00 | 11.49 |
| | 4 | 17.83 | 04.93 | 04.57 | 06.05 | 07.68 | 08.88 |
| | 5 | 23.30 | 04.84 | 04.49 | 05.52 | 06.66 | 07.52 |
| | 6 | 26.22 | 04.16 | 03.87 | 04.76 | 05.79 | 06.63 |
| Clay loam | 1 | 04.58 | 06.44 | 05.92 | 08.93 | 12.05 | 13.66 |
| | 2 | 08.25 | 05.88 | 05.40 | 08.24 | 11.21 | 12.99 |
| | 3 | 12.48 | 05.42 | 04.99 | 07.87 | 10.96 | 12.80 |
| | 4 | 16.11 | 04.86 | 04.49 | 06.76 | 09.23 | 10.74 |
| | 5 | 20.58 | 04.65 | 04.29 | 05.93 | 07.69 | 08.69 |
| | 6 | 22.98 | 04.22 | 03.89 | 05.54 | 07.32 | 08.38 |
| Loam | 1 | 02.04 | 14.83 | 12.77 | 19.91 | 26.68 | 28.48 |
| | 2 | 06.87 | 13.96 | 13.59 | 20.39 | 26.78 | 28.33 |
| | 3 | 11.18 | 11.17 | 10.22 | 17.06 | 23.69 | 25.63 |
| | 4 | 13.93 | 08.47 | 07.72 | 13.20 | 18.35 | 19.43 |
| | 5 | 16.71 | 08.52 | 07.77 | 12.94 | 17.81 | 18.83 |
| | 6 | 20.78 | 07.47 | 06.86 | 11.39 | 15.84 | 17.11 |
| Loamy sand | 1 | 01.25 | 06.96 | 06.42 | 09.88 | 13.54 | 15.47 |
| | 2 | 06.19 | 04.98 | 04.62 | 07.34 | 10.41 | 12.27 |
| | 3 | 08.21 | 04.43 | 04.10 | 05.89 | 07.89 | 09.12 |

RESULTS

| | | | | | | | |
|--|---|-------|-------|-------|-------|-------|-------|
| | 4 | 11.57 | 05.24 | 04.85 | 06.35 | 08.00 | 08.94 |
| | 5 | 14.30 | 05.97 | 05.51 | 06.96 | 08.48 | 09.23 |
| | 6 | 16.42 | 04.93 | 04.54 | 06.35 | 08.27 | 09.25 |

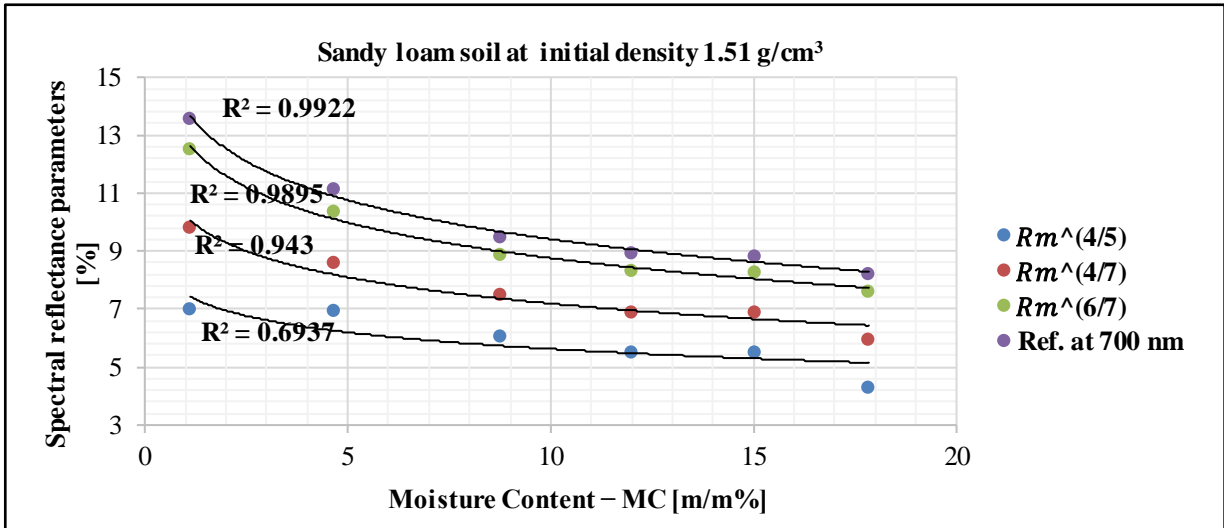


Figure 4.11. Spectral reflectance parameter – moisture content relationship for sandy loam.

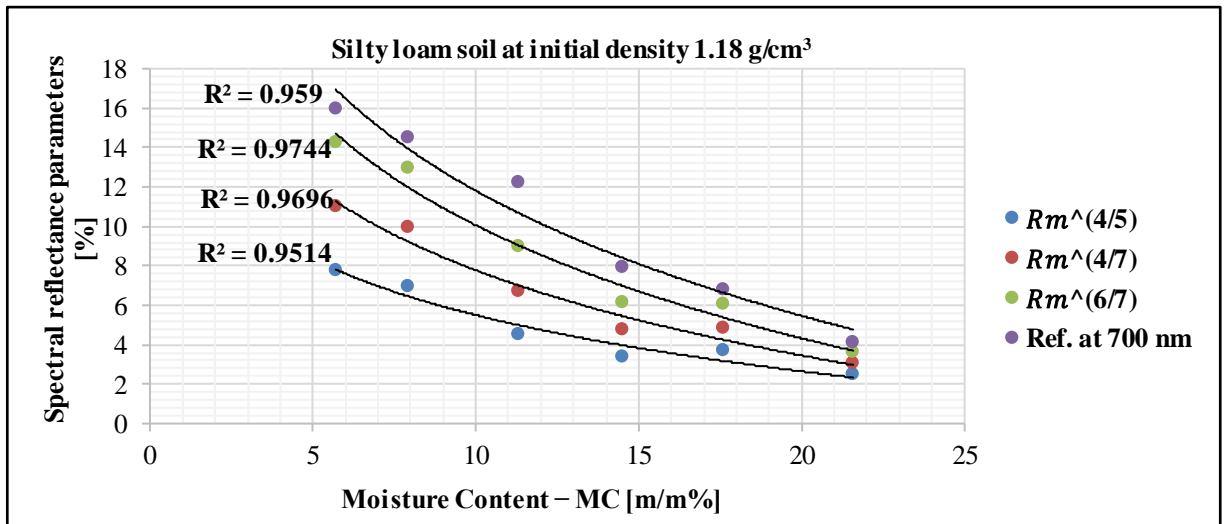


Figure 4.12. Spectral reflectance parameter – moisture content relationship for silty loam.

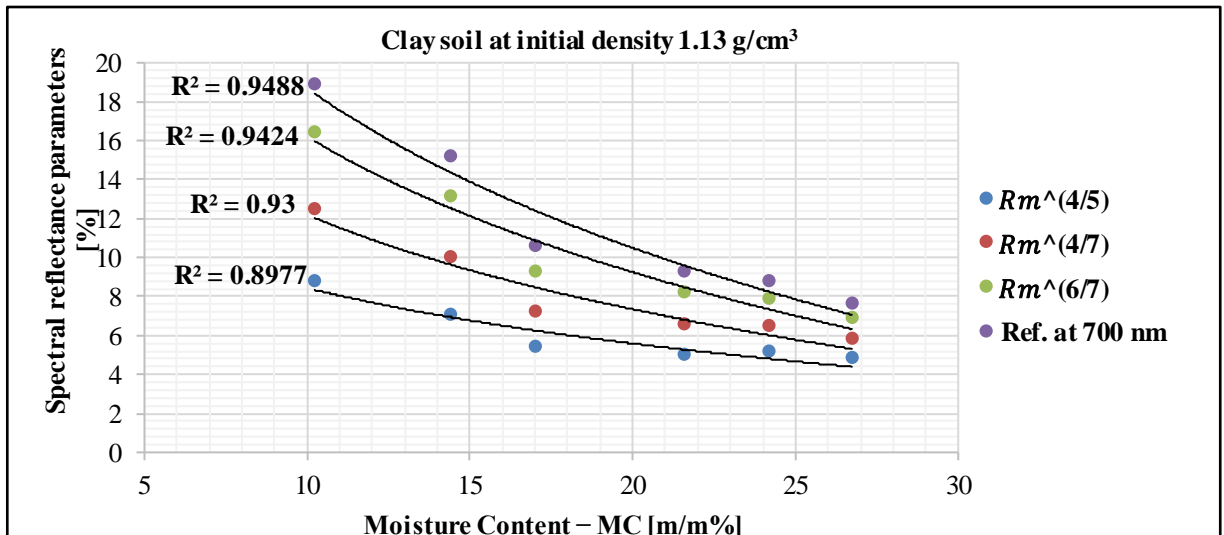


Figure 4.13. Spectral reflectance parameter – moisture content relationship for clay.

RESULTS

Based on the analysis of Table 4.2, the three soil textures in Figures 4.11 – 4.13 and five soil textures as in Appendix A6, it can be concluded that the reflectance at 700 nm exhibits greater sensitivity to moisture content and warrants consideration when evaluating spectral reflectance.

4.4 Soil properties underload and the spectral reflectance at 700 nm

4.4.1 Relative density ratio – spectral reflectance at 700 nm relationship

Based on the results (see Figures 4.14 – 4.16, and appendix A7) the relationship between the reflectance at 700 nm and the soil density ratio demonstrates that an increase in reflectance corresponds to a decrease in the soil density ratio. Consequently, this correlation indicates a reduction in sinkage (signifying high load-bearing capacity) and vice versa.

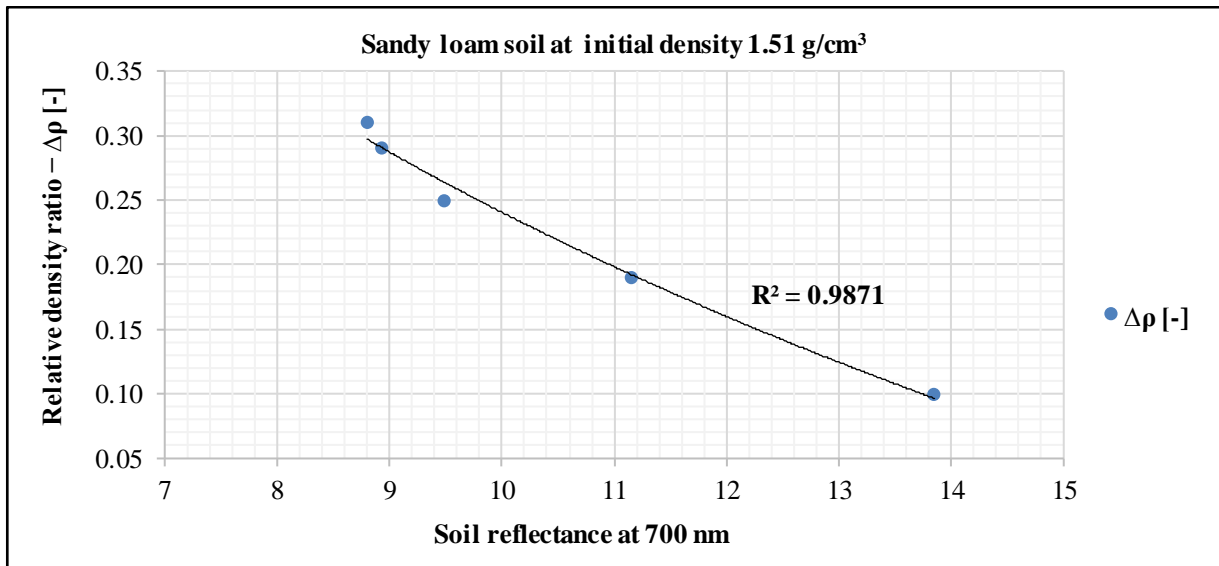


Figure 4.14. Soil relative density ratio – Spectral reflectance at 700 nm relationship for sandy loam.

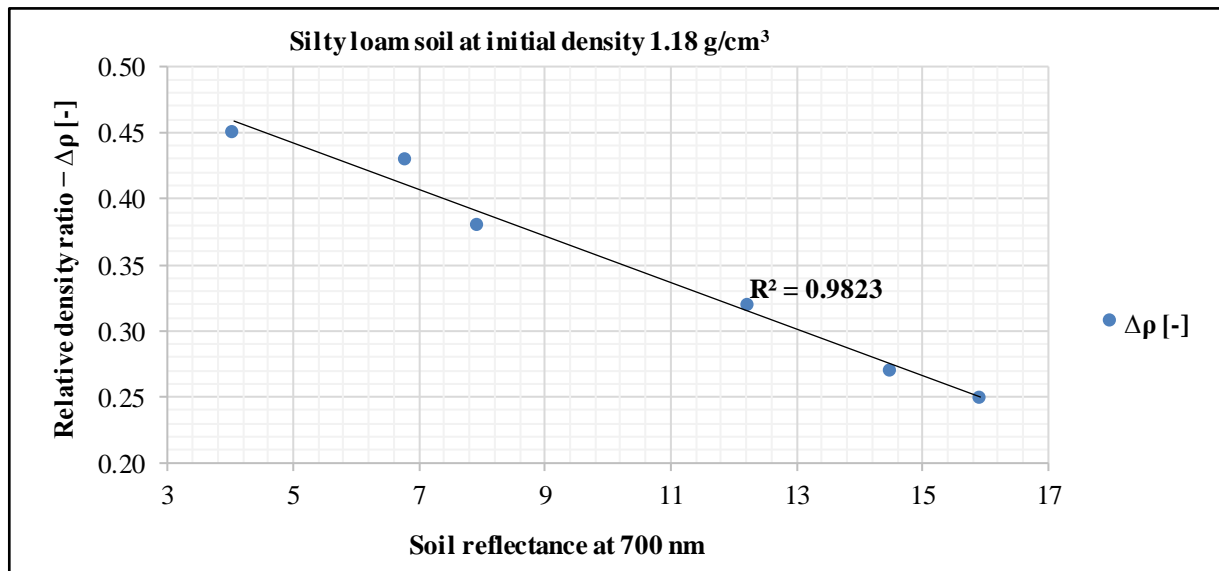


Figure 4.15. Soil relative density ratio – Spectral reflectance at 700 nm relationship for silty loam.

RESULTS

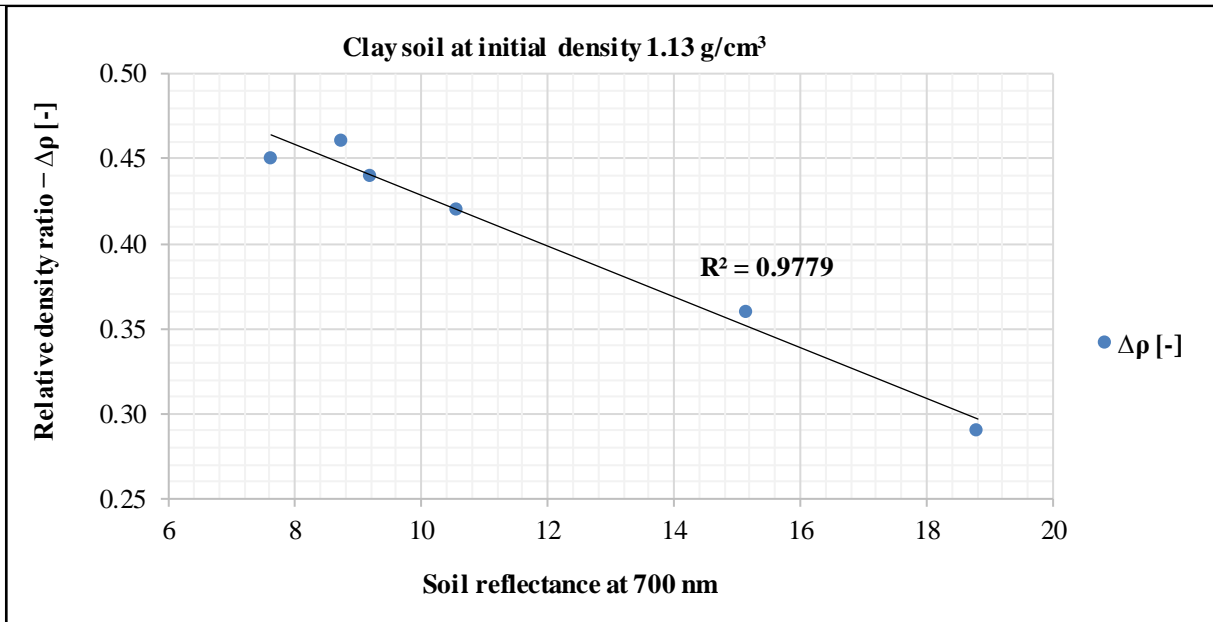


Figure 4.16. Soil relative density ratio – Spectral reflectance at 700 nm relationship for clay.

4.4.2 Relative sinkage – spectral reflectance at 700 nm relationship

The relationship between the reflectance at 700 nm and the relative sinkage, as illustrated in Figures 4.18 – 4.20, and appendix A8 demonstrates that an increase in reflectance corresponds to a decrease in the soil's relative sinkage. Consequently, this indicates a reduction in sinkage (signifying the high load-bearing capacity) and vice versa.

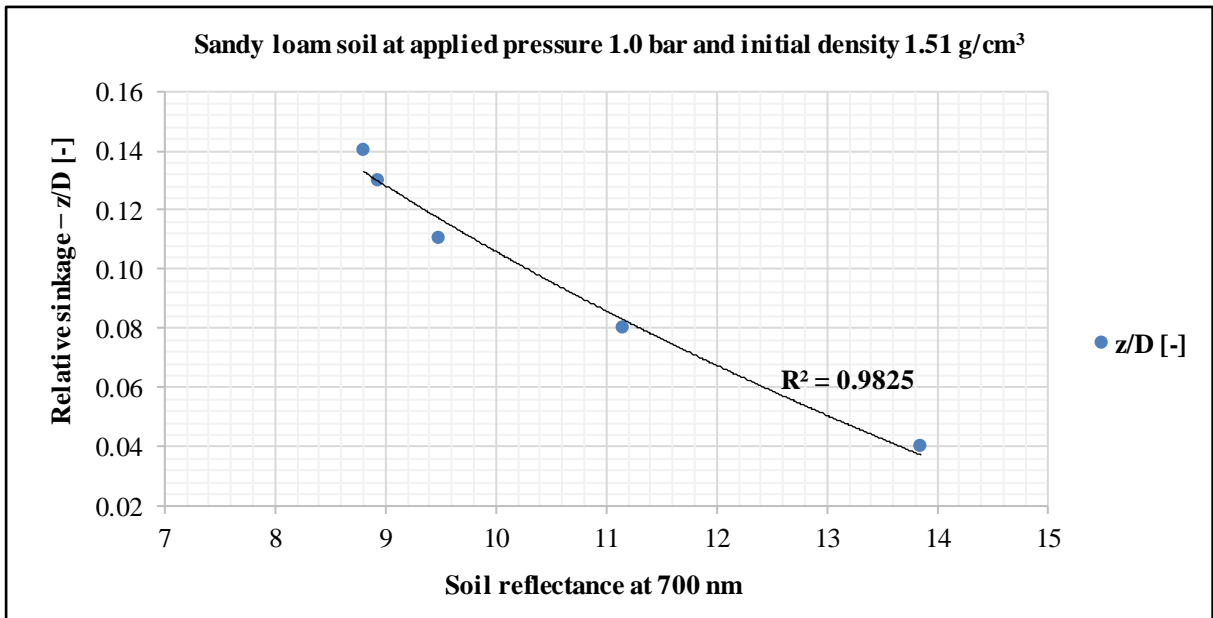


Figure 4.17. Soil relative sinkage – Spectral reflectance at 700 nm relationship for sandy loam.

RESULTS

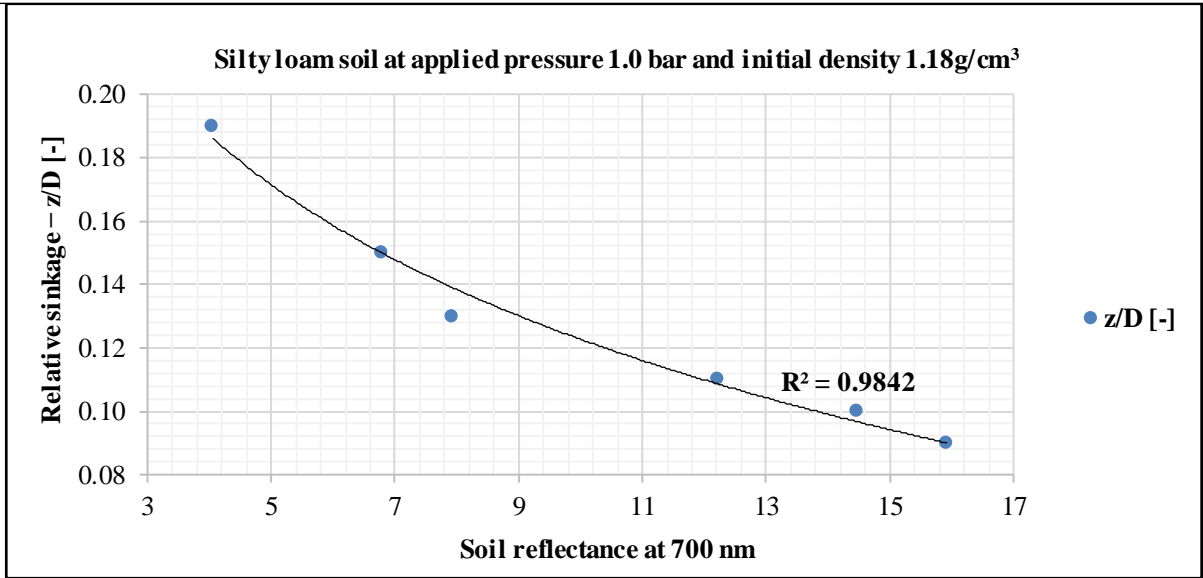


Figure 4.18. Soil relative sinkage – Spectral reflectance at 700 nm relationship for silty loam.

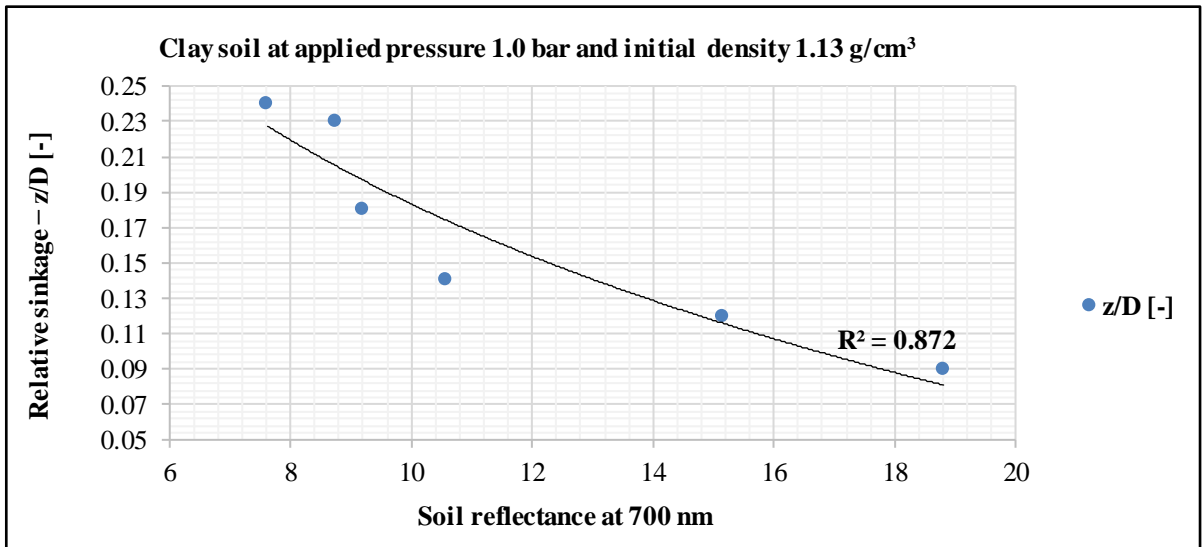


Figure 4.19. Soil relative sinkage – Spectral reflectance at 700 nm relationship for clay.

4.5 Estimation of soil-specific constants and moisture content calculations

The soil samples were oven-dried at 105°C for 24 hours to achieve a near-zero moisture content. The objective of this analysis was to determine the values of the constants \hat{A} and \hat{n} for each soil type, as outlined in Table 4.3. These values were subsequently used to calculate the reference reflectance $R_{0\%}^{700}$ using Equation 4.6. With $R_{0\%}^{700}$ established, we then applied equation 4.7 to estimate the moisture content for each soil sample.

$$R_{MC\%}^{700} = R_{0\%}^{700} - \hat{A} \cdot MC\%^{\hat{n}} \quad (4.6)$$

$$MC\% = \sqrt[\hat{n}]{\frac{R_{0\%}^{700} - R_{MC\%}^{700}}{\hat{A}}} \quad (4.7)$$

The soil spectral behaviour at 700 nm with the moisture content for three soil textures as in Figures 4.20 – 4.22 (The results for the other five soil textures are provided in Appendix A9). The curves were made using equation 4.6.

RESULTS

Table 4.3 Values of the constants for Equations (4.6) and (4.7)

| Soil texture | \hat{A} [-] | \hat{n} [-] | $R_{0\%}^{700}$ [%] |
|--------------|---------------|---------------|---------------------|
| Sandy loam | 1.20 | 0.84 | 14.30 |
| Silty loam | 0.37 | 0.85 | 12.20 |
| Clay | 0.41 | 0.83 | 15.80 |
| Sand | 0.66 | 0.83 | 17.50 |
| Silty clay | 0.57 | 0.84 | 18.40 |
| Clay loam | 0.55 | 0.83 | 19.70 |
| Loam | 0.85 | 0.79 | 20.50 |
| Loamy sand | 0.56 | 0.83 | 34.40 |

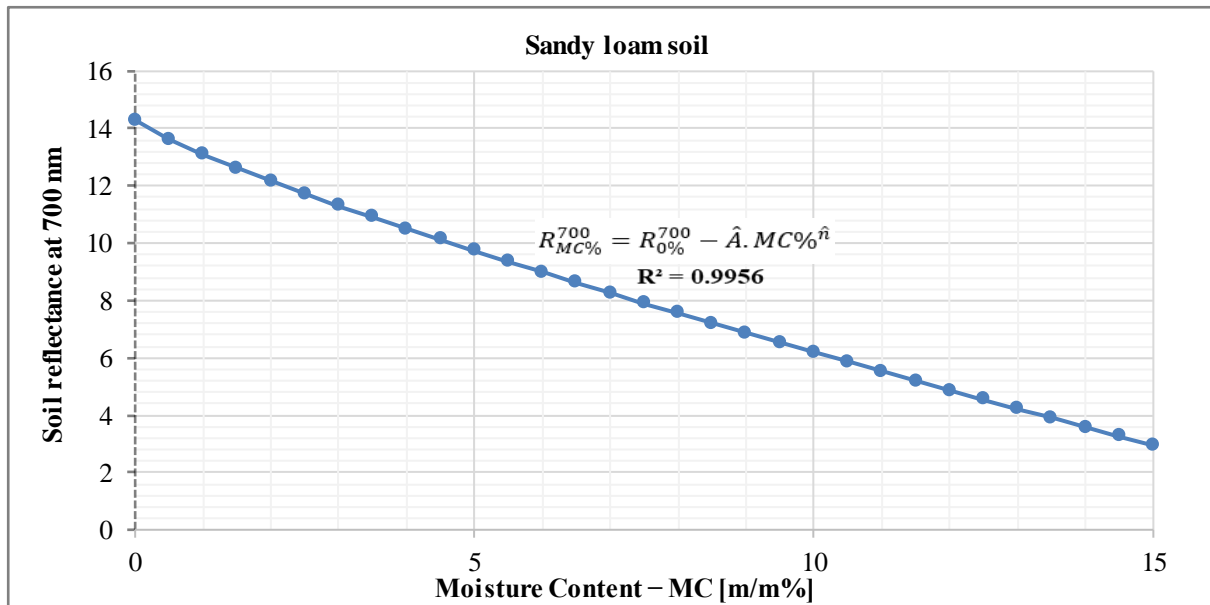


Figure 4.20. Spectral reflectance at 700 nm – soil moisture content relationship for sandy loam.

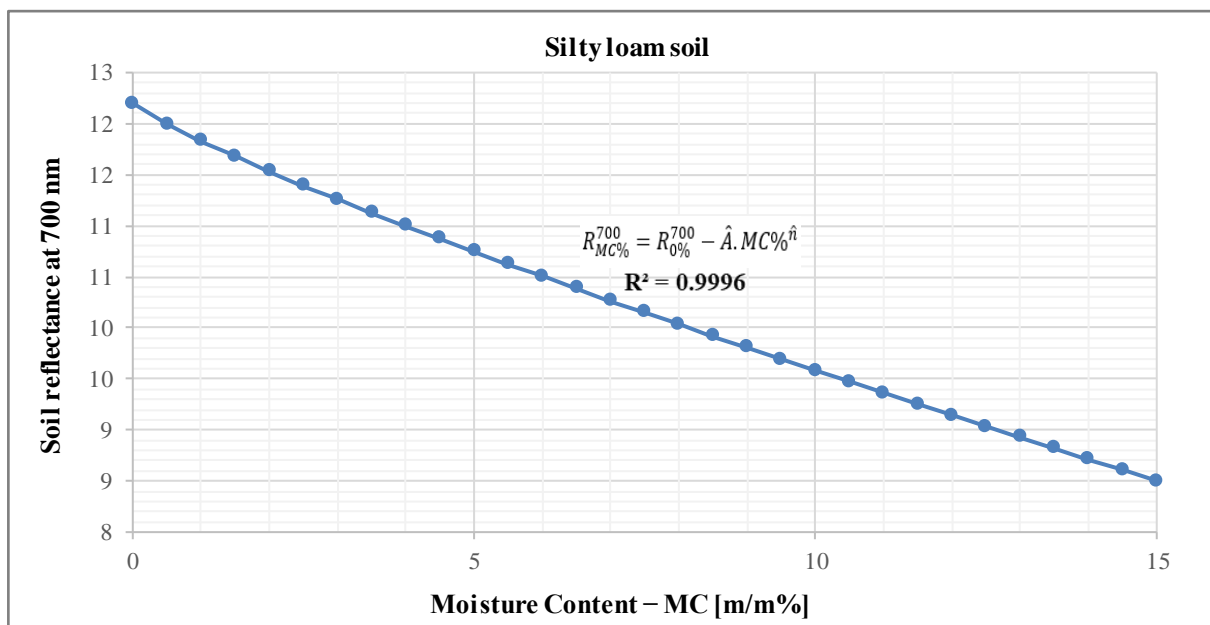


Figure 4.21. Spectral reflectance at 700 nm – soil moisture content relationship for silty loam.

RESULTS

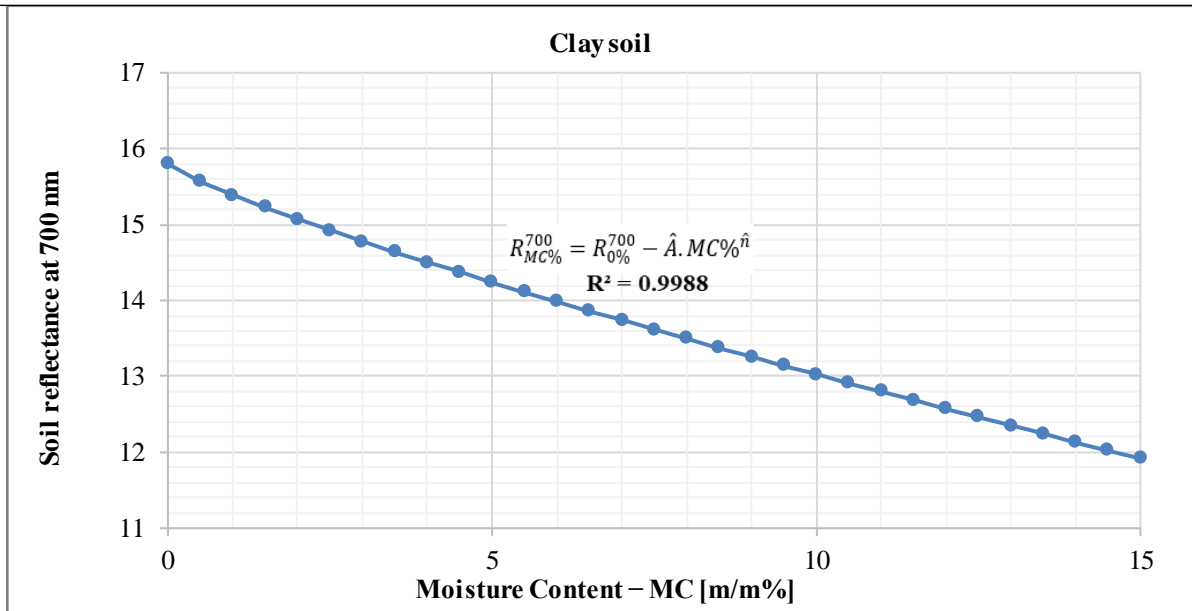


Figure 4.22. Spectral reflectance at 700 nm – soil moisture content relationship for clay.

4.6 Soil load-bearing capacity – optical reflectance relationship

At the beginning of the compaction, there is a small transient phenomenon when the soil conforms to the pressure plate and settles. Based on the measurements, this ends at approximately $z/D = 0.05$ and from there the curve follows according to the discovered function. This will be the starting point of the curve.

$$p_0 = k_0 \cdot \left(\frac{z_0}{D}\right)^n \quad (4.8)$$

where:

$n=0.8$ for sandy loam,

Substituting the given values:

$$p_0 = k_0 \cdot 0.1 \quad (4.9)$$

The change in soil pressure under the plate is given by:

$$\Delta p = p_0 - p \quad (4.10)$$

Rearranging for p :

$$p = p_0 - \Delta p \quad (4.11)$$

The pressure difference due to moisture content (MC%) is:

RESULTS

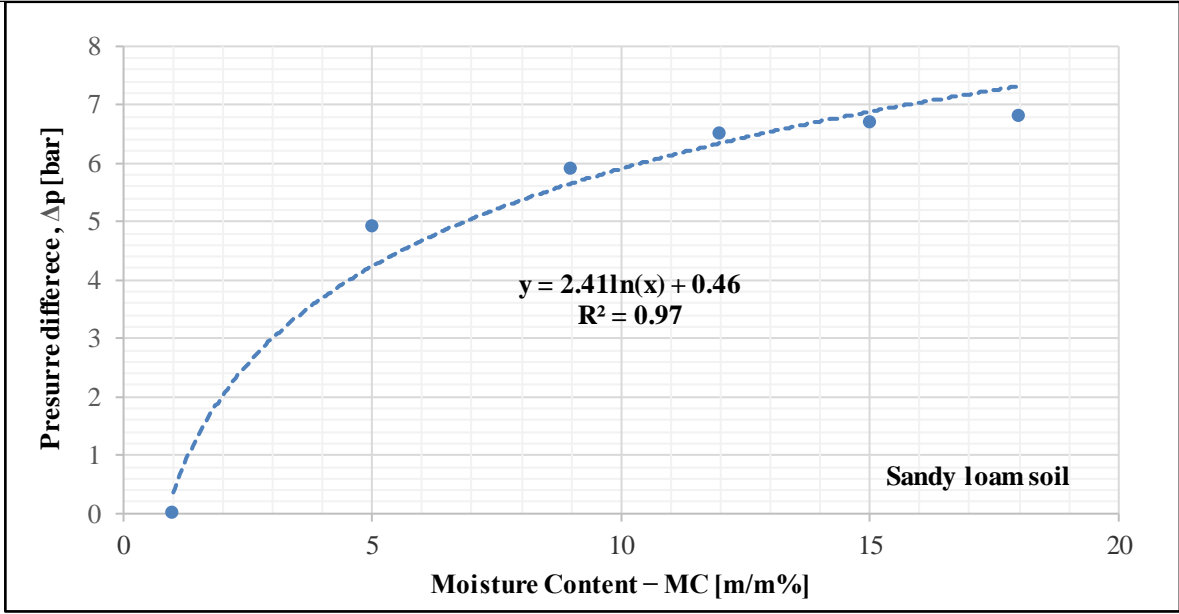


Figure 4.23. Pressure difference – soil moisture content relationship for sandy loam.

$$\Delta p = 2.41 \cdot \ln(MC\%) + 0.46 \quad (4.12)$$

Since the moisture content is related to spectral reflectance by:

$$MC\% = \left(\frac{R_{0\%}^{700} - R_{MC\%}^{700}}{2.75} \right)^{\frac{1}{0.35}} \quad (4.13)$$

Substituting (4.13) into (4.12) and into the pressure equation (4.11):

$$p = k_0 \cdot 0.1 - 2.41 \cdot \ln \left[\left(\frac{R_{0\%}^{700} - R_{MC\%}^{700}}{2.75} \right)^{\frac{1}{0.35}} \right] + 0.46 \quad (4.14)$$

We add one to the input variable of the ln function so that it will be valid from zero.

Thus, the corrected equation for load-bearing capacity is:

$$p = k_0 \cdot 0.1 - 2.41 \cdot \ln \left[1 + \left(\frac{R_{0\%}^{700} - R_{MC\%}^{700}}{2.75} \right)^{\frac{1}{0.35}} \right] + 0.46 \quad (4.15)$$

The final formulation:

$$p = a \cdot k_0 - c - f \cdot \ln \left[1 + \left(\frac{R_{0\%}^{700} - R_{MC\%}^{700}}{\hat{A}} \right)^{\frac{1}{\hat{n}}} \right] \quad (4.16)$$

where a , c , f , \hat{A} , and \hat{n} are empirical constants dependent on soil texture and spectral properties. During validation, it was revealed that c is a negative constant. We take this into account in the equation.

RESULTS

4.7 Soil saturation- spectral reflectance relationship

This study investigated sand and loamy sand soil, utilizing known reflectance parameters of dry soil and saturated soil, and employing the saturation " ε " with the following equation, where " R_{Sat}^{700} " represents the reflectance of fully saturated soil:

$$\varepsilon = \frac{R_0^{700} - R^{700}}{R_0^{700} - R_{Sat}^{700}} \quad (4.17)$$

The higher saturation values observed in the sand indicate a more substantial reduction in reflectance when saturated, which is indicative of its rapid drainage and lower water retention capacity. Loamy sand exhibited lower saturation values, suggesting a more stable reflectance due to its finer texture and enhanced moisture retention properties (Table 4.4).

Table 4.4 Shows the data of soil textures investigated as follows:

| Soil texture | Dry | Fully saturated | | Reflectance range | Soil particle distribution | | |
|--------------|-----------------|---------------------|---------------------------|-------------------|----------------------------|----------|----------|
| | R_0^{700} [%] | R_{Sat}^{700} [%] | MC _{Sat} [m/m %] | ΔR_{Max} | Clay [%] | Silt [%] | Sand [%] |
| Sand | 17.30 | 06.86 | 30.00 | 10.40 | 02.20 | 02.10 | 95.70 |
| Sandy loam | 14.30 | 08.20 | 35.00 | 06.10 | 05.80 | 12.10 | 82.10 |

4.8 The effect of the plate size on the sinkage

This study examined soil pressure-sinkage behaviour using plates of various sizes with a constant height-to-diameter (H/D) ratio of 0.5. A uniform load of 12 bar was applied to plates of 15 cm and 20 cm diameters to evaluate their impact on soil sinkage. The results (Figures 4.57 and 4.58) showed that the smaller plate (15 cm) caused more sinkage than the larger plate (20 cm) under the same load conditions. The increased sinkage with the smaller plate is due to the load being concentrated over a smaller area, leading to higher localized pressure and greater soil deformation. In contrast, the larger plate distributes the load over a wider area, reducing pressure and minimizing sinkage.

These findings align with classical soil mechanics theories, such as Bekker's pressure-sinkage model, which suggests that a larger contact area decreases normal stress and limits sinkage under constant loading. This study highlights the importance of plate size in off-road applications, where optimized load distribution is essential for reducing soil compaction and enhancing vehicle mobility on soft terrains.

RESULTS

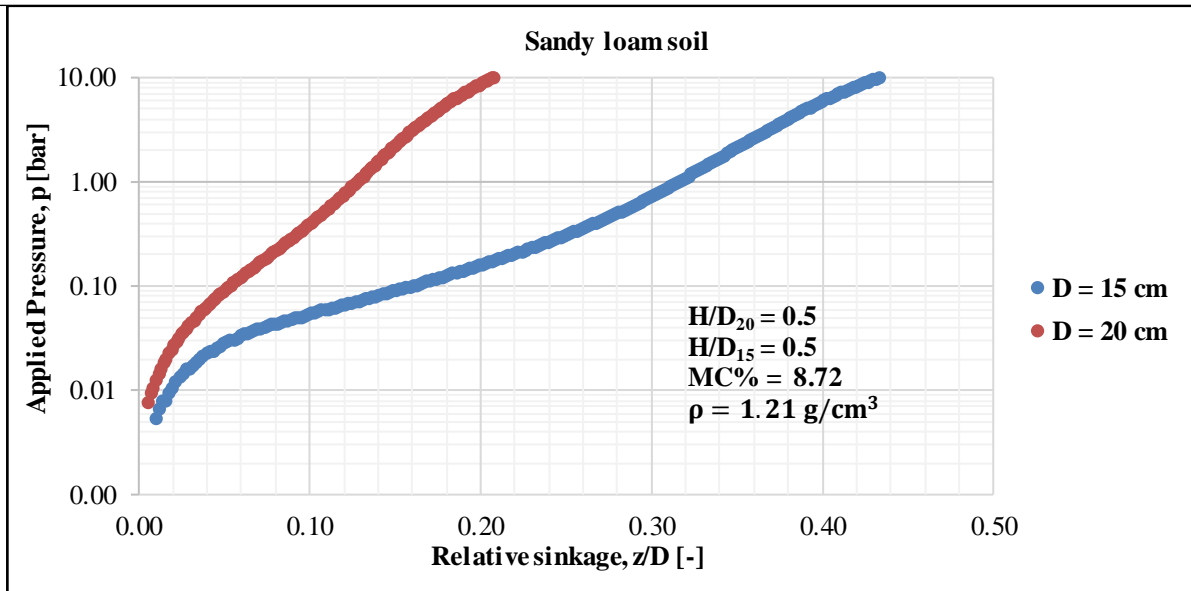


Figure 4.24. The plate size affects the sinkage of sandy loam soil.

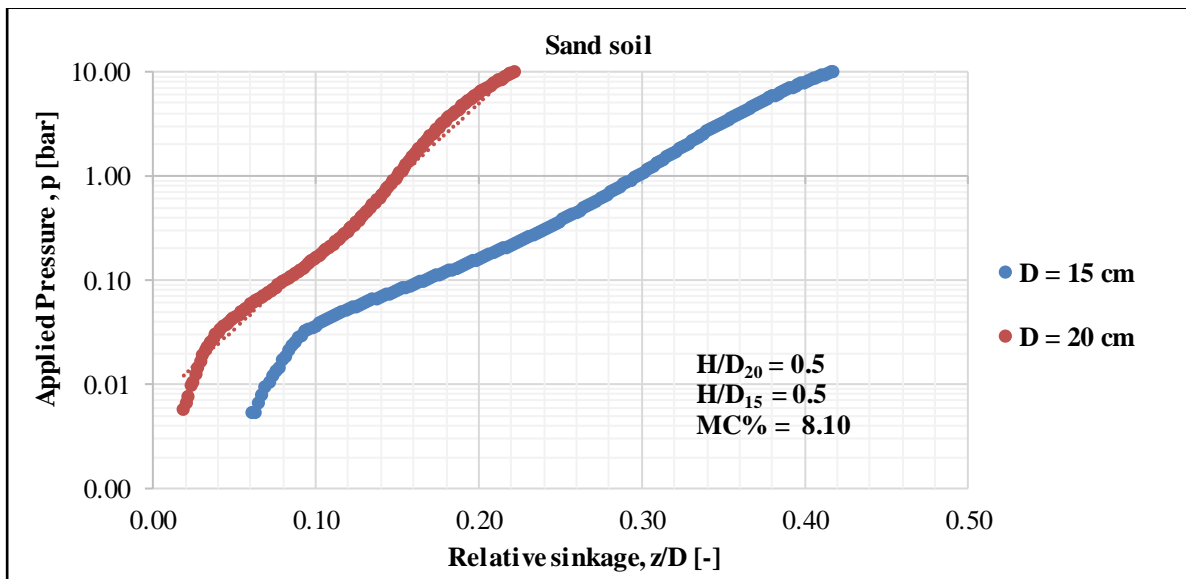


Figure 4.25. The plate size affects the sinkage of sand soil.

4.9 The effect of the load velocity on the soil sinkage

In examining the load-bearing capacity of a homogeneous soil layer under different load velocities, a significant correlation between velocity and soil sinkage was found. Higher load velocities resulted in reduced sinkage, while lower velocities led to increased sinkage (Figures 4.59 and 4.60). This is due to the soil's mechanical response to varying loading rates. At lower velocities, the soil had more time to compact, becoming denser and more resistant to deformation, hence increasing sinkage. Conversely, at higher velocities, the soil experienced less compaction because of the rapid load application, leading to lower sinkage.

These findings align with terramechanics principles, where the soil's response to load depends on time, pressure, and material properties. The increased sinkage at slower velocities may be due to the soil's ability to adjust and redistribute particles over time, resulting in a more compacted, less penetrable layer. At higher velocities, rapid load application limits soil rearrangement, resulting in

RESULTS

less compaction and reduced sinkage. This velocity-soil deformation relationship is critical for off-road vehicle design and soil interaction models, optimizing performance across varying terrains and load conditions. Further analysis of soil texture, moisture content, and particle size distribution could provide additional insights into this behaviour.

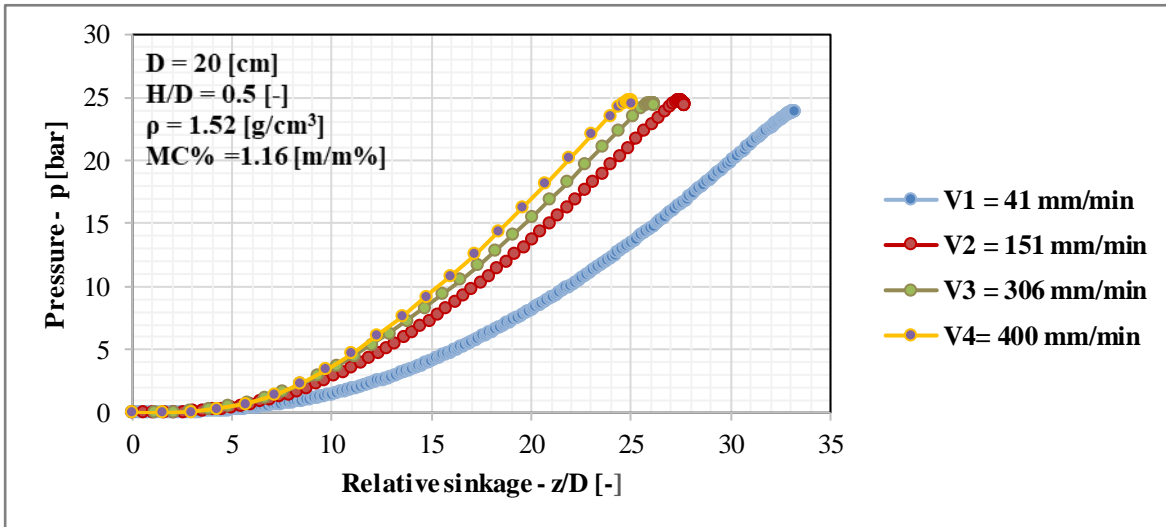


Figure 4.26. The load velocity affects the sinkage of sandy loam soil.

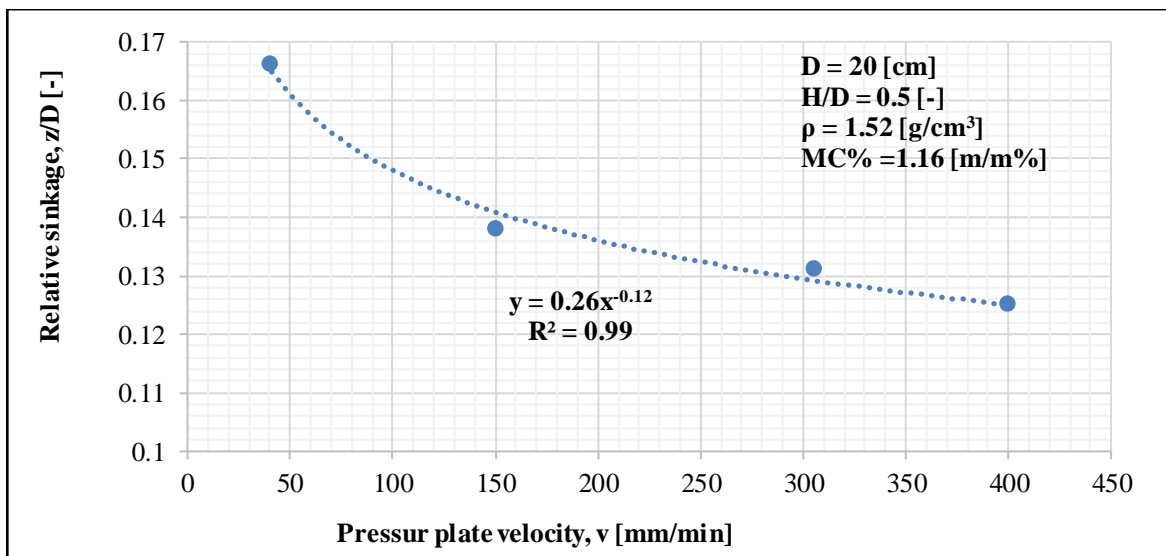


Figure 4.27. The sinkage as a function of velocity for sandy loam soil.

4.10 Cone penetrometer technique with colour measurement (field measurements)

Data were collected using two primary methods: the cone index (CI) to evaluate soil penetration resistance and a spectrophotometer to measure soil spectral behaviour under different moisture conditions. Results indicate a clear correlation between moisture content, soil compaction, and strength (see Figures 4.61 and 4.62). Increased moisture content lubricates soil particles, enhancing interparticle cohesion and resistance to penetration, consistent with this study's findings.

Furthermore, soil spectral behaviour analysis shows that soil reflectance decreases as moisture content rises due to water's absorption properties, which diminish the soil minerals' reflective

RESULTS

characteristics. This behaviour aligns with established principles in soil physics and remote sensing, where moisture significantly alters the soil's optical properties.

These findings highlight a complex interaction between moisture content, soil strength, and spectral reflectance, with implications for soil mechanics and remote soil condition monitoring. The insights could guide future research on optimizing soil management practices, particularly in off-road engineering and precision agriculture, where understanding soil behaviour under varying moisture conditions is crucial.

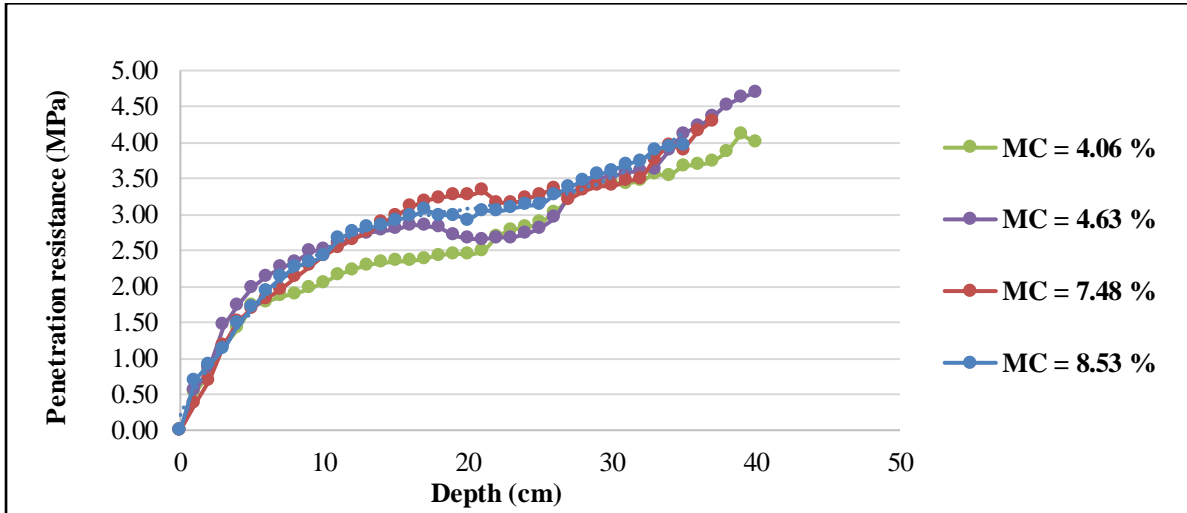


Figure 4.28. The Penetration resistance (MPa) – Depth (cm) at different moisture contents of sandy loam soil.

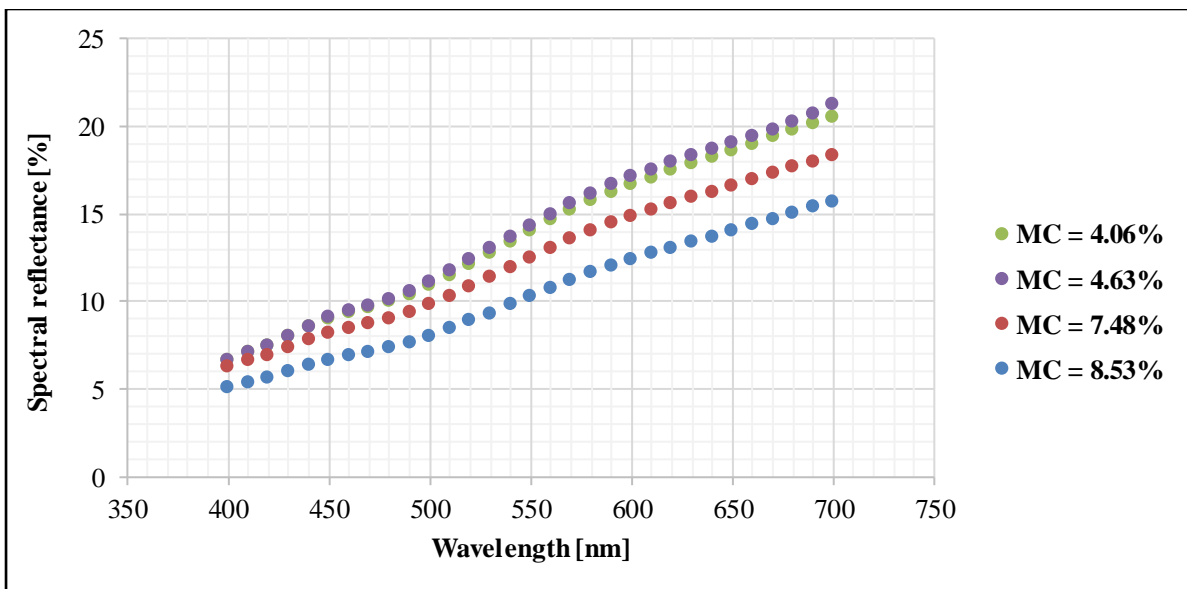


Figure 4.29. The Spectral reflectance (%) – Wavelength (nm) at different moisture contents of sandy loam soil.

5. NEW SCIENTIFIC RESULTS

This chapter presents the new scientific findings from this research work as follows:

1. Soil saturation- spectral reflectance relationship

I investigated sand and sandy loam soil, knowing the reflectance parameters of dry soil and saturated soil, the saturating level " ε " can be calculated by the following equation, where " R_{Sat}^{700} " is the reflectance of fully saturated soil, " R_0^{700} " is the reflectance of the dry soil and the " R^{700} " is the measured reflectance:

$$\varepsilon = \frac{R_0^{700} - R^{700}}{R_0^{700} - R_{Sat}^{700}}$$

Traditional methods for measuring soil saturation rely on collecting physical samples and conducting laboratory analyses. In contrast, this method utilizes reflectance measurements, enabling field-based assessments of soil water saturation without the need for sample collection. By first obtaining reflectance measurements for both fully saturated and completely dry soil, subsequent reflectance readings can be used to calculate the current saturation level of the soil. This approach offers a more efficient and convenient way to monitor soil moisture conditions in agricultural settings.

Data of soil textures investigated are listed as follows:

| Soil texture | Dry | Fully saturated | | Reflectance range | Soil particle distribution | | |
|--------------|-----------------|---------------------|--------------------------|-------------------|----------------------------|----------|----------|
| | R_0^{700} [%] | R_{Sat}^{700} [%] | MC _{Sat} [m/m%] | ΔR_{Max} | Clay [%] | Silt [%] | Sand [%] |
| Sand | 17.30 | 06.86 | 30.00 | 10.40 | 02.20 | 02.10 | 95.70 |
| Sandy loam | 14.30 | 08.20 | 35.00 | 06.10 | 05.80 | 12.10 | 82.10 |

2. Soil moisture content from soil spectral reflectance

At a 700 nm wavelength, I found a correlation between soil surface moisture content and measured reflectance. Calculating moisture content using this correlation requires knowing three constants specific to the soil texture, including the reflectance of the dry soil at 700 nm. These constants for each analyzed soil texture are presented in the table below.

$$MC\% = \sqrt{\frac{\hat{n} (R_{0\%}^{700} - R_{MC\%}^{700})}{\hat{A}}}$$

The value of the constants is as follows:

| Soil texture | \hat{A} [-] | \hat{n} [-] | R_0^{700} [%] |
|--------------|---------------|---------------|-----------------|
| Sandy loam | 1.20 | 0.84 | 14.30 |
| Silty loam | 0.37 | 0.85 | 12.20 |
| Clay | 0.41 | 0.83 | 15.80 |
| Sand | 0.66 | 0.83 | 17.50 |
| Silty clay | 0.57 | 0.84 | 18.40 |

NEW SCIENTIFIC RESULTS

| | | | |
|------------|------|------|-------|
| Clay loam | 0.55 | 0.83 | 19.70 |
| Loam | 0.85 | 0.79 | 20.50 |
| Loamy sand | 0.56 | 0.83 | 34.40 |

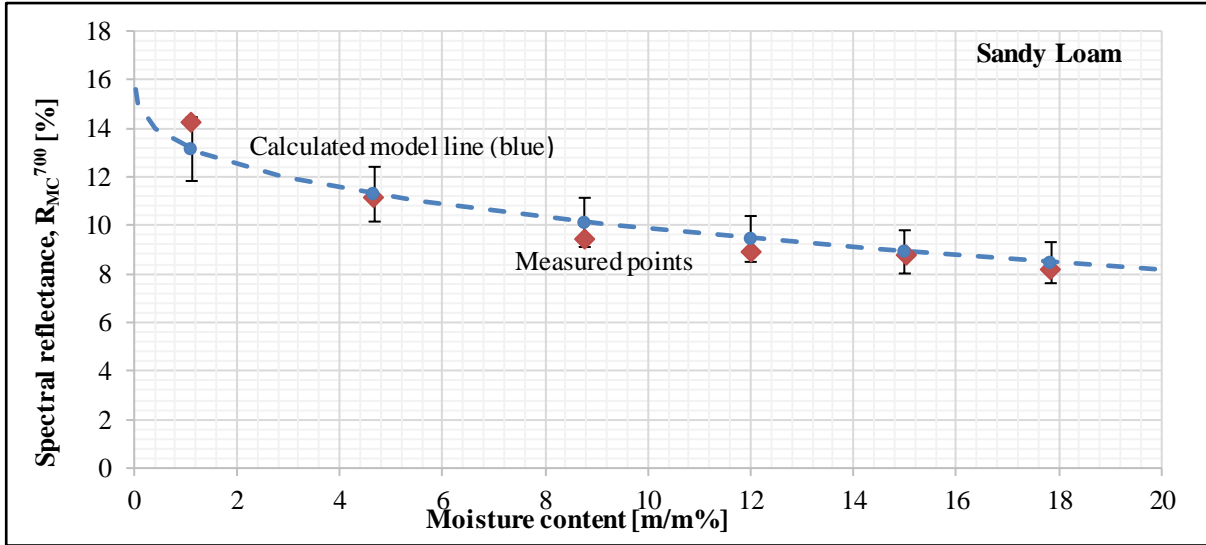


Figure 5.1. Model accuracy for sandy loam soil.

3. The load-bearing capacity and the spectral behaviour of soil relationship

For a homogeneous soil volume under confined compression with a H/D ratio of 0.5, I established a relationship between the soil's surface reflectance at 700 nm and its load-bearing capacity (p , [bar]). This relationship incorporates specific constants listed in the diagram. Furthermore, the equation contains the load-bearing capacity factor (k_0 , [bar]) at a relative sinkage (z/D , [-]) of 0.05 in a dry state, and the reflectance of dry soil (R_0^{700} , [%]) at 700 nm. The reflectance of the soil at 700 nm with a given moisture content ($R_{MC\%}^{700}$, [%]) serves as the independent variable.

$$p = a \cdot k_0 - c - f \cdot \ln \left[1 + \left(\frac{R_0^{700} - R_{MC\%}^{700}}{\hat{A}} \right)^{\frac{1}{\hat{n}}} \right]$$

The validity limit is the reflectance of dry soil to saturated soil. For sandy loam 14.3-8.2%

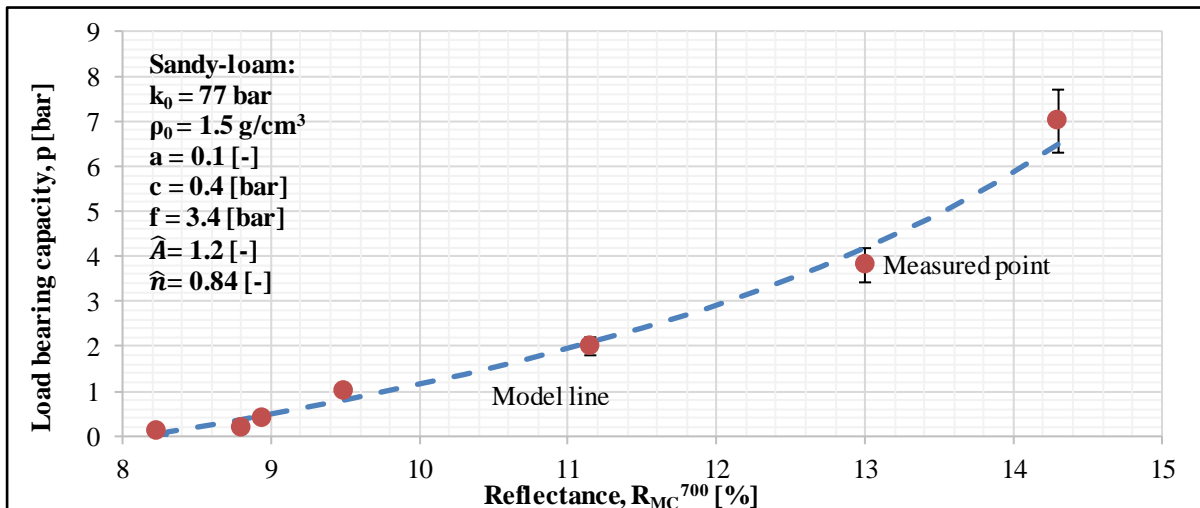


Figure 5.2. Reflectance-load bearing capacity relationship for sandy loam.

4. Pressure plate displacement as a function of its velocity

Under the conditions illustrated in the diagram, I determined a power function relationship between the pressure plate's velocity (rate of descent) and its sinkage. This relationship is expressed with two dimensionless constants, A and b, that include the effect of the soil properties and its initial condition. Further incorporates the plate diameter (D) and its velocity (v) as independent variables. The validity range of the equation for the velocity is between 40-400 mm/min.

$$z = D \cdot A \cdot v^{-b}$$

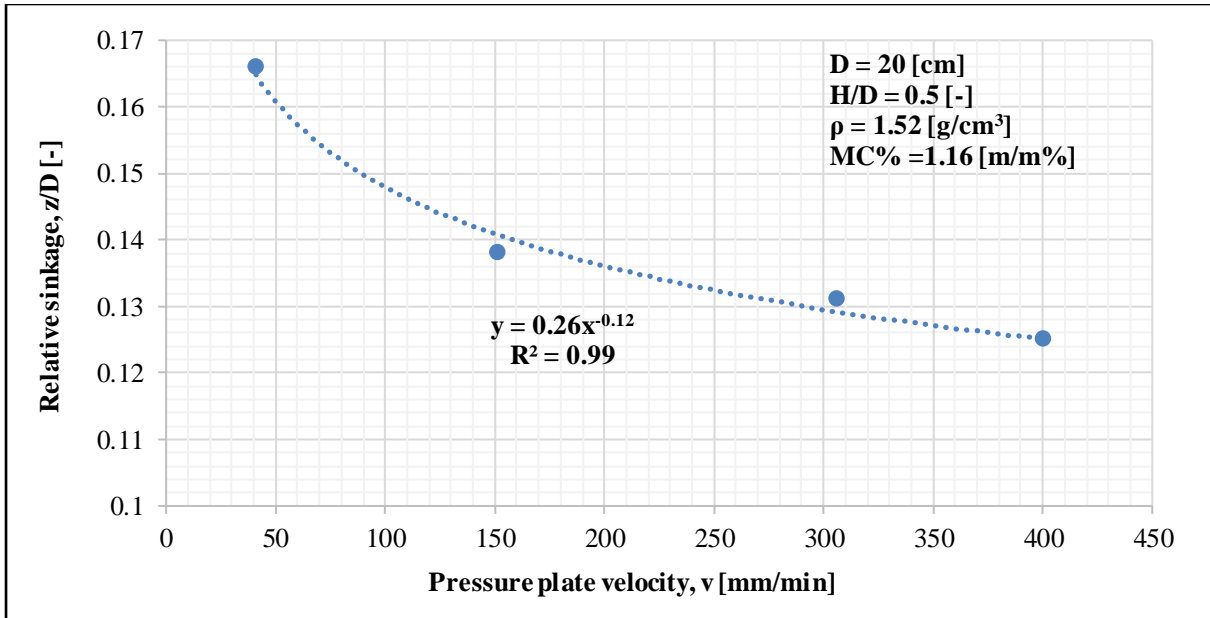


Figure 5.3. The relative sinkage as function of the pressure plate's velocity.

5. Soil relative sinkage – moisture content relationship

Based on the measured data, I developed a new equation to determine the relative sinkage (z/D). This equation is valid for the given initial density as a function of moisture content, where A₁ and B₁ are constants depending on the soil texture. They are listed in the table below for different soil textures at 1.0 bar tyre inflation pressure, which is commonly utilized in agriculture applications.

$$z/D = A_1 \cdot MC\% + B_1$$

| Soil texture | A ₁ [-] | B ₁ [-] | Regression, R ² | MC[m/m%] |
|--------------|--------------------|--------------------|----------------------------|----------|
| Sandy loam | 0.0072 | 0.0404 | 0.9647 | 01 – 16 |
| Silty loam | 0.0061 | 0.0488 | 0.9583 | 01 – 22 |
| Clay | 0.0096 | 0.0154 | 0.9764 | 10 – 27 |
| Sand | 0.0053 | 0.0437 | 0.9798 | 01 – 16 |
| Silty clay | 0.0084 | 0.0208 | 0.9720 | 04 – 27 |
| Clay loam | 0.0106 | 0.0139 | 0.9919 | 04 – 23 |
| Loam | 0.0125 | 0.0208 | 0.9510 | 02 – 21 |
| Loamy sand | 0.0105 | 0.0710 | 0.9654 | 01 – 17 |

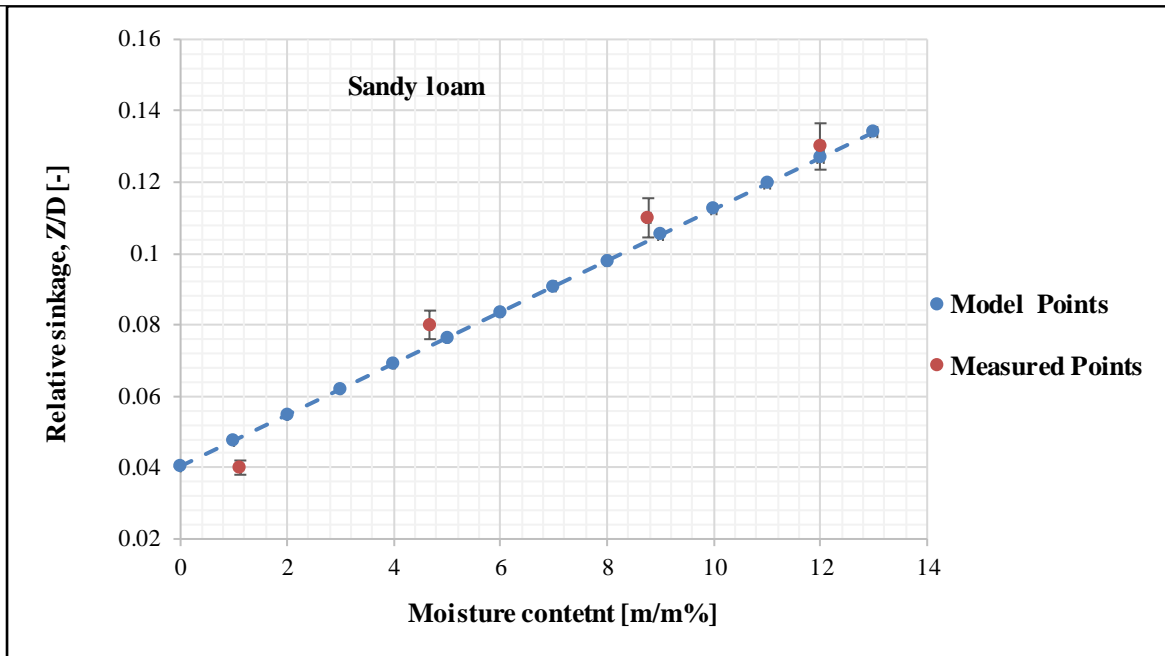


Figure 5.4. Soil relative sinkage – moisture content relationship for sandy loam.

6. Soil relative sinkage – spectral reflectance relationship

I experimentally determined and measured the soil spectral behaviour and load-bearing capacity (pressure-sinkage relationship) simultaneously under controlled moisture content conditions. Based on the experimental results, I focused on soil reflectance at 700 nm in relation to soil relative sinkage (z/D) under an applied pressure of 1.0 bar, corresponding to the typical tyre inflation pressure in vehicle mobility, as a function of moisture content. Through the analysis of graphs derived from the experiments, I experimentally revealed that soil spectral reflectance is inversely proportional to soil relative sinkage (z/D). Consequently, I developed a novel equation to determine the relative sinkage as a function of soil reflectance at 700 nm, where A_2 and B_2 are constants dependent on soil texture and soil spectral reflectance, as presented in the table below:

$$z/D = -A_2 \cdot \ln (R_{MC\%}^{700}) + B_2$$

| Soil texture | A_2 [-] | B_2 [-] | Regression, R^2 | MC[m/m%] |
|--------------|-----------|-----------|-------------------|----------|
| Sandy loam | 0.211 | 0.5921 | 0.9825 | 01 – 16 |
| Silty loam | 0.071 | 0.2845 | 0.9842 | 01 – 22 |
| Clay | 0.162 | 0.5558 | 0.8720 | 10 – 27 |
| Sand | 0.218 | 0.6499 | 0.9326 | 01 – 16 |
| Silty clay | 0.208 | 0.6372 | 0.9879 | 04 – 27 |
| Clay loam | 0.376 | 1.0693 | 0.9788 | 04 – 23 |
| Loam | 0.455 | 1.5836 | 0.9980 | 02 – 21 |
| Loamy sand | 0.231 | 0.7096 | 0.9768 | 01 – 17 |

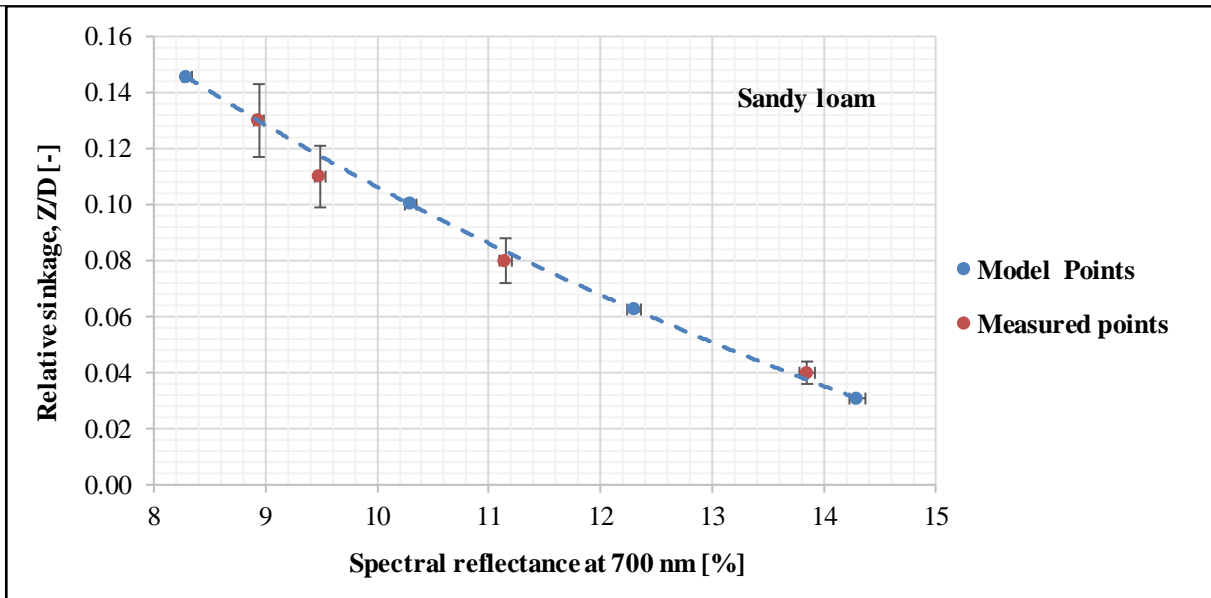


Figure 5.5. Soil relative sinkage – spectral reflectance relationship for sandy loam.

6. CONCLUSION AND SUGGESTIONS

In conclusion, experimental analysis has been conducted to study the load-bearing capacity and the spectral behaviour of the eight soil textures as homogenous. The load-bearing capacity is represented by the pressure-sinkage relationship. The bevameter apparatus has been used to examine the load-bearing capacity and soil properties via applied normal load on the soil surface. The experiments were conducted using a circular sinkage plate (20 cm) with soil thicknesses (10 cm) and at soil density. The applied force, time and plate displacement were recorded by Catman4.5 software through Spider8. These experimental data were employed to determine the applied pressure (p) and the relative sinkage (z/D) relationship at different moisture content levels. The pressure–sinkage curves of soil measurement were plotted by using a logarithmic scale. The densities before and after the measurement along with the soil mass were identified to calculate the relative density ratio ($\Delta\rho$). For the soil spectral behaviour, we measured the soil reflectance behaviour for the same soil sample as it was prepared to be measured by the bevameter technique. Based on the measurements and the findings of the current study, it is possible to make the following inferences:

- The pressure-sinkage relationship curves for eight soil textures at varying moisture content levels, based on the experimental results, demonstrated that the sinkage (the relative sinkage (z/D)) increases proportionally with applied pressure (defined as the applied force divided by the plate area) at each moisture content level, as well as the relative density ratio ($\Delta\rho$).
- From the pressure-sinkage relationship curves and based on the moisture content, new equations have been introduced for both the relative sinkage and the relative density ratio.
- The spectral reflectance–wavelength curves of all examined soil textures at different moisture content levels (before pressing the soil) indicated that the reflected wavelength increased with an increase in the value of the sent wavelength at the same moisture content. Furthermore, a comparison of the spectral behaviour of soil at different moisture contents with an increase in moisture content at a fixed sent wavelength revealed that the reflected wavelength decreased.
- To determine the effect of soil moisture content on the spectral behavior of soil, calculations were performed for each moisture content; the reflected wavelengths at 700 nm, the mean for reflected wavelengths in the range 400 – 500 nm, 400 – 700 nm range, and 600 – 700 nm. It was concluded that the reflectance at 700 nm is more sensitive to moisture content and should be considered when evaluating spectral reflectance.
- The experiment revealed, through the moisture content, the relationship of the relative sinkage and the spectral reflectance at 700 nm, as well as the relative density ratio with the soil spectral reflectance at 700 nm.
- Sand and loamy sand soil were investigated, and it was determined that knowing the reflectance parameters of dry soil and saturated soil, the saturation level can be ascertained by the soil reflectance parameters.
- The experiment of the soil at zero (or near-zero) moisture content level revealed that the soil moisture content level can be determined by the soil reflectance parameters.

CONCLUSION AND SUGGESTION

- The effect of the plate size on the soil bearing capacity was investigated, and the experimental results demonstrated that when applying an equivalent load to the same soil layer, the smaller plate size (15 cm) resulted in greater sinkage compared to the larger plate size (20 cm). This phenomenon can be attributed to the fact that the load is more concentrated when utilizing the 15 cm plate and more distributed when employing the 20 cm plate.
- The impact of the load speed on the load-bearing capacity of the same soil layer at varying load speeds was investigated. Based on the measurements, it was observed that higher load speeds resulted in reduced sinkage, while lower speeds led to increased sinkage. This phenomenon occurred due to the soil becoming more densely packed when subjected to lower speeds and less dense when exposed to higher speeds.
- Field measurements were conducted for the soil penetration resistance and the soil reflectance. The results indicated that greater resistance to penetration occurs when the moisture content increases and the soil reflectance decreases.

As a suggestion, additional experiments should be performed with inhomogeneous soil samples, first in laboratory environments and then in the field. These studies should seek to confirm the newly proposed correlations between load-bearing capacity and moisture levels, as well as between load-bearing capacity and spectral characteristics. Moreover, these investigations should strive to verify the generalized relationship linking load-bearing capacity to spectral reflectance

7. SUMMARY

INFLUENCE OF MOISTURE CONTENT ON SOIL BEARING CAPACITY AND SPECTRAL REFLECTANCE

This study conducted comprehensive experiments and analyses to establish the relationship between load-bearing capacity and spectral behaviour (soil colour) across eight different soil textures. Soil samples from various locations in Hungary were treated as homogeneous for the investigation. The bevameter apparatus measured the load-bearing capacity, while a spectrophotometer assessed spectral reflectance (soil colour). Both properties were measured under controlled conditions, maintaining constants such as moisture content, initial density, and a H/D ratio of 0.5.

The bevameter tests identified the relative density ratio and relative sinkage at various moisture levels, while the spectrophotometer assessed soil reflectance under different moisture conditions.

Results from both tests were categorized into:

1. A novel equation for determining the relative sinkage (z/D) was developed based on experimental results of load-bearing capacity (pressure sinkage relationship), as a function of moisture content.
2. Furthermore, a relationship of the relative soil density ratio ($\Delta\rho$) was found based on experimental results of load-bearing capacity (pressure sinkage relationship), as a function of moisture content.
3. A novel relationship concerning the relative sinkage (z/D) with the soil reflectance at 700 nm was proposed based on experimental results.
4. Additionally, a new relationship of the relative soil density ratio ($\Delta\rho$) with the soil reflectance at 700 nm was proposed based on experimental results.
5. Soil saturation-reflectance was investigated for sand and loamy sand soil, considering the reflectance parameters of dry soil and saturated soil.
6. A new moisture content equation (MC%) derived from the soil spectral reflectance has been proposed for eight soil textures according to the experimental results.
7. A novel equation was developed to determine the relationship between the load-bearing capacity and the soil spectral reflectance, based on experimental results of load-bearing capacity (pressure sinkage relationship), as a function of moisture content.
8. A novel equation developed for determining the sinkage as a function of the velocity for sandy loam soil.
9. It was concluded that the reflectance at 700 nm exhibits greater sensitivity to moisture content and should be considered when evaluating spectral reflectance.
10. Based on the comprehensive measurements of soil load-bearing capacity and spectral behaviour, it was observed that there exists a definitive function between the two parameters, demonstrating a proportional relationship. This correlation is valid for a given soil density, as different soil densities yield similar tendencies with varying relative sinkage and relative soil density ratios. Furthermore, it was noted that soil spectral behaviour exhibits a mirroring effect at the point of soil failure (the failing point), which is not requisite as the soil has failed to sustain the applied load.

As a recommendation, further experimental investigations should be conducted with inhomogeneous soil, initially in laboratory settings and subsequently in field conditions, to validate

SUMMARY

the proposed new relationships between load-bearing capacity and moisture content, as well as between load-bearing capacity and spectral behaviour. Additionally, these studies should aim to validate the generalized load-bearing capacity with the spectral reflectance relationship.

8. ÖSSZEFOGLALÁS (SUMMARY IN HUNGARIAN)

A NEDVESSÉGTARTALOM HATÁSA A TALAJ TEHERBÍRÓ KÉPESSÉGÉRE ÉS SPEKTRÁLIS REFLEXIÓJÁRA

Ez a disszertáció átfogó kísérleteket és elemzéseket tartalmaz annak érdekében, hogy meghatározzam a talaj teherbíró képesség és a spektrális viselkedés (talajszín) közötti kapcsolatot nyolc különböző talajtextúra esetében. A különböző magyarországi helyszínekről származó talajmintákat homogénként kezeltem a vizsgálat során. A teherbíró képességet a bevameter készülékkel mértem, míg a spektrális visszaverődést (talajszín) spektrofotométerrel vizsgáltam. Mindkét tulajdonságot kontrollált körülmények között mértem, a nedvességtartalom, a kezdeti sűrűség és a H/D arány (0,5) állandóságának fenntartásával.

A bevameter-tesztek a relatív sűrűségi arányt és a relatív süllyedést különböző nedvességi szinteken határozza meg, míg a spektrofotométer különböző nedvességi körülmények között értékelte a talaj visszaverődését. A vizsgálatok eredményeit a következő kategóriákba soroltam:

1. Új egyenletek kerültek kidolgozásra a relatív mélység (z/D) meghatározására a teherbíró képesség (nyomás-süllyedés kapcsolat) kísérleti eredményei alapján, a nedvességtartalom függvényében.
2. Továbbá, új egyenletek születtek a relatív talajsűrűségi arány ($\Delta\rho$) meghatározására a teherbíró képesség (nyomás-süllyedés kapcsolat) kísérleti eredményei alapján, a nedvességtartalom függvényében.
3. Kísérleti eredmények alapján új kapcsolatot javaslok a relatív mélység (z/D) és a talaj 700 nm-en mért visszaverődése között.
4. Emellett új kapcsolatot javaslok a relatív talajsűrűségi arány ($\Delta\rho$) és a talaj 700 nm-en mért visszaverődése között kísérleti eredmények alapján.
5. Vizsgáltam a talaj telítettség-visszaverődést homok és homokos vályogtalaj esetében, figyelembe véve a száraz és telített talaj visszaverődési paramétereit.
6. A kísérleti eredmények alapján egy új nedvességtartalom egyenletet (MC%) vezettem le a talaj spektrális visszaverődéséből, nyolc talajtextúrára vonatkozóan.
7. Megállapítottam, hogy a 700 nm-en mért visszaverődés nagyobb érzékenységet mutat a nedvességtartalom iránt, és figyelembe kell venni a spektrális visszaverődés értékelése során.
8. Új egyenletet hoztam létre homokos vályog talaj esetén a nyomólap besüllyedésének meghatározására a sebesség függvényében.
9. Arra a következtetésre jutottam, hogy a 700 nm-es reflexió nagyobb érzékenységet mutat a nedvességtartalomra, és ezt figyelembe kell venni a spektrális reflexió értékelésekor.
10. A talaj teherbíró képességére és spektrális viselkedésére vonatkozó átfogó méréseim alapján megfigyeltem, hogy egyértelmű összefüggés létezik a két paraméter között, amely arányos kapcsolatot mutat. Ez az összefüggés adott talajsűrűség esetén érvényes, mivel eltérő talajsűrűségek hasonló tendenciákat mutatnak különböző relatív mélységgel és relatív talajsűrűségi arányokkal. Továbbá megállapítottam, hogy a talaj spektrális viselkedése tükrözési hatást mutat a talaj tönkremenetelének pontjánál, amikor a talaj nem képes tovább fenntartani az alkalmazott terhelést.

Ajánlásként javasolt további kísérleti vizsgálatokat végezni inhomogén talajokkal, kezdetben laboratóriumi körülmények között, majd terepi feltételek mellett is, hogy megerősítsék az újonnan javasolt összefüggéseket a teherbíró képesség és a nedvességtartalom, valamint a teherbíró

képesség és a spektrális viselkedés között. Emellett ezeknek a vizsgálatoknak célja a spektrális visszaverődés alapján általánosított teherbíró képesség érvényesítése is

9. APPENDICES

A1. Bibliography

1. Ageykin, Y. S. (1973). Evaluation of ground deformability concerning vehicle mobility. *Journal of Terramechanics*, 10(1), 105–111.
2. Ahmed, A. E. E.; El Hariri, A.; Kiss, P. Soil strength and load bearing capacity measurement techniques. *HAE* 2021, 40, pp. 16-27. ISSN 0864-7410. <https://doi.org/10.17676/HAE.2021.40.16>.
3. Ahmed, A.E.E.; El Hariri, A.; Kiss, P. Soil Spectral Behavior Related to Its Load-Bearing Capacity Based on Moisture Content. *Appl. Sci.* 2023, 13, 3498. <https://doi.org/10.3390/app13063498>
4. Ahmed E.E.A., Kiss P., (2022): Homokos Vályogtalaj Teherbíróképességének Yizsgálata Bevaméterrel, *Mezőgazdasági Technika*, ISSN 0026-1890 : 63 (6), pp 2-6
5. Ahmed E. E. A., Pillinger G., Kiss P., (2022): The influence of sandy loam soil moisture content on its load-bearing capacity, *Mechanical Engineering Letters*, Gödöllő, Hungary, 2021, Vol. 22, Pp.15-25. HU ISSN 2060-3789.
6. Ahmed, A.E.E.; Pillinger, G.; Kiss, P. Moisture content impacts on soil load bearing capacity and its spectral behaviour. In *Proceedings of the 16th European-African Regional Conference of the ISTVS*, Lublin University of Technology, Poland, (11-13 October 2023), <https://doi.org/10.56884/DTUX6735>
7. Ahmed, S. I.; Siddiqua, S. Compressibility Behavior of Soils: A Statistical Approach. *Geotechnical and Geological Engineering*, 2016, 34(6), pp. 2063–2070. <https://doi.org/10.1007/s10706-016-9996-7>.
8. Aitkenhead, M.; Coull, M.; Towers, w.; Hudson, G.; Black, H. Prediction of soil characteristics and colour using data from the National Soils Inventory of Scotland, *Geoderma* 2013, 200–201, pp. 99-107, ISSN 0016-7061, <https://doi.org/10.1016/j.geoderma.2013.02.013>.
9. Alakukku, L., Weisskopf, P., Chamen, W.C., Tijink, F.G., van der Linden, J., Pires, S., Sommer, C., Spoor, G., 2003. Prevention strategies for field traffic-induced subsoil compaction: a review. *Soil Tillage Res.* 73, 145–160. [https://doi.org/10.1016/S0167-1987\(03\)00107-7](https://doi.org/10.1016/S0167-1987(03)00107-7)
10. Alamanis, N.; Lokkas, P.; Chrysanidis, T.; Christodoulou, D.; Paschalis, E. Assessment Principles for the Mechanical Behavior of Clay Soils. *WSEAS Transactions on Applied and Theoretical Mechanics*, 2021, 16, pp. 47-61, ISSN: 2224-3429 [DOI:10.37394/232011.2021.16.6](https://doi.org/10.37394/232011.2021.16.6).
11. ASAE, (1988). *ASAE Standards: Standards, Engineering Practices and Data Adopted by the American Society of Agricultural Engineers*, Volume 35, Part 1988, the University of Wisconsin - Madison, ISBN 0916150933, 9780916150938

12. Basarygina, E. M., Zyalov, V., Pakhomova, N. A., & Akulich, O. E. (2022). Information-analytical modeling of soil composition based on spectral analysis. IOP Conference Series: Earth and Environmental Science, 949, 012129. <https://doi.org/10.1088/1755-1315/949/1/012129>
13. Bekker, M. G. (1956). Theory of land locomotion. University of Michigan Press. <https://doi.org/10.3998/mpub.969040>
14. Bekker, M. G. (1960). Off-the-road locomotion. University of Michigan Press.
15. Bekker, M. G. (1969). Introduction to terrain-vehicle systems. The University of Michigan Press; First Edition edition, 1969.
16. Bernstein, R. Probleme zur experimentellen motorpflugmechanik'. Der Motorwagen. Berlin, Germany, 1913, pp.199-206 [Google Scholar](#)
17. Bigham, J. M., Ciolkosz, E. J., Luxmoore, R. J., (1993). Soil Color: Proceedings of a Symposium Sponsored by Divisions S-5 and S-9 of the Soil Science Society of America in San Antonio, Texas, Soil Science Society of America.
18. Bloch, I.; Hosen, J.; Kracht, E.; Lefebvre, M.; Jazmine-Lopez, C.; Woodcock, R.; Keegan, W. Is it better to be objectively wrong or subjectively, right? testing the accuracy and consistency of the Munsell capture spectroradiometer for Archaeological applications, *adv. Archaeol. Pract* 2021, 9(2), pp.132–144. <https://doi.org/10.1017/aap.2020.53>
19. Boussinesq, J.: Application des potentials a l'etude de l'equilibre et due mouvement des solides elastique, Gauthier-Villars, Paris, 1885. [Google Scholar](#)
20. Bouyoucos, G. J. (1962). Hydrometer method improved for making particle size analyses of soils. *Agronomy Journal*, 54(5), 464-465. <https://doi.org/10.2134/agronj1962.00021962005400050028x>
21. Campbell, G. S., & Norman, J. M. (1998). An introduction to environmental biophysics. Springer. <https://doi.org/10.1007/978-1-4612-1626-1>
22. Cerato, A.B., Lutenecker, A.J., 2006. Bearing Capacity of Square and Circular Footings on a Finite Layer of Granular Soil Underlain by a Rigid Base. *J. Geotech. Geoenvironmental Eng.* 132, 1496–1501. [https://doi.org/10.1061/\(ASCE\)1090-0241\(2006\)132:11\(1496\)](https://doi.org/10.1061/(ASCE)1090-0241(2006)132:11(1496))
23. Chen, X.; & Chen, X. Soil spectral behaviour and its effect on soil properties. *Biosystems Engineering* 2015, 141, pp. 61-70.
24. Cierniewski, J. (2020). Spectral Reflectance of Soil. In: Kokhanovsky, A. (eds) Springer Series in Light Scattering. Springer Series in Light Scattering. Springer, Cham. https://doi.org/10.1007/978-3-030-38696-2_4
25. Clarke, G., Topp, T., & Ferré, P. (2006). Measuring soil water content.

<https://doi.org/10.1002/0470848944.HSA076>

26. Corina, Sandu., Adrian, Sandu., Lin, Li. (2005). 5. Stochastic Modeling of Terrain Profiles and Soil Parameters. SAE transactions, doi: [10.4271/2005-01-3559](https://doi.org/10.4271/2005-01-3559)
27. Cresswell, H. P., & Hamilton, G. J. (2002). *Particle size analysis*. In N. McKenzie, K. Coughlan, & H. Cresswell (Eds.), *Soil physical measurement and interpretation for land evaluation* (pp. 224-239). CSIRO Publishing. <https://doi.org/10.1071/9780643100731>
28. Csanády, E.; Magoss, E.; Tolvaj, L. Colour Characterization of Wood. In: Quality of Machined Wood Surfaces. Springer, Cham. 2015. https://doi.org/10.1007/978-3-319-22419-0_3.
29. Csanády, E.; Kovács, Z.; Magoss, E.; Ratnasingam, J. Principles of Optimization. In: Optimum Design and Manufacture of Wood Products. Springer, Cham. 2019. https://doi.org/10.1007/978-3-030-16688-5_3.
30. Das, B.M., 2017. Shallow Foundations. CRC Press, Third edition. | Boca Raton : CRC Press, 2017. <https://doi.org/10.1201/9781315163871>
31. Ding, L.; Gao, H.; Deng, Z.; Li, Y.; Liu, G. New perspective on characterizing pressure–sinkage relationship of terrains for estimating interaction mechanics, Journal of Terramechanics, 2014, 52, pp.57–76. <https://doi.org/10.1016/j.jterra.2014.03.001>.
32. Dewhirst, D. L. (1964). A load-sinkage equation for lunar soils. AIAA Journal, 2(4), 761–762. <https://doi.org/10.2514/3.2421>
33. Dexter, A.R., (1988). Advances in characterization of soil structure}, Journal of Soil and Tillage Research, vol,11(3), Pp.199-238, Proceedings 11th Conference of ISTRO: Tillage and Traffic in Crop Production, ISSN 0167-1987,[https://doi.org/10.1016/0167-1987\(88\)90002-5](https://doi.org/10.1016/0167-1987(88)90002-5).
34. Dwivedi, R.S. (2017). Spectral Reflectance of Soils. In: Remote Sensing of Soils. Springer, Berlin, Heidelberg. https://doi.org/10.1007/978-3-662-53740-4_6
35. E., L., Skidmore., J., D., Dickerson., H., Schimmelpfennig. (1975). 1. Evaluating Surface-Soil Water Content by Measuring Reflectance1. Soil Science Society of America Journal, doi: [10.2136/SSSAJ1975.03615995003900020009X](https://doi.org/10.2136/SSSAJ1975.03615995003900020009X)
36. Earl, R. (1996). Prediction of trafficability and workability using tensiometers. Journal of Agricultural Engineering Research, 63(1), 27–33. <https://doi.org/10.1006/jaer.1996.0004>
37. Edwards, M. B., Dewoolkar, M. M., Huston, D. R., & Creager, C. (2017). bevameter testing on simulant Fillite for planetary rover mobility applications. Journal of Terramechanics, 70, 13–26. <https://doi.org/10.1016/j.jterra.2016.10.004>
38. Egorov, K.E., 1961. Deformation of a foundation bed of finite thickness. Soil Mech. [in Russ. Res. Inst. Found. 43.

39. Emori, R., & Schuring, D. (1966). Static and dynamic penetration tests of soil. *Journal of Terramechanics*, 3(1), 23–30.
40. Escadafal, R. Remote sensing of soil colour: principles and applications, *Remote Sensing Rev*, 1993. 7, pp.261–279.
41. Freitag, D. R. (1966). A dimensional analysis of the performance of pneumatic tires on clay. *Journal of Terramechanics*, 3(3), 51–68. [https://doi.org/10.1016/0022-4898\(66\)90106-6](https://doi.org/10.1016/0022-4898(66)90106-6)
42. Fröhlich OK. *Druckverteilung im Baugrunde. Mit Besonderer Berücksichtigung der Plastischen Erscheinungen*. Julius Springer: Wien, 1934.
43. Gill, W. R., & Glen E. Berg. (1967). *Soil dynamics in tillage and traction*(1st ed.). U.S. Department of Agriculture, Agricultural Research Service.
44. Godwin, R. J., Warner, N. L., & Smith, D. L. O. (1991). The development of a dynamic drop-cone device for the assessment of soil strength and the effects of machinery traffic. *Journal of Agricultural Engineering Research*, 48(C), 123–131. [https://doi.org/10.1016/0021-8634\(91\)80009-4](https://doi.org/10.1016/0021-8634(91)80009-4)
45. Grahn, M. (1991). Prediction of sinkage and rolling resistance for off-the-road vehicles considering penetration velocity. *Journal of Terramechanics*, 28(4), 339–347. [https://doi.org/10.1016/0022-4898\(91\)90015-X](https://doi.org/10.1016/0022-4898(91)90015-X)
46. Hallonborg, U. (1996). Super ellipse as tyre-ground contact area. *Journal of Terramechanics*, 33(3), 125–132. [https://doi.org/10.1016/S0022-4898\(96\)00013-4](https://doi.org/10.1016/S0022-4898(96)00013-4)
47. He, R., Sandu, C., Khan, A.K., Guthrie, A.G., Schalk Els, P., Hamersma, H.A., 2019. Review of terramechanics models and their applicability to real-time applications. *J. Terramechanics* 81, 3–22. <https://doi.org/10.1016/j.jterra.2018.04.003>
48. Hettiaratchi, D. R. P., & Liang, Y. (1987). Nomograms for the estimation of soil strength from indentation tests. *Journal of Terramechanics*, 24(3), 187–198. [https://doi.org/10.1016/0022-4898\(87\)90040-1](https://doi.org/10.1016/0022-4898(87)90040-1)
49. Hillel, D. (1998). *Environmental soil physics: Fundamentals, applications, and environmental considerations*. Academic Press. <https://doi.org/10.1016/B978-012348525-0/50001-0>
50. Inns, F. M., & Kilgour, J. (1978). *Agricultural tyres*. London: Dunlop. Retrieved from http://books.google.co.uk/books/about/Agricultural_tyres.html?id=JB8NAQAAMAAJ&pgis=1
51. Janosi, Z., & Hanamoto, B. (1961). The analytical determination of drawbar pull as a function of slip for tracked vehicles in deformable soils. In 1st international conference on the mechanics of soil-vehicle systems (p. 22). Torino: Edizioni Minerva Tecnica.

-
52. José, Alexandre, Melo, Demattê., Fabrício, da, Silva, Terra., Carlos, Fernando, Quartaroli. (2012). Spectral behaviour of some modal soil profiles from São Paulo State, Brazil. *Bragantia*, [doi: 10.1590/S0006-87052012005000038](https://doi.org/10.1590/S0006-87052012005000038)
53. Jun-Jie Poh and Wei-Ling Wu and Nicholas Wei-Jie Goh and Samuel Ming-Xuan Tan and Samuel Ken-En Gan,(2021).Spectrophotometer on-the-go: The development of a 2-in-1 UV–Vis portable Arduino-based spectrophotometer}, *Sensors and Actuators A: Physical*, vol,325, Pp.112698, ISSN 0924-4247,<https://doi.org/10.1016/j.sna.2021.112698>
54. Keller, T. (2005). A model for the prediction of the contact area and the distribution of vertical stress below agricultural tyres from readily available tyre parameters. *Biosystems Engineering*, 92(1), 85–96. <https://doi.org/10.1016/j.biosystemseng.2005.05.012>
55. Kogure, K., Ohira, Y., & Yamaguchi, H. (1983). Prediction of sinkage and motion resistance of a tracked vehicle using plate penetration test. *Journal of Terramechanics*, 20(3–4), 121–128. [https://doi.org/10.1016/0022-4898\(83\)90043-5](https://doi.org/10.1016/0022-4898(83)90043-5)
56. Konica Minolta (2024). CM-700d Instruction Manual. Retrieved from https://www.konicaminolta.com/instruments/download/instruction_manual/color/pdf/cm-700d_instruction_eng.pdf
57. Kulhawy, F.H., Hirany, A., 2003. Foundations, in: *Encyclopedia of Physical Science and Technology*. Elsevier, pp. 145–166. <https://doi.org/10.1016/B0-12-227410-5/00874-7>
58. Kwanele Phinzi, N., & Njoya Silas Ngetar. (2019). The assessment of water-borne erosion at catchment level using GIS-based RUSLE and remote sensing: A review. *International Soil and Water Conservation Research*, 7(1).
59. Li, X.; Su, Z. Soil spectral behaviour and its relation to soil properties. *Advances in Applied Science Research* 2011, 2(2), pp.691-699.
60. Lyasko, M. (2010). LSA model for sinkage predictions. *Journal of Terramechanics*, 47(1), 1–19. <https://doi.org/10.1016/j.jterra.2009.06.004>
61. Marcia M. Mauli*, Adriana M. Meneghetti and Lúcia H. P. Nóbrega, Terpenes Behavior in Soil, *Terpenoids: Recent Advances in Extraction, Biochemistry and Biotechnology* (2022), Pp: 169-199 (31), [DOI: 10.2174/9781681089645122010010](https://doi.org/10.2174/9781681089645122010010)
62. Mašin, D. Soil Mechanical Behaviour and Its Modelling. In: *Modelling of Soil Behaviour with Hypoplasticity*. Springer Series in Geomechanics and Geoengineering, Springer, Cham, 2019, pp.13–42. ISBN 978-3-030-03975-2. https://doi.org/10.1007/978-3-030-03976-9_2.
63. Mastinu, G., & Pairana, E. (1992). Parameter identification and validation of a pneumatic tyre model. *Vehicle System Dynamics*, 21(sup001), 58–81. <https://doi.org/10.1080/00423119208969999>
64. Meirion-Griffith, G., & Spenko, M. (2011). A modified pressure-sinkage model for small,

- rigid wheels on deformable terrains. *Journal of Terramechanics*, 48(2), 149–155. <https://doi.org/10.1016/j.jterra.2011.01.001>
65. Meirion-Griffith, G., & Spenko, M. (2013). A pressure-sinkage model for small-diameter wheels on compactive, deformable terrain. *Journal of Terramechanics*, 50(1), 37–44. <https://doi.org/10.1016/j.jterra.2012.05.003>
66. Micklethwait, E. W. E. (1944). *Soil mechanics in relation to fighting vehicles*. Britain: Military College of Science.
67. Mouazen, A.; Karoui, R.; Deckers, J.; De Baerdemaeker, J.; Ramon, H. Potential of visible and near-infrared spectroscopy to derive colour groups utilising the Munsell soil colour charts, *Biosyst. Eng.* 2007, 97(2), pp.131–143, ISSN 1537-5110. <https://doi.org/10.1016/j.biosystemseng.2007.03.023>.
68. Nickerson, D. Uniform colour scales: Munsell conversion of OSA committee selection. *Journal of the Optical Society of America* 1975, 65(2), pp.205–207. <https://doi.org/10.1364/JOSA.65.000205>.
69. Ohtomo, K., & Andy Tan, C. C. (2001). Direct measurement of soil deformation using the bead-grid method. *Journal of Agricultural and Engineering Research*, 78(3), 325–332. <https://doi.org/10.1006/jaer.2000.0611>
70. Onafeko, O., & Reece, A. R. (1967). Soil stress and deformation beneath rigid wheels. *Journal of Terramechanics*, 59(1), 59–80.
71. Orna, M. V. The chemical origins of colour, *J. Chem. Ed.*, 1978,55, pp.478–484.
72. Pavia, D. L., Lampman, G. M., & Kriz, G. S. (2001). *Introduction to Spectroscopy* (3rd ed.). Belmont, CA: Thomson Brooks/Cole.
73. Pillinger, G.; Kiss, P.; Géczy, A.; Hudoba, Z. Determination of soil density by cone index data, *J. Terramechanics* 2018, 77, pp. 69-74, ISSN 0022-4898. <https://doi.org/10.1016/j.jterra.2018.03.003>.
74. Pillinger, G. "Deformation and damping of soil under tire". (PhD dissertation,). Szent Istvan University, 2016.
75. Pope, R. G. (1969). The effect of sinkage rate on pressure sinkage relationships and rolling resistance in real and artificial clays. *Journal of Terramechanics*, 6(4), 31–38. [https://doi.org/10.1016/0022-4898\(69\)90015-9](https://doi.org/10.1016/0022-4898(69)90015-9)
76. Pytka, J.A., 2016. *Dynamics of Wheel-Soil Systems*. CRC Press. <https://doi.org/10.1201/b12729>
77. R.E., Eckert., M.K., Wood., W.H., Blackburn., F.F., Peterson. (1979). 1. Impacts of off-road vehicles on infiltration and sediment production of two desert soils. *Journal of Range Management*, [doi: 10.2307/3898025](https://doi.org/10.2307/3898025)

-
78. Rabenhorst, M.; Schmeehling, A.; Thompson, J.; Hirmas, D.; Graham, R.; Rossi, A. Reliability of soil color standards, *Soil Sci. Soc. Am. J.*, 2015, 79(1), pp.193–199. <https://doi.org/10.2136/sssaj2014.10.0401>.
79. Rabot, E., Wiesmeier, M., Schlüter, S. & Vogel, H.-J. (2018). Soil structure as an indicator of soil functions: A review,(*Geoderma*), vol.(314), Pp. (122-137), ISSN 0016-7061,<https://doi.org/10.1016/j.geoderma.2017.11.009>.
80. Raghavan, G. S. V., McKyes, E., Amir, I., Chassé, M., & Broughton, R. S. (1976). Prediction of soil compaction due to off-road vehicle traffic. *Transactions of the ASABE*, 19(3), 153–157. <https://doi.org/10.13031/2013.36079>
81. Randall K. Wood, Larry G. Wells,(1985). Characterizing Soil Deformation by Direct Measurement Within the Profile, Published in *Transactions of the ASAE*, vol. 28, issue 6, Pp. 1754-1758.© 1985 American Society of Agricultural Engineers, <https://doi.org/10.13031/2013.32513>
82. Rawls, W. J., Brakensiek, D. L., & Miller, N. J. (2003). Estimation of soil water properties. *Transactions of the ASAE*, 46(6), 1493-1500.
83. Rawls, W.J., Brakensiek, D.L. (1989). Estimation of Soil Water Retention and Hydraulic Properties. In: Morel-Seytoux, H.J. (eds) *Unsaturated Flow in Hydrologic Modeling*. NATO ASI Series, vol 275. Springer, Dordrecht. https://doi.org/10.1007/978-94-009-2352-2_10
84. Reece, A. R. (1965). Principles of soil-vehicle mechanics. *Proceedings of the Institution of Mechanical Engineers*, 180(1), 45–66. https://doi.org/10.1243/PIME_AUTO_1965_180_009_02
85. Rohani, B., & Baladi, G. Y. (1981). Correlation of mobility cone index with fundamental engineering properties of soil. U.S. Army Engineer Waterways Experiment Station, Vicksburg.
86. Robert, H., Webb. (1982). 4. Off-road Motorcycle Effects on a Desert Soil. *Environmental Conservation*, doi: [10.1017/S0376892900020403](https://doi.org/10.1017/S0376892900020403)
87. Rodnei, Rizzo., Wanderson, de, Souza, Mendes., Nélida, Elizabet, Quiñonez, Silvero., Fabrício, da, Silva, Terra., André, Carnieletto, Dotto., Natasha, Valadares, dos, Santos., Benito, Roberto, Bonfatti., Raúl, Roberto, Poppiel., José, Alexandre, Melo, Demattê. (2021). Point and Imaging Spectroscopy in Geospatial Analysis of Soils. In: Mitran, T., Meena, R.S., Chakraborty, A. (eds) *Geospatial Technologies for Crops and Soils*. Springer, Singapore. https://doi.org/10.1007/978-981-15-6864-0_8
88. Roy-Choudhury, A. K. (2014). Colour measurement instruments. In **Principles of Colour and Appearance Measurement** (pp. 1-12). Woodhead Publishing.
89. SAE. (1967). *Off-road Vehicle Mobility Evaluation*. S.A.E.
90. S. -L. Muraru, V. Muraru, P. Condruz, C. Muraru-Ionel and R. Sfiru, "Soil Spectral

- Analysis," 2021 13th International Conference on Electronics, Computers and Artificial Intelligence (ECAI), Pitesti, Romania, 2021, pp. 1-7, [doi: 10.1109/ECAI52376.2021.9515028](https://doi.org/10.1109/ECAI52376.2021.9515028)
91. S., A., Bowers., S., J., Smith. (1972). 2. Spectrophotometric Determination of Soil Water Content. Soil Science Society of America Journal, [doi: 10.2136/SSSAJ1972.03615995003600060045X](https://doi.org/10.2136/SSSAJ1972.03615995003600060045X)
92. Saakyan, S. 'Soil resistance under load'. Sbornik trudov po zeml 1965. 3, pp.24-31 [Google Scholar](https://scholar.google.com/).
93. Sahar Taghdis, Mohammad Hady Farpoor, Majid Mahmoodabadi, Pedological assessments along an arid and semi-arid transect using soil spectral behavior analysis, CATENA, Volume 214,2022,106288, ISSN 0341-8162, <https://doi.org/10.1016/j.catena.2022.106288>.
94. Salman, N.D.; Pillinger, G.; Hanon, M.M.; Kiss, P. A Modified Pressure–Sinkage Model for Studying the Effect of a Hard Layer in Sandy Loam Soil. Appl. Sci. 2021,11(12), 5499.<https://doi.org/10.3390/app11125499>.
95. Salman, N.D. Load bearing capacity of soil as a homogeneous finite half-space. (PhD dissertation,). Hungarian University of Agriculture and Life Sciences, Szent István Campus, Gödöllő, Hungary, 2022.
96. Salman, N.D.; Pillinger, G.; Kiss, P. Soil behaviour of shallow homogenous upper layer soil, Journal Of Applied Science And Engineering,2022,25(1), pp.159-164. [https://doi.org/10.6180/jase.202202_25\(1\).0016](https://doi.org/10.6180/jase.202202_25(1).0016).
97. Salman, N.D.; Pillinger, G.; Hanon, M.M.; Kiss, P. Design and performance evaluation of bevameter equipment, Journal of Advanced Mechanical Design, Systems, and Manufacturing, 2020, 14(6), PagesAMDSM0084, ISSN18813054. <https://doi.org/10.1299/jamdsm.2020jamdsm0084>.
98. Sánchez-Marañón,M.,Soriano, M., Melgosa,M., Delgado, G.,Delgado,R., (2021).Quantifying the effects of aggregation, particle size and components on the colour of Mediterranean soils, European Journal of Soil Science: Vol.55, Pp. 551-565 Issue 3, <https://doi.org/10.1016/j.sna.2021.112698>
99. Sánchez-Marañón,M, García,P.A., Huertas,R., Hernández-Andrés,J.,Melgosa,M.,(2021). Influence of Natural Daylight on Soil Color Description: Assessment Using a Color-Appearance Model, Soil Science Society of America: Vol.75, Pp. 984-993, Issue 3, <https://doi.org/10.2136/sssaj2010.0336>
100. Scott, C. R. (1994). An Introduction to Soil Mechanics and Foundations. Boston, MA: Springer US. <https://doi.org/10.1007/978-1-4899-7250-7>
101. Siegfried, O., Auer. (1978). Apparatus for measurement of soil moisture content.

-
102. Sitkei, G. "Sinkage and rolling resistance of wheels" *Progress in Agricultural Engineering Sciences*, 2015, 11(1): pp.85–94
103. Sitkei, G., Pillinger, G., Máthé, L., Gurmai, L., Kiss, P., 2019. Methods for generalization of experimental results in terramechanics. *J. Terramechanics* 81, 23–34. <https://doi.org/10.1016/j.jterra.2018.05.004>
104. Sitkei, G. Further studies on the characterization of wood colours 2020. Anomalies of the CIE-Lab system. Department of Wood Engineering, University of Sopron, Hungary. ISSN 2060-3649, ISBN 978-963-359-100-0.
105. Skoog, D. A., Holler, F. J., & Crouch, S. R. (2007). *Principles of Instrumental Analysis* (6th ed.). Belmont, CA: Thomson Brooks/Cole.
106. Sohen, W. (1958). Fundamentals of pressure distribution and soil compaction under tractor tires. *Agricultural Engineering*, 39.
107. Susha Lekshmi, S. U., Singh, D. N., & Shojaei Baghini, M. (2014). A critical review of soil moisture measurement. *Measurement*, 54, 92–105. <https://doi.org/10.1016/j.measurement.2014.04.007>
108. Soydan, H. (2014). Effects of Soil Salinity on Soil Spectral Behaviour.
109. Taghavifar, H., & Mardani, A. (2017). *Off-road Vehicle Dynamics* (Vol. 70). Switzerland: Springer International Publishing. <https://doi.org/10.1007/978-3-319-42520-7>
110. Terzaghi, K., 1943. *Theoretical Soil Mechanics*. John Wiley & Sons, Inc., Hoboken, NJ, USA. <https://doi.org/10.1002/9780470172766>
111. Topp, G. C., Davis, J. L., & Annan, A. P. (1980). *Electromagnetic determination of soil water content: Measurements in coaxial transmission lines*. *Water Resources Research*, 16(3), 574-582. <https://doi.org/10.1029/WR016i003p00574>
112. Upadhyaya, S. K., Wulfsohn, D., & Mehlschau, J. (1993). An instrumented device to obtain traction-related parameters. *Journal of Terramechanics*, 30(1), 1–20. [https://doi.org/10.1016/0022-4898\(93\)90027-U](https://doi.org/10.1016/0022-4898(93)90027-U)
113. Viscarra Rossel, R. A., Minasny, B., Roudier, P., McBratney, A.B. Colour space models for soil science, *Geoderma* 2006,133(3–4), pp.320-337, ISSN 0016-7061. <https://doi.org/10.1016/j.geoderma.2005.07.017>.
114. Whitlow, R. (1995). *Basic Soil Mechanics* (3rd ed.). England: Longman Group Limited.
115. William J. Chancellor. J. Soil physical properties. In *Advances in soil dynamics*; Shrini K. Upadhyaya, William J. Chancellor, John V. Perumpral, Dvoralai Wulfsohn, Thomas R. Way; American Society of Agricultural Engineers (ASAE): 2950 Niles Road, St. Joseph, Michigan 49085-9659, USA, 1994, 1, pp. 21–254. <https://doi.org/10.13031/2013.22670>

-
116. Wismer, R. D., & Luth, H. J. (1973). Off-road traction prediction for wheeled vehicles. *Journal of Terramechanics*, 10(2), 49–61. [https://doi.org/10.1016/0022-4898\(73\)90014-1](https://doi.org/10.1016/0022-4898(73)90014-1)
117. Wong, J. Y. (1979). Soil mechanics for off-road vehicle engineering: Book review. *Canadian Geotechnical Journal*, 16(3), 624–626. <https://doi.org/10.1139/t79-072>
118. Wong, J. Y. (1983). Evaluation of soil strength measurements. Canada: National Research Council.
119. Wong, J. Y. (2001). *Theory of Ground Vehicles (Third)*. Canada: John Wiley & Sons.
120. Wong, J.Y. Performance of Off-Road Vehicles. *Terramechanics and Off-Road Vehicle Engineering*, 2nd Eds.; Ottawa-Canada, 2010a; pp. 129-153. ISBN 9780750685610. <https://doi.org/10.1016/B978-0-7506-8561-0.00006-3>.
121. Wong, J. Y. (2010). *Terramechanics and Off-Road Vehicle Engineering (Second)*. Oxford, UK: Elsevier Ltd. <https://doi.org/10.1016/C2009-0-00403-6>
122. Wong, J. Y., & Asnani, V. M. (2008). Study of the correlation between the performances of lunar vehicle wheels predicted by the Nepean wheeled vehicle performance model and test data. *Proceedings of the Institution of Mechanical Engineers, Part D: Journal of Automobile Engineering*, 222(11), 1755–1770. <https://doi.org/10.1243/09544070JAUTO811>
123. Wong, J. Y., & Preston-Thomas, J. (1983). On the characterization of the shear stress-displacement relationship of terrain. *Journal of Terramechanics*, 19(4), 225–234. [https://doi.org/10.1016/0022-4898\(83\)90028-9](https://doi.org/10.1016/0022-4898(83)90028-9)
124. Xuewu, J., Jide, Z., & Xiding, Q. (1996). Effects of loading patterns on the pressure-sinkage relation of dry loose sand. *Journal of Terramechanics*, 33(1), 13–20. [https://doi.org/10.1016/0022-4898\(96\)00005-5](https://doi.org/10.1016/0022-4898(96)00005-5)
125. Yong, R. N., Fattah, E. A., & Skiadas, N. (1984). *Vehicle Traction Mechanics*. Amsterdam: Elsevier Science.
126. Youssef, A.-F. A., & Ali, G. A. (1982). Determination of Soil Parameters using Plate Test. *Journal of Terramechanics*, 19(2), 129–147. [https://doi.org/10.1016/0022-4898\(82\)90016-7](https://doi.org/10.1016/0022-4898(82)90016-7)

A2. Publications related to the dissertation

Referred papers in foreign languages:

1. **Ahmed A.E.E.**, El Hariri A., Kiss P., (2023): Soil Spectral Behavior Related to Its Load-Bearing Capacity Based on Moisture Content. Applied Sciences.13(6):3498. <https://doi.org/10.3390/app13063498> (Q2)
2. El Hariri A., **Ahmed E. E. A.**, Kiss P., (2023): Review on soil shear strength with loam sand soil results using direct shear test, Journal of Terramechanics, vol. 107, Pp.47-59, ISSN 0022-4898,<https://doi.org/10.1016/j.jterra.2023.03.003>. (Q1)
3. Pillinger G., **Ahmed E.E.A.**, Kornél B., Kiss P.,(2023): Correlations between moisture content and colour spectrum of sandy soils, Journal of Terramechanics, vol.108, Pp. 39-45, ISSN 0022-4898,<https://doi.org/10.1016/j.jterra.2023.05.002>. (Q1)
4. El Hariri A., **Ahmed A.E.E.**, Kiss P., (2023): Sandy Loam Soil Shear Strength Parameters and Its Colour. Applied Sciences. 2023; 13(6):3847. <https://doi.org/10.3390/app13063847> (Q2)
5. **Ahmed E. E. A.**, Pillinger G., Kiss P., (2022): The influence of sandy loam soil moisture content on its load-bearing capacity, Mechanical Engineering Letters, Gödöllő, Hungary, 2021, Vol. 22, Pp.15-25. HU ISSN 2060-3789.
6. **Ahmed A.E.E.**, El Hariri A., Kiss P., (2021): Soil strength and load bearing capacity measurement techniques. Hungarian Agricultural Engineering (40). pp. 16-27. ISSN 0864-7410 <https://doi.org/10.17676/HAE.2021.40.16>
7. MohammedZein, M. A., Michéli, E., Rotich, B., Justine, P. N., **Ahmed, A. E. E.**, Tharwat, H., Csorba, Á. (2023): Rapid Detection of Soil Texture Attribute based on Mid-Infrared Spectral Library In Salt Affected Soils of Hungary. Hungarian Agricultural Engineering: periodical of the committee of Agricultural and Biosystem Engineering of the Hungarian Academy of Sciences and Hungarian University of Agriculture and Life Sciences Institute of Technology (42). Pp. 5-13. ISSN 0864-7410 (print); 2415-9751 <https://doi.org/10.17676/HAE.2023.42.5>
8. **Ahmed A. E. E.**, Pillinger G., Kiss P., (2025). The Connection of Sandy Loam Soil Moisture Content to the Load-Bearing Capacity. Ingineria automobilului, (x), xx-xx. ISSN xxxx – xxxx <https://siar.ro/publicatii/> (accepted)

Refereed papers in Hungarian:

9. **Ahmed E.E.A.**, Kiss P., (2022): Homokos Vályogtalaj Teherbíróképességének vizsgálata Bevaméterrel, *Mezőgazdasági Technika*, ISSN 0026-1890 : 63 (6), pp 2-6

International conference proceedings:

10. **Ahmed E. E. A.**, Pillinger G., Kiss P., (2023): Moisture content impacts on soil load bearing capacity and its spectral behaviour. 16th European-African Regional Conference of the ISTVS, Lublin, Poland, October 11-13, 2023, <https://doi.org/10.56884/DTUX6735>
11. Pillinger G., **Ahmed E. E. A.**, Kiss P., (2024): Effect of initial soil colour on sandy soil moisture content determination, 21st International and 12th Asia-Pacific Regional Conference of the ISTVS, Yokohama, Japan, October 28-31, 2024, <https://doi.org/10.56884/GV41C6MW>

International conference abstracts:

12. **Ahmed E. E. A.**, Pillinger G., Kiss P., (2024): Investigating the spectral behaviour and load bearing of soil, In Bakacsi, Zsófia; Horel, Ágota; Mészáros, János; Rékási, Márk; Takács, Tünde (eds.), *Alternatives to Reduce Soil Degradation (ARSD2024) - Book of abstracts*, Conference: Budapest, Hungary 2024.05.07., -2024.05.07. Bp: HUN-REN Centre for Agricultural Research, Vol. 62, Pp. 35-35, ISBN: 9786155387128
13. **Ahmed E. E. A.**, Pillinger G., Kiss P., (2024): Correlation Between Soil Moisture, Spectral Response, and Load Capacity, In *Annual Conference 2024 Abstract Book: British Society of Soil Science (BSSS) (2024)* 115 p. pp. 107-107. , 1 p.

A3. Pressure-sinkage curves

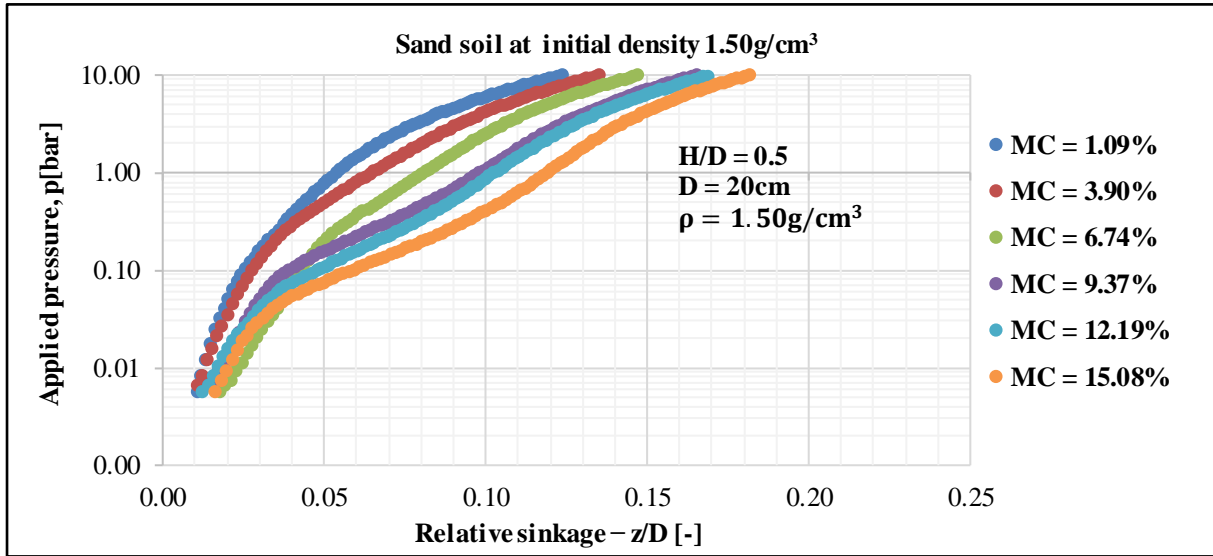


Figure A3.1. Sand soil texture pressure – sinkage relationship at different moisture contents for 1.50 g/cm³ density.

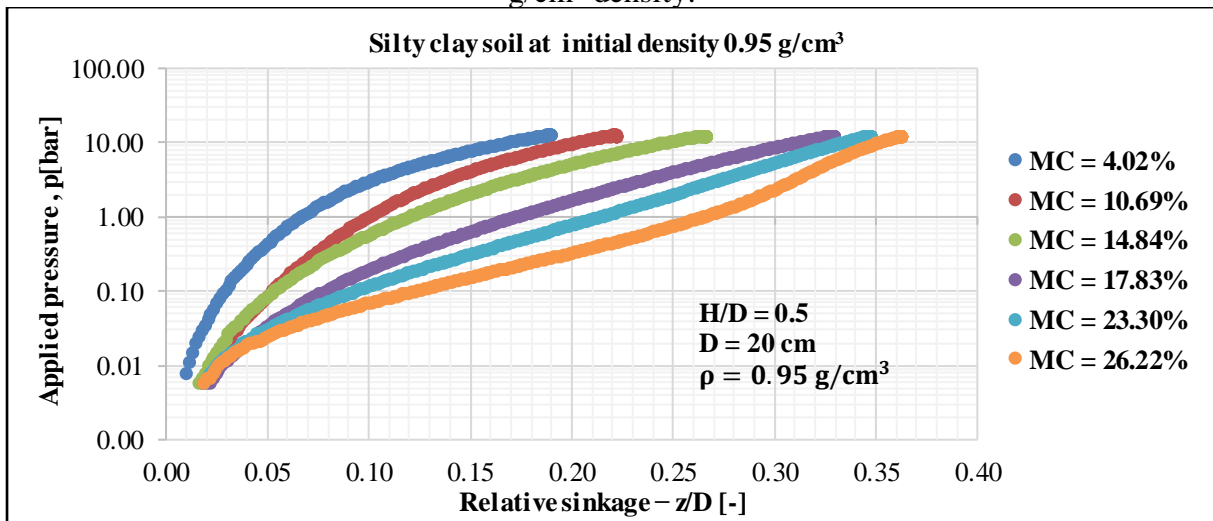


Figure A3.2. Silty clay soil texture pressure – sinkage relationship at different moisture contents for 0.95 g/cm³ density.

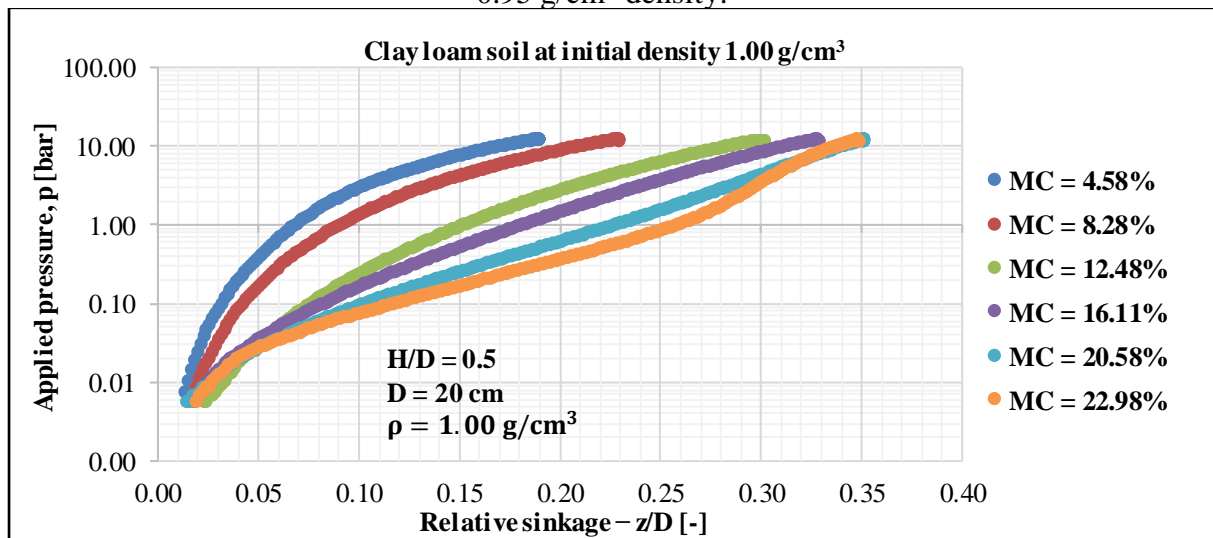


Figure A3.3. Clay loam soil texture pressure – sinkage relationship at different moisture contents for 1.00 g/cm³ density.

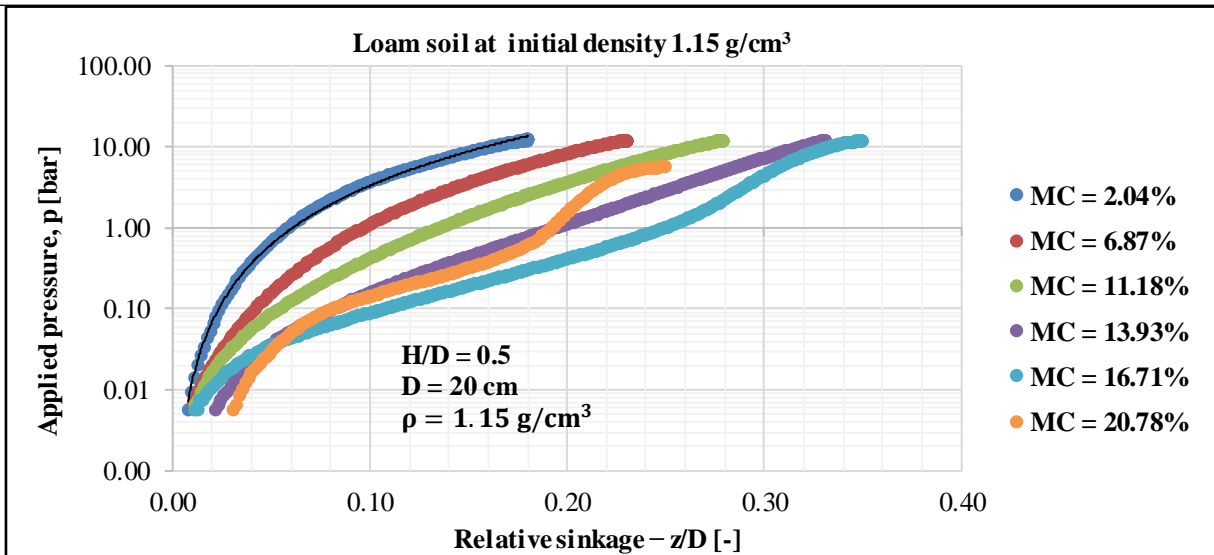


Figure A3.4. Loam soil texture pressure – sinkage relationship at different moisture contents for 1.15 g/cm³ density.

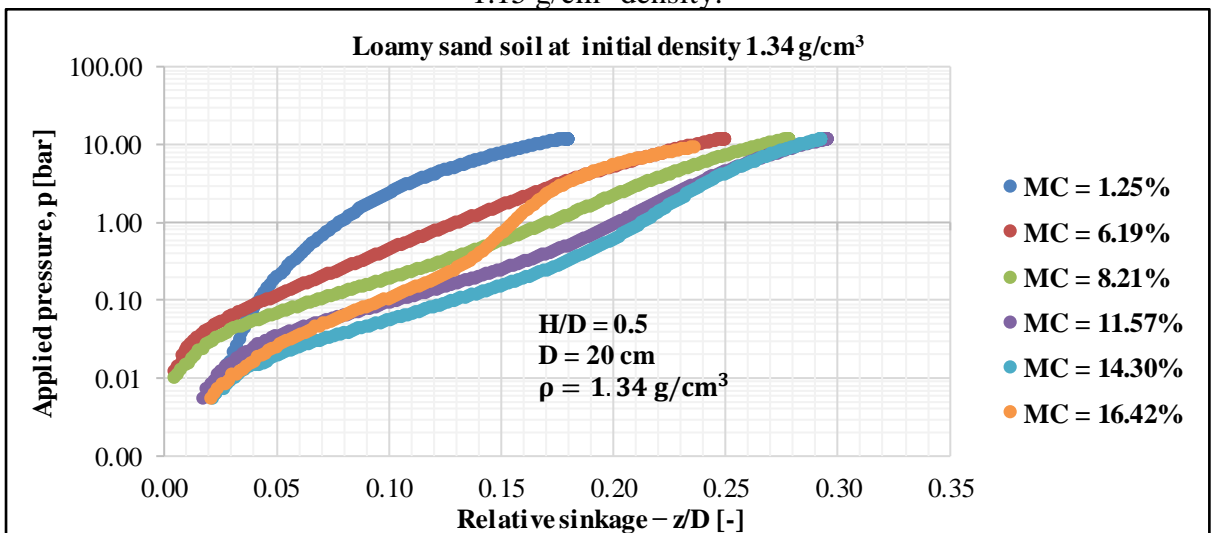


Figure A3.5. Loamy sand soil texture pressure – sinkage relationship at different moisture contents for 1.34 g/cm³ density.

A4. Influence of moisture content on soil relative sinkage and relative density ratio curves

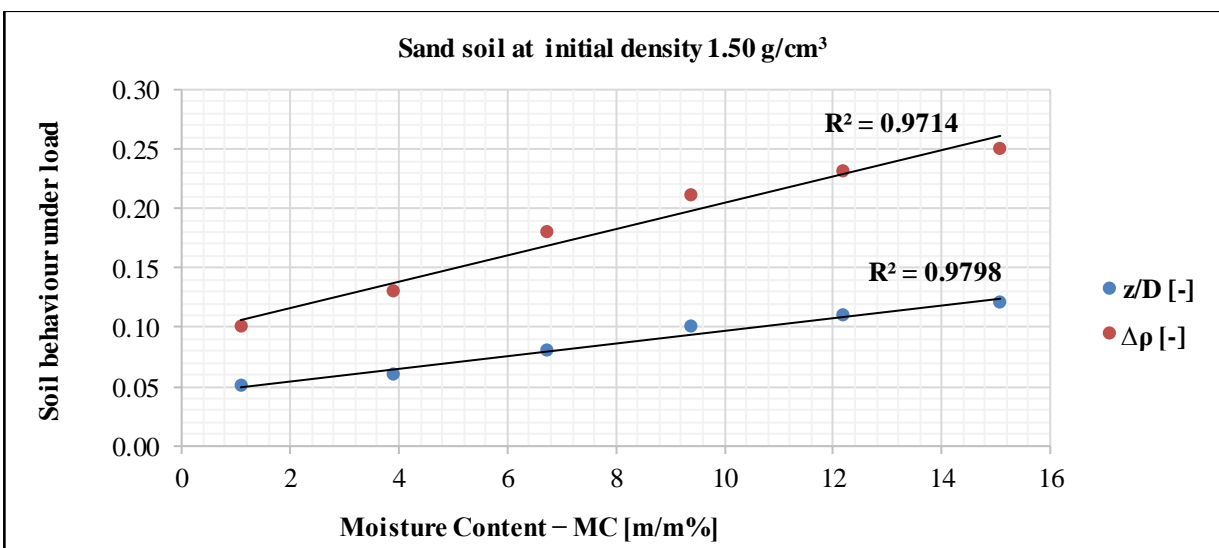


Figure A4.1. The relative sinkage and density ratio of sand soil as a function of moisture content.

APPENDICES

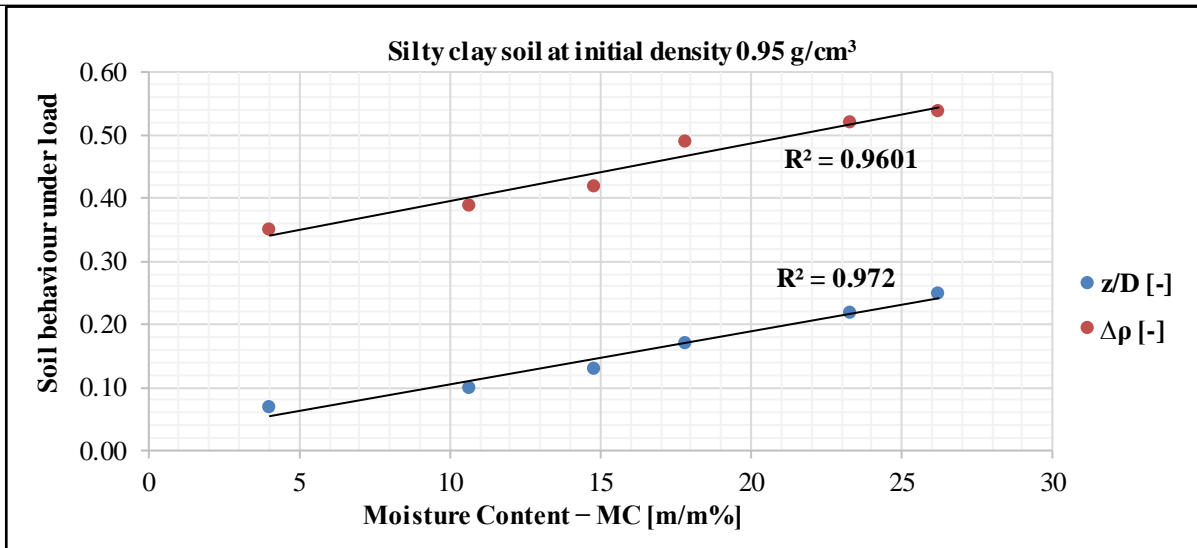


Figure A4.2. The relative sinkage and density ratio of silty clay soil as a function of moisture content.

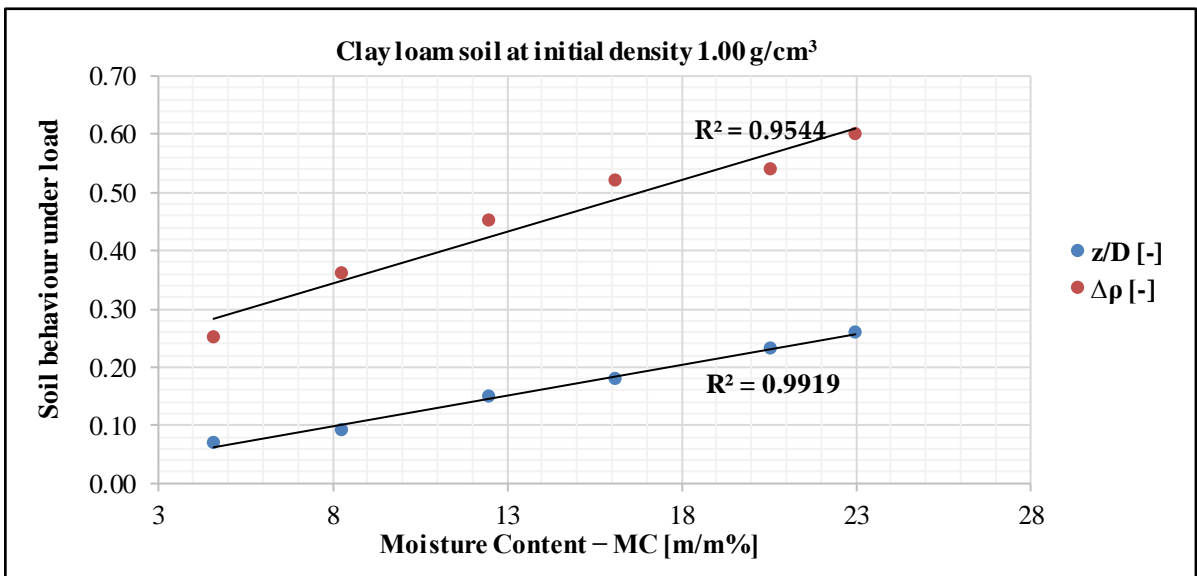


Figure A4.3. The relative sinkage and density ratio of clay loam soil as a function of moisture content.

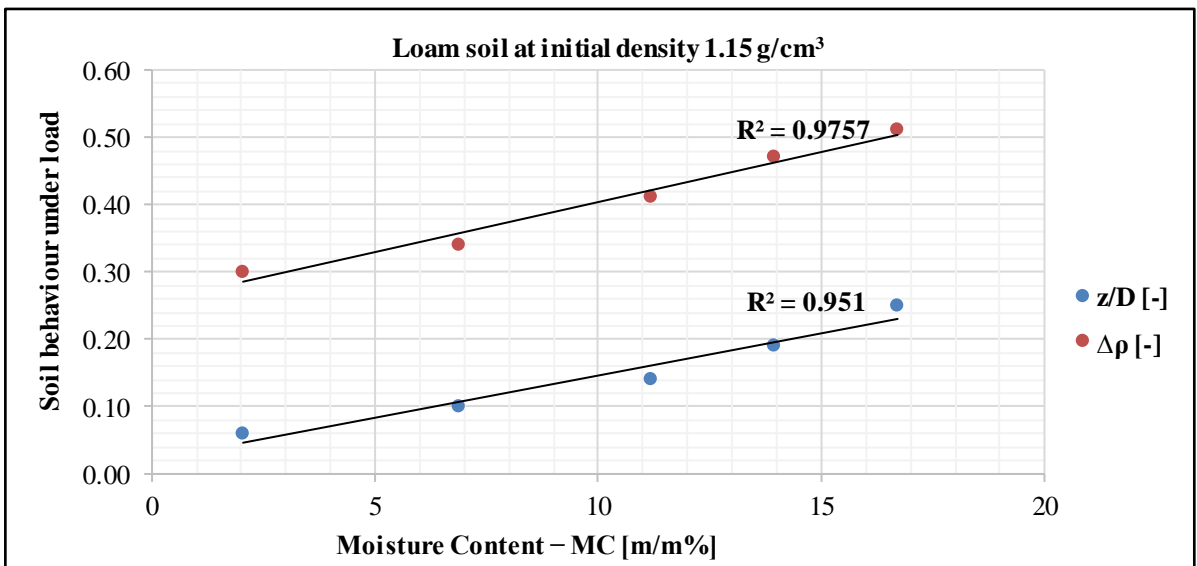


Figure A4.4. The relative sinkage and density ratio of loam soil as a function of moisture content.

APPENDICES

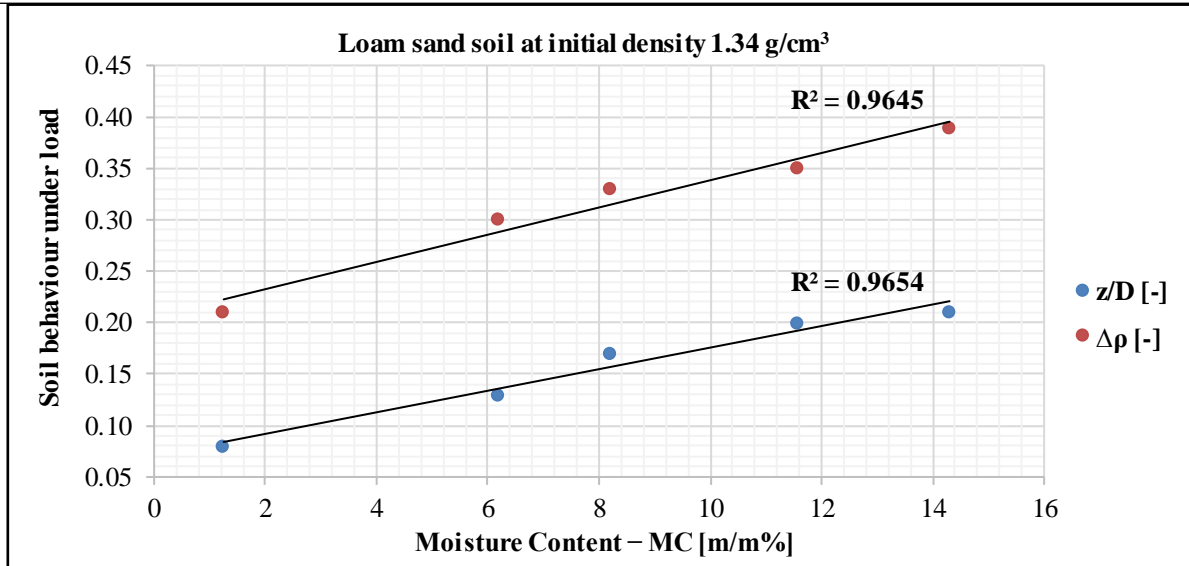


Figure A4.5. The relative sinkage and density ratio of loamy sand soil as a function of moisture content.

A5. Soil spectral behaviour curves

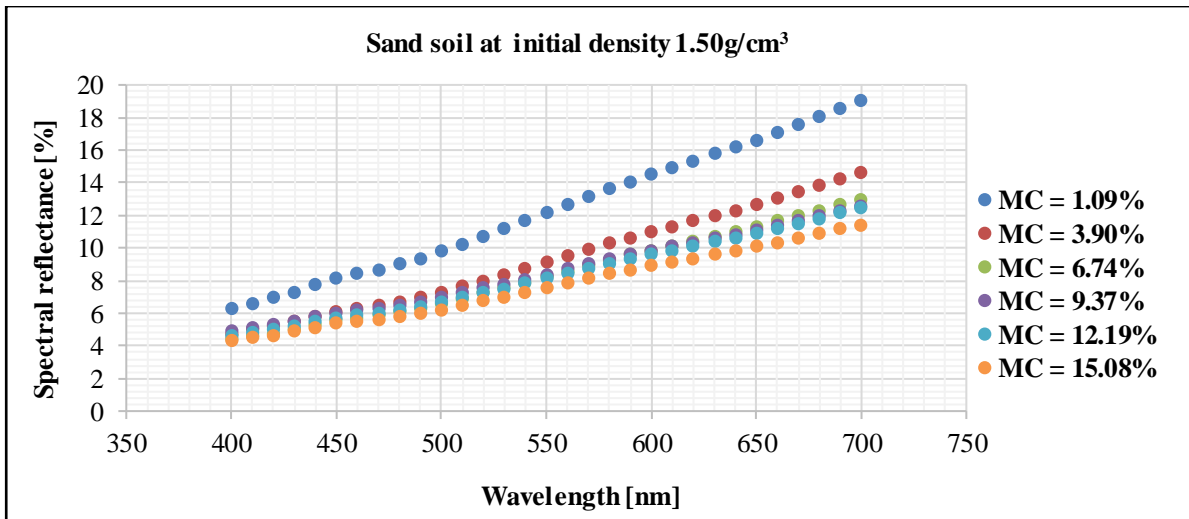


Figure A5.1. The spectral reflectance of sand soil in the visible range at varying moisture content levels.

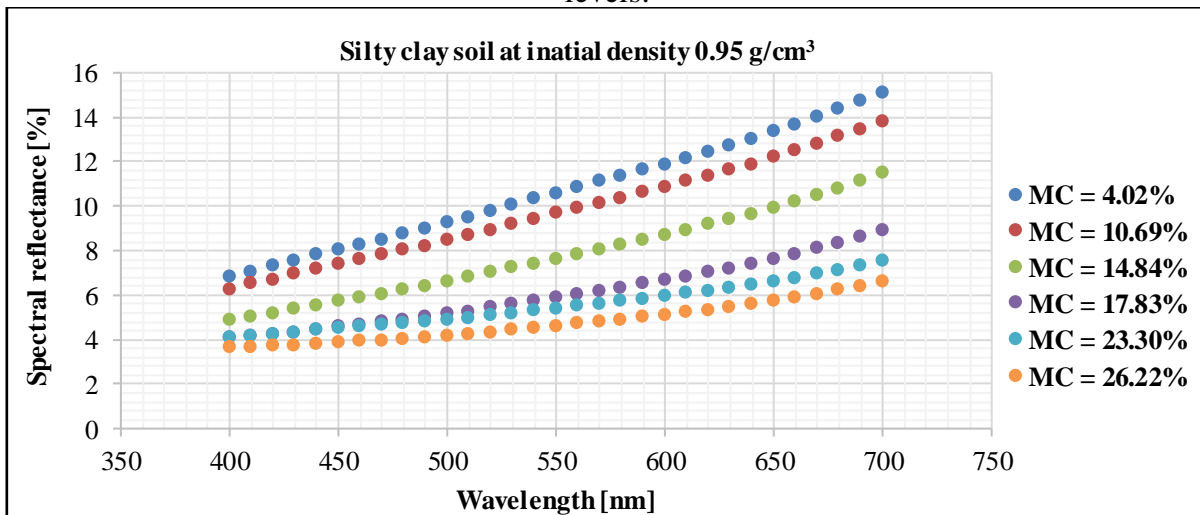


Figure A5.2. The spectral reflectance of silty clay soil in the visible range at varying moisture content levels.

APPENDICES

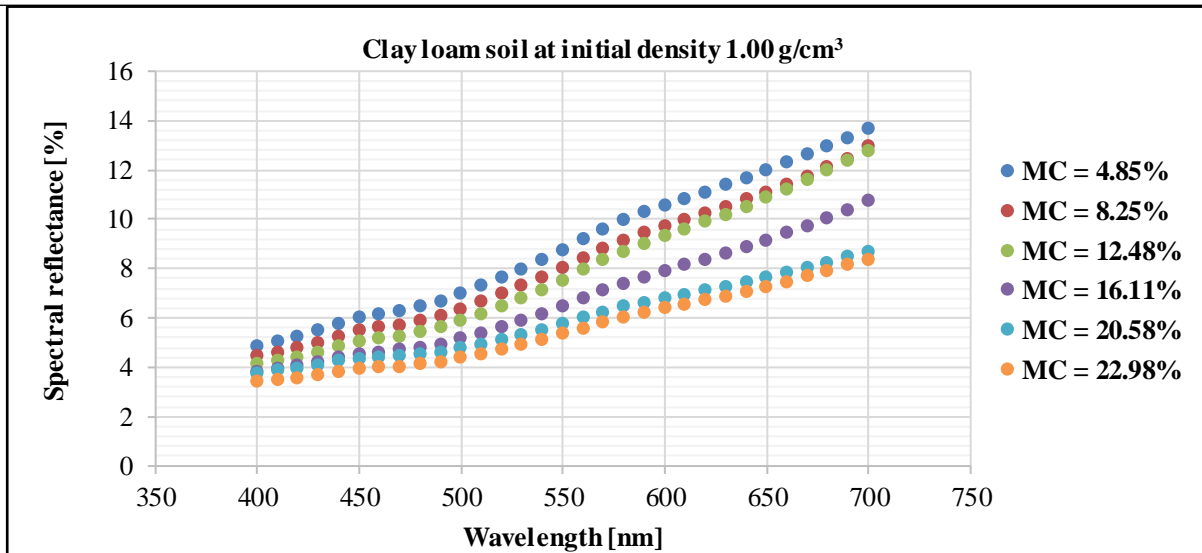


Figure A5.3. The spectral reflectance of clay loam soil in the visible range at varying moisture content levels.

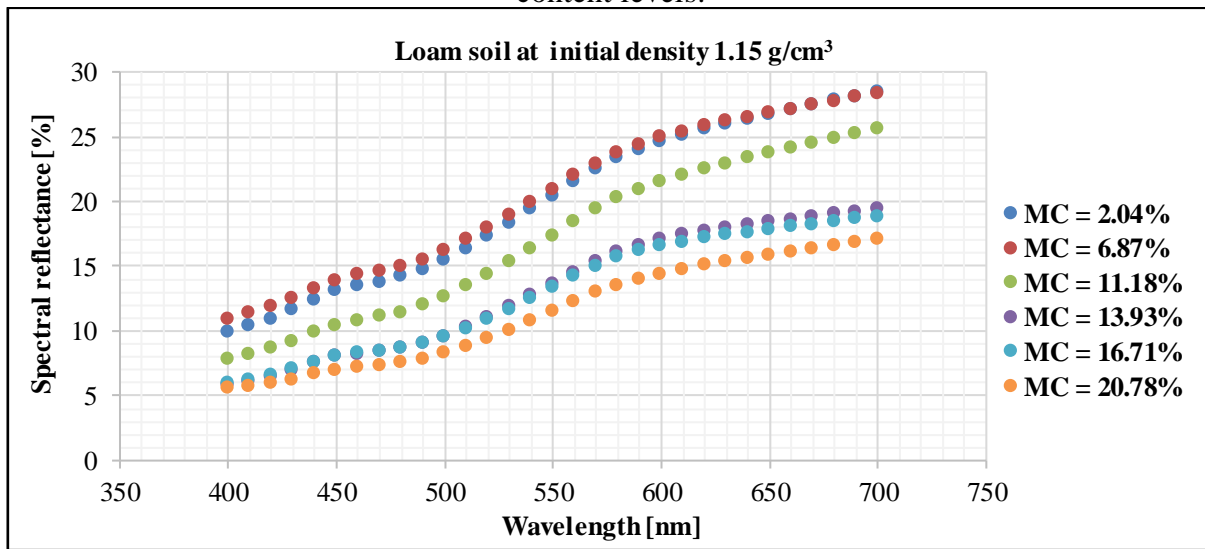


Figure A5.4. The spectral reflectance of loam soil in the visible range at varying moisture content levels.

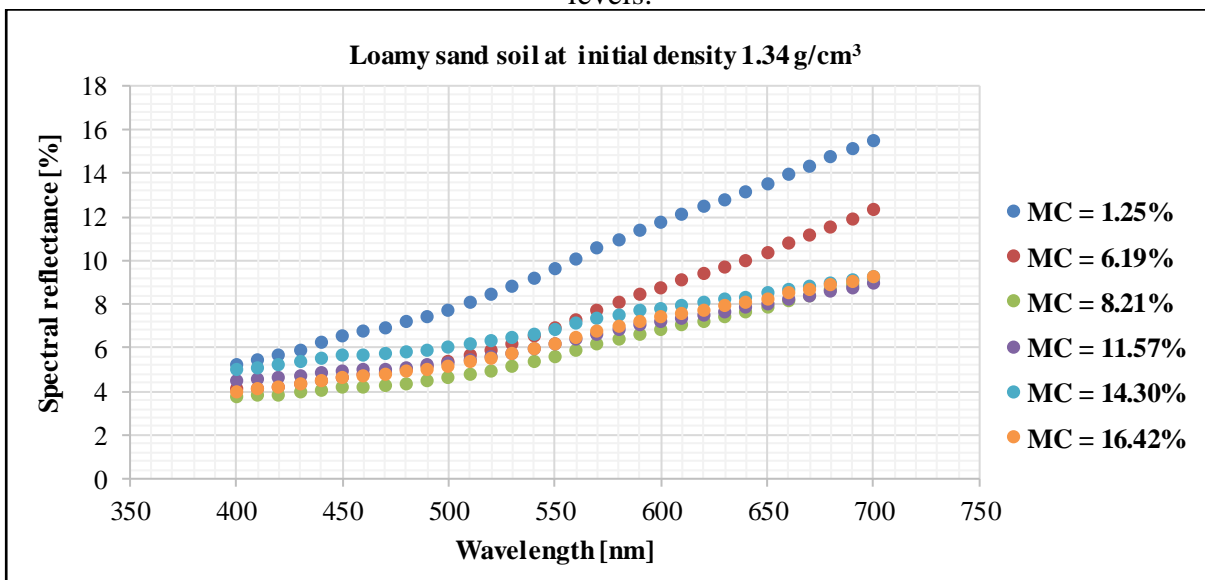


Figure A5.5. The spectral reflectance of loamy sand soil in the visible range at varying moisture content levels.

A6. Influence of moisture content on spectral reflectance curves

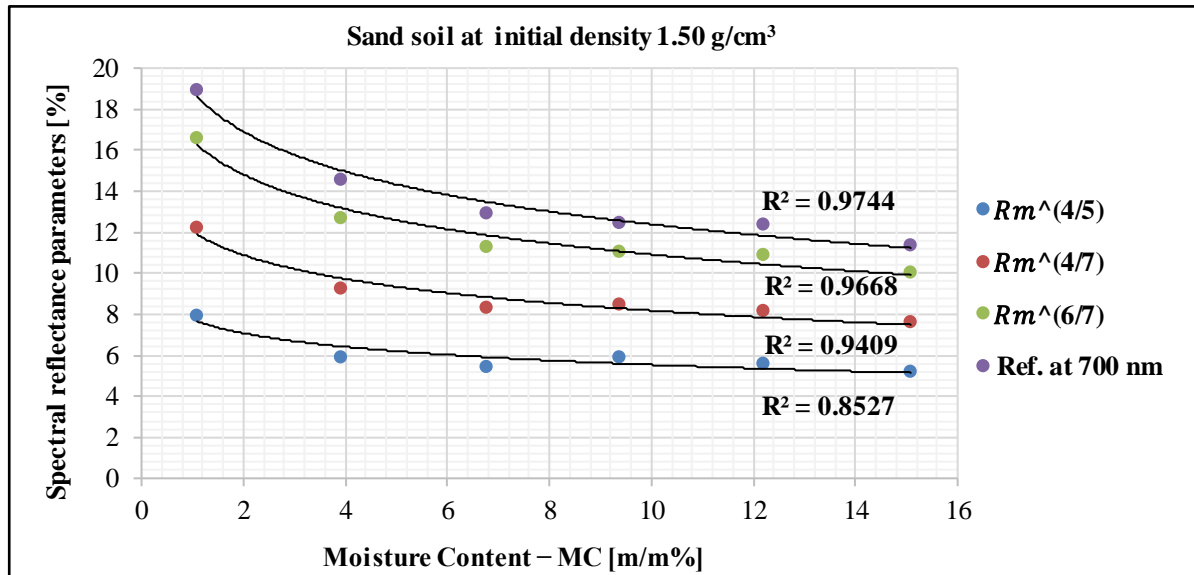


Figure A6.1. Spectral reflectance parameter – moisture content relationship for sand.

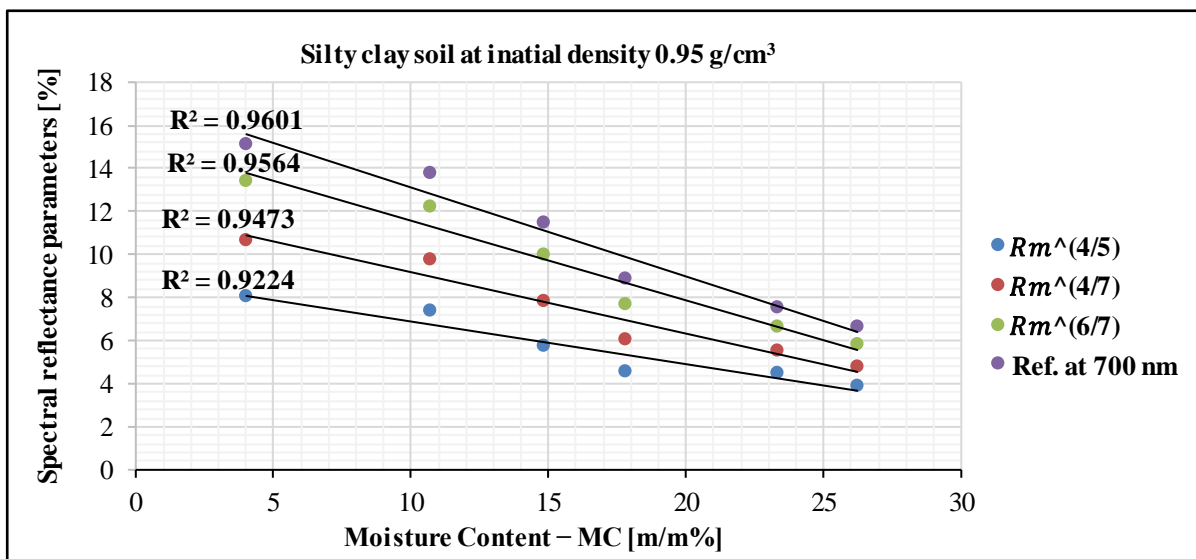


Figure A6.2. Spectral reflectance parameter – moisture content relationship for silty clay.

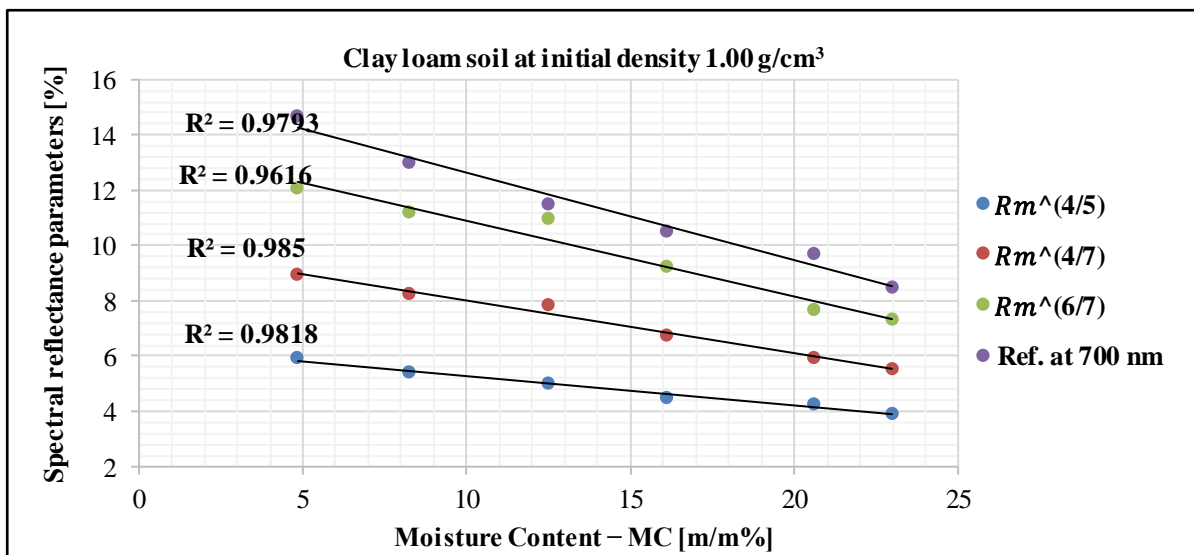


Figure A6.3. Spectral reflectance parameter – moisture content relationship for clay loam.

APPENDICES

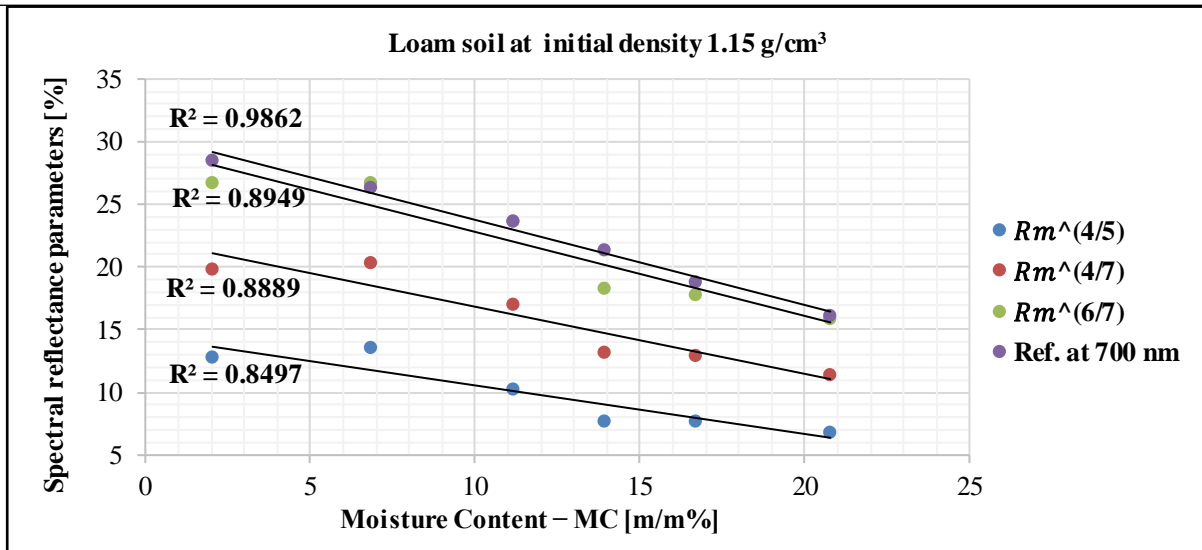


Figure A6.4. Spectral reflectance parameter – moisture content relationship for loam.

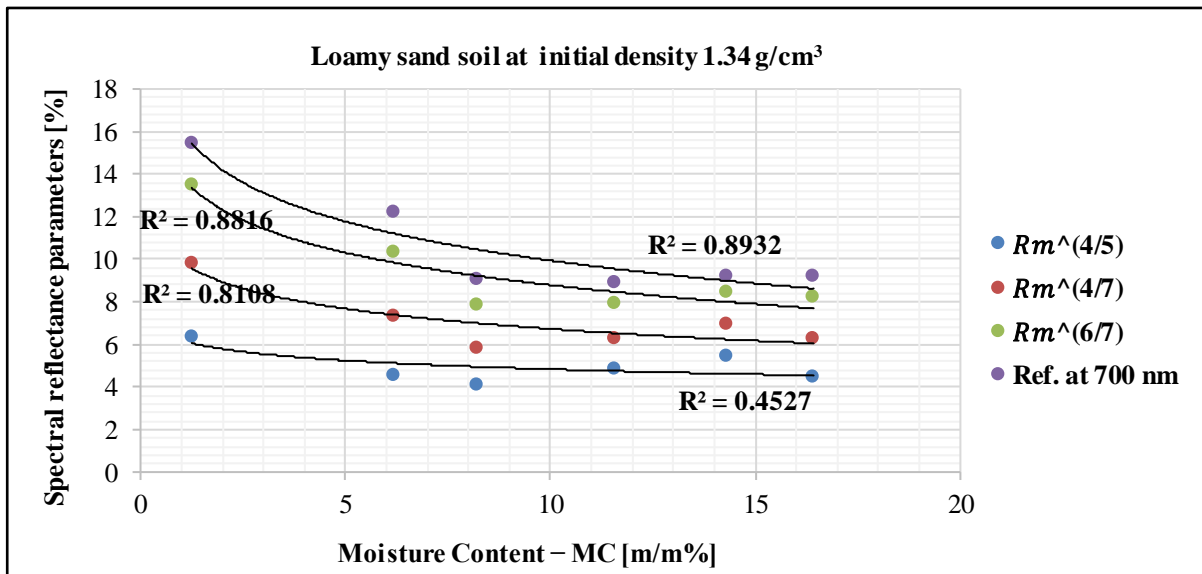


Figure A6.5. Spectral reflectance parameter – moisture content relationship for loamy sand.

A7. Soil relative density ratio – spectral reflectance at 700 nm relationship curves

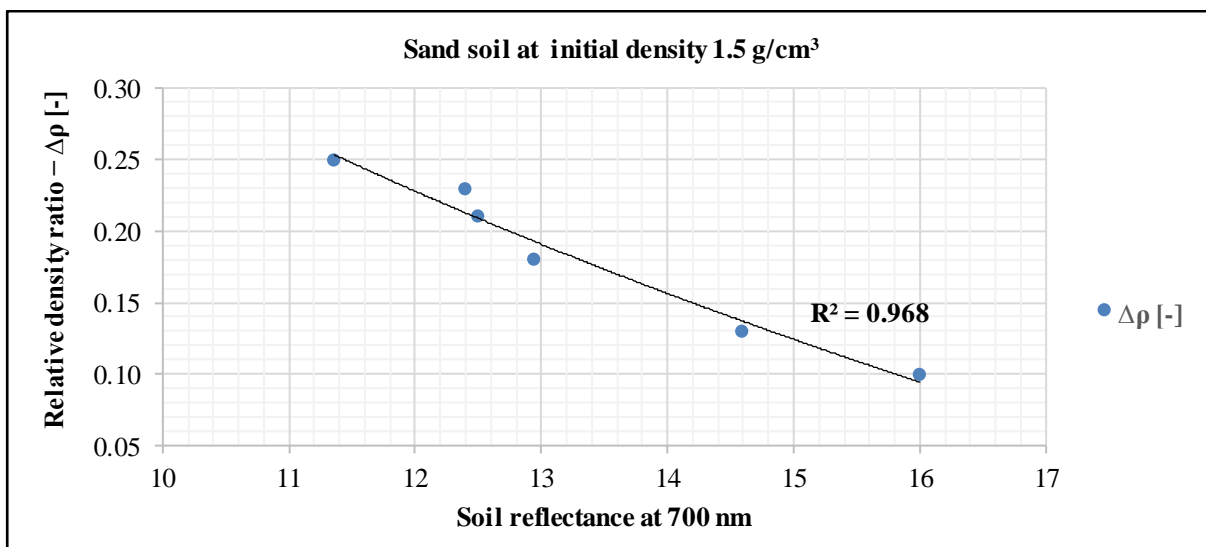


Figure A7.1. Soil relative density ratio – Spectral reflectance at 700 nm relationship for sand.

APPENDICES

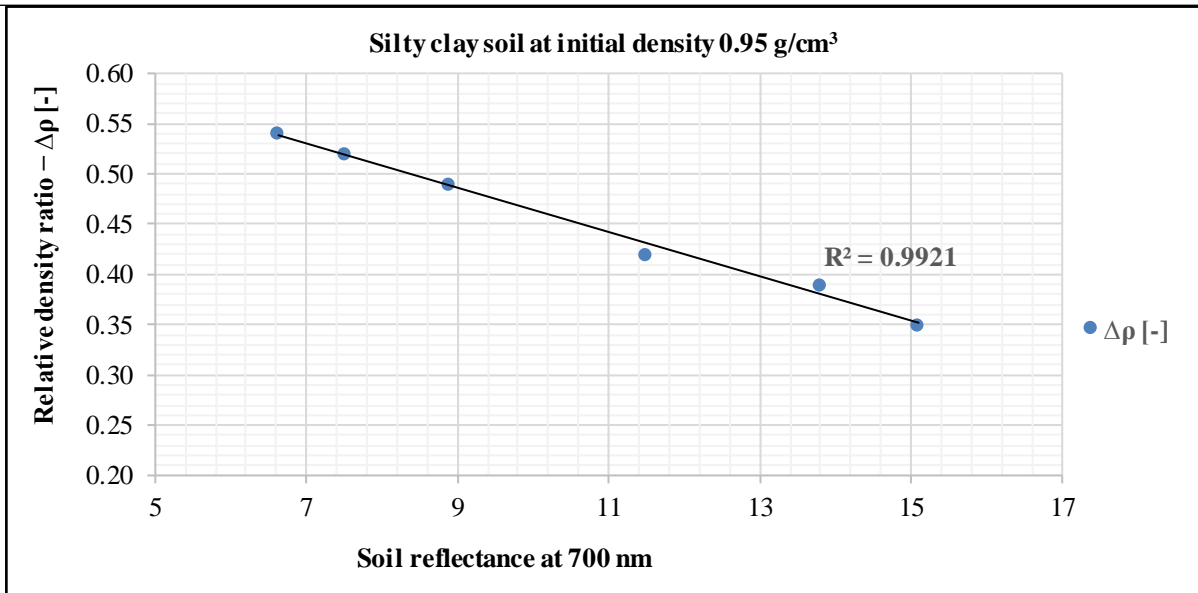


Figure A7.2. Soil relative density ratio – Spectral reflectance at 700 nm relationship for silty clay.

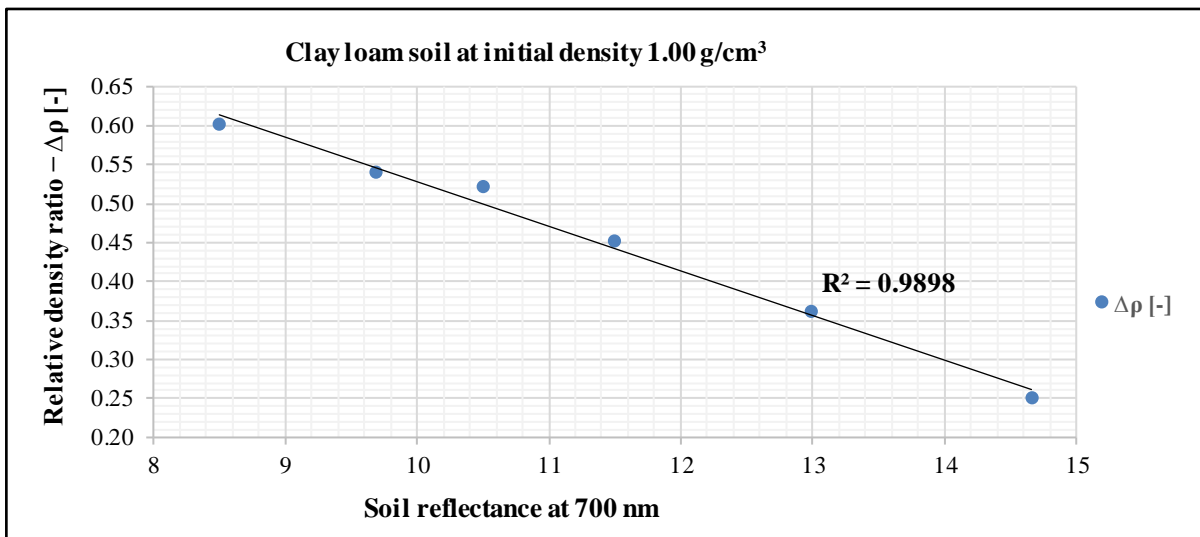


Figure A7.3. Soil relative density ratio – Spectral reflectance at 700 nm relationship for clay loam.

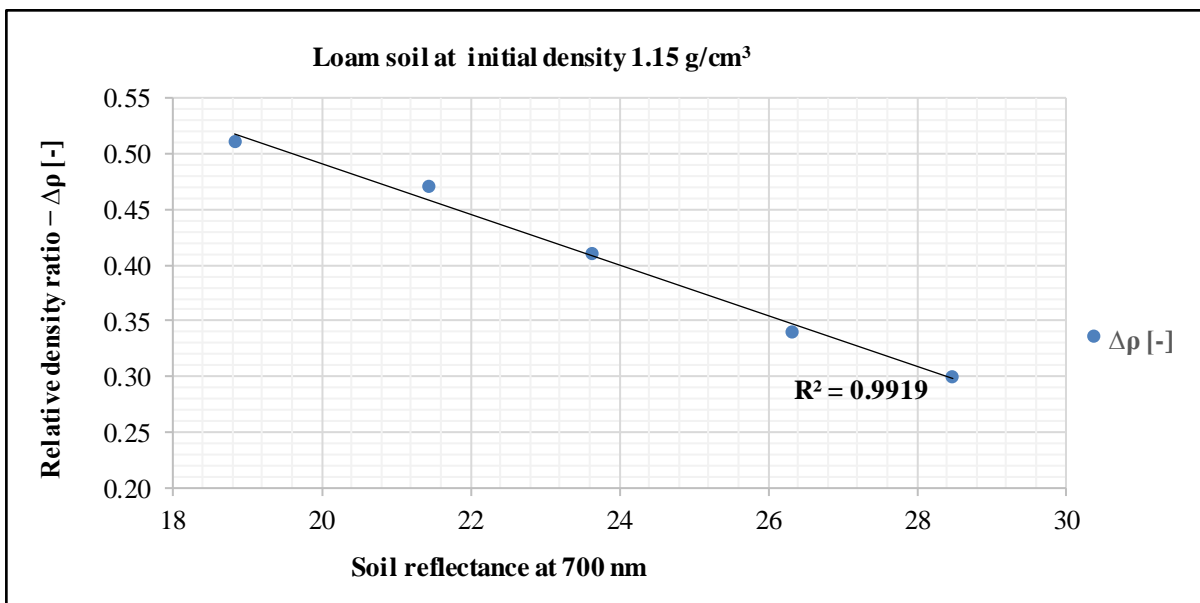


Figure A7.4. Soil relative density ratio – Spectral reflectance at 700 nm relationship for loam.

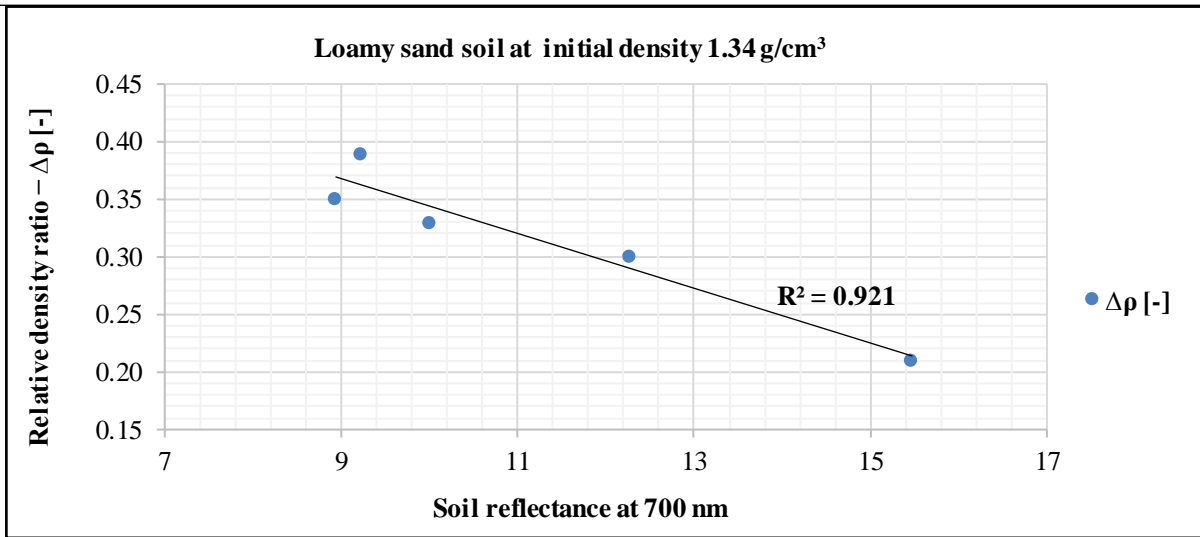


Figure A7.5. Soil relative density ratio – Spectral reflectance at 700 nm relationship for loamy sand.

A8. Soil relative sinkage – spectral reflectance at 700 nm relationship curves

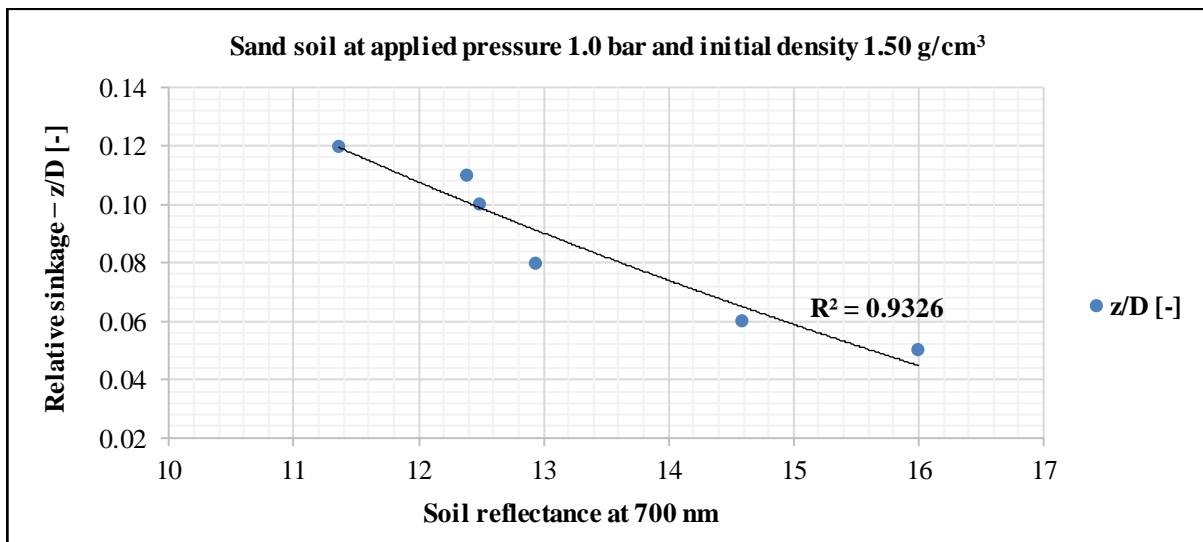


Figure A8.1. Soil relative sinkage – Spectral reflectance at 700 nm relationship for sand.

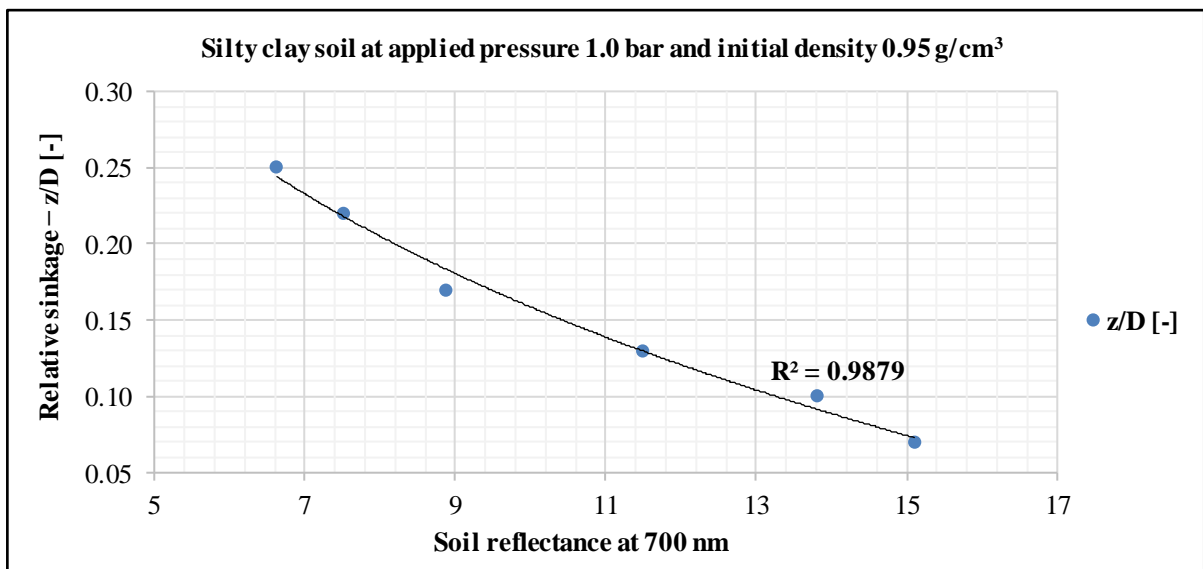


Figure A8.2. Soil relative sinkage – Spectral reflectance at 700 nm relationship for silty clay.

APPENDICES

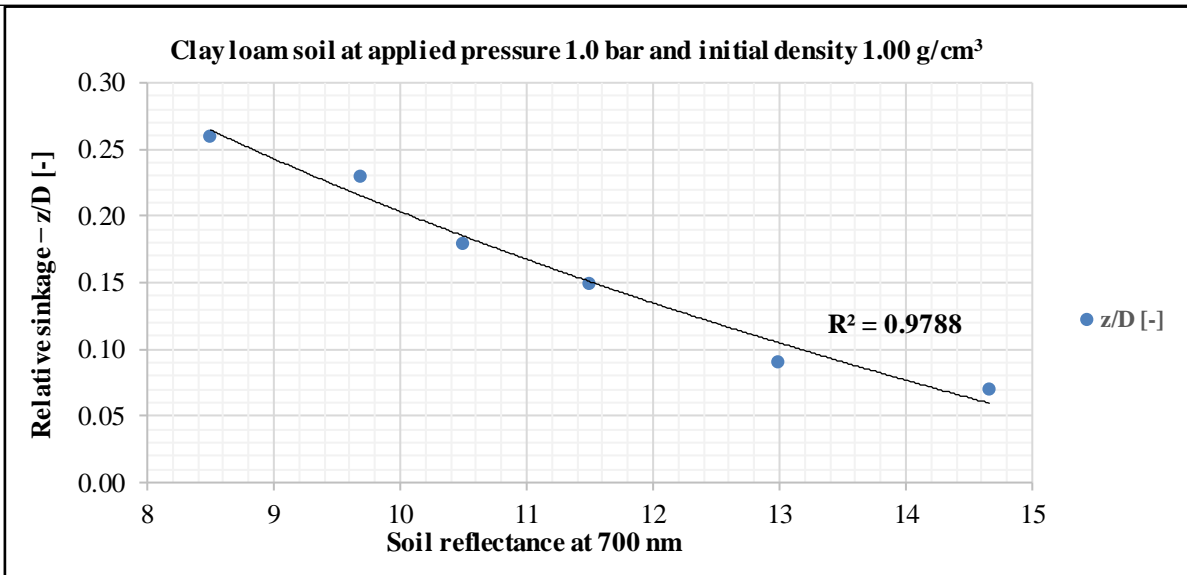


Figure A8.3. Soil relative sinkage – Spectral reflectance at 700 nm relationship for clay loam.

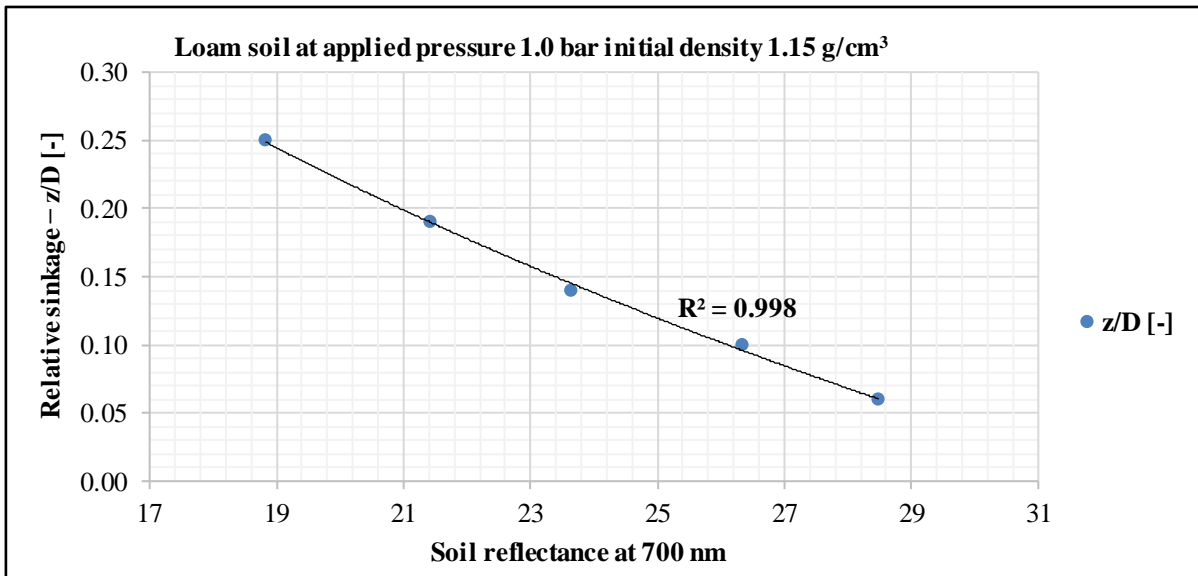


Figure A8.4. Soil relative sinkage – Spectral reflectance at 700 nm relationship for loam.

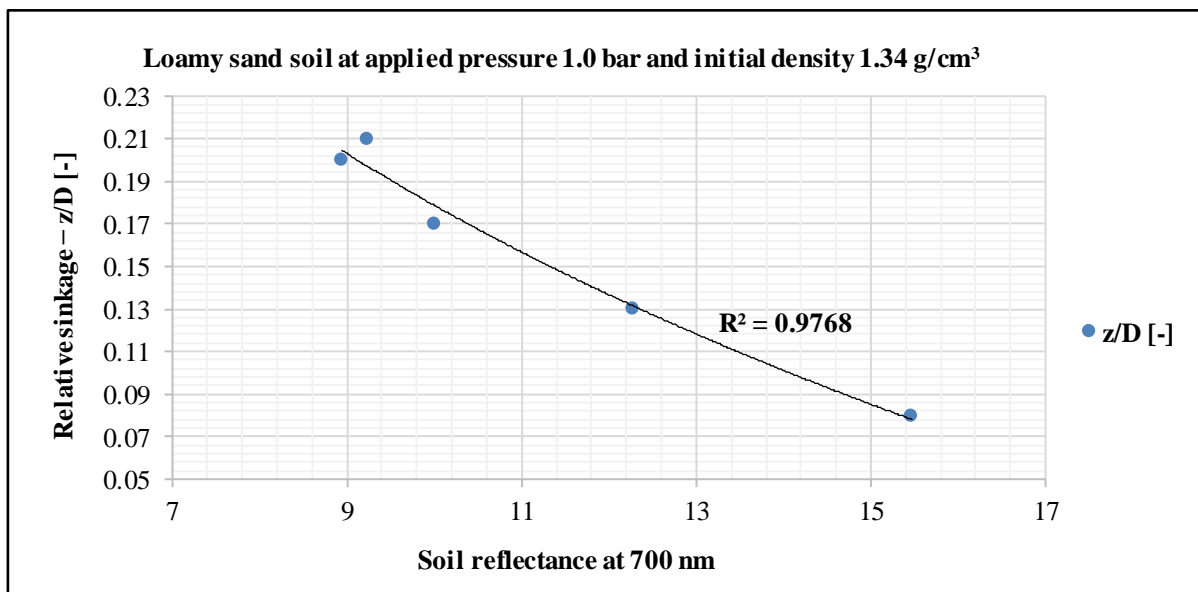


Figure A8.5. Soil relative sinkage – Spectral reflectance at 700 nm relationship for loam sand

A9. Influence of moisture content on spectral reflectance curves

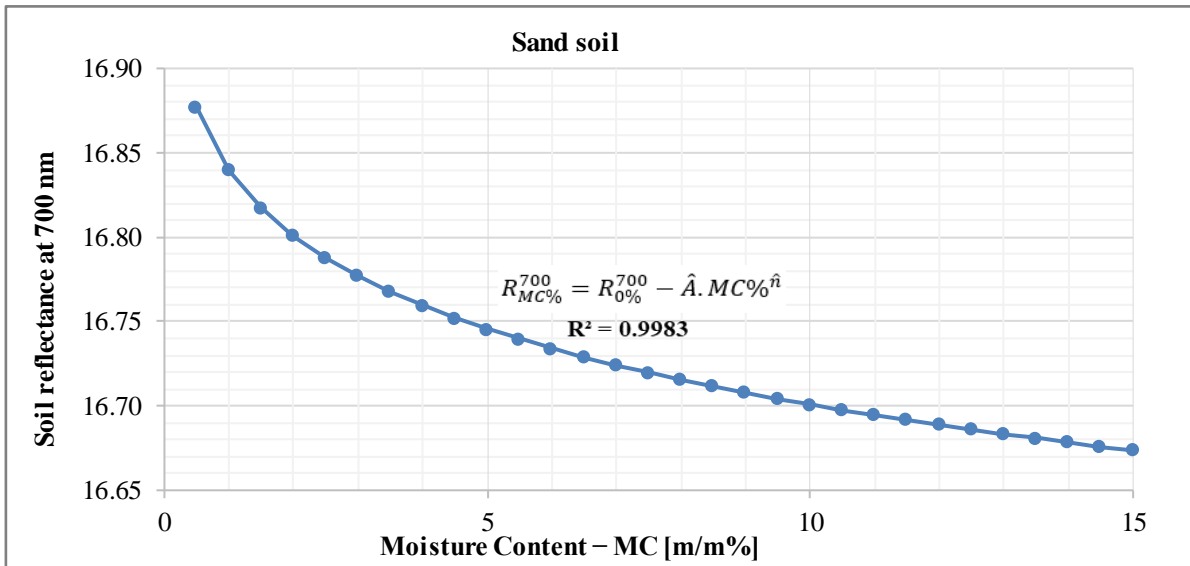


Figure A9.1. Spectral reflectance at 700 nm – soil moisture content relationship for sand.

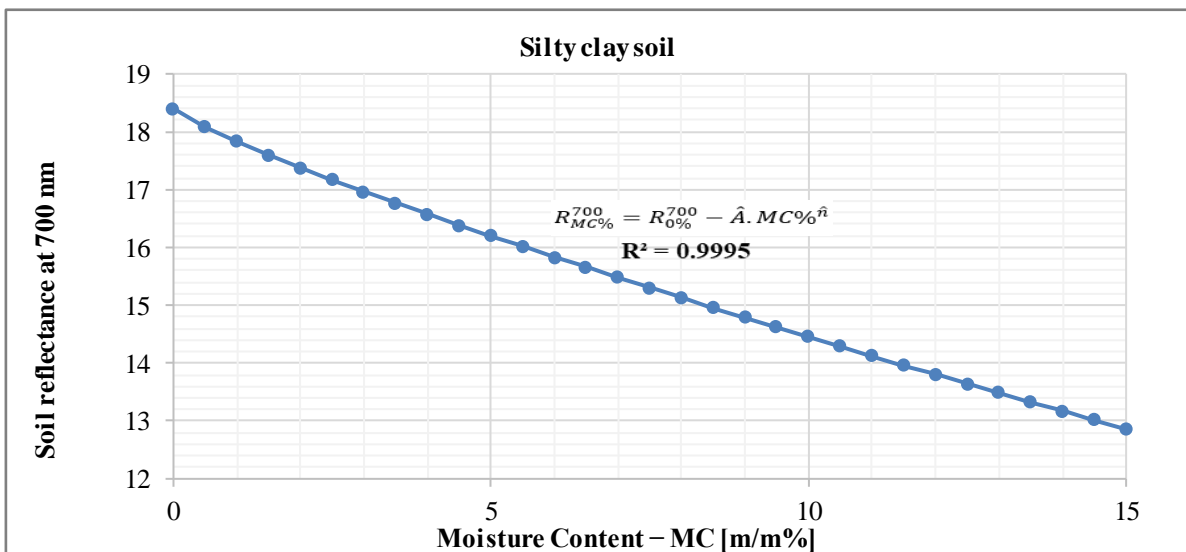


Figure A9.2. Spectral reflectance at 700 nm – soil moisture content relationship for silty clay.

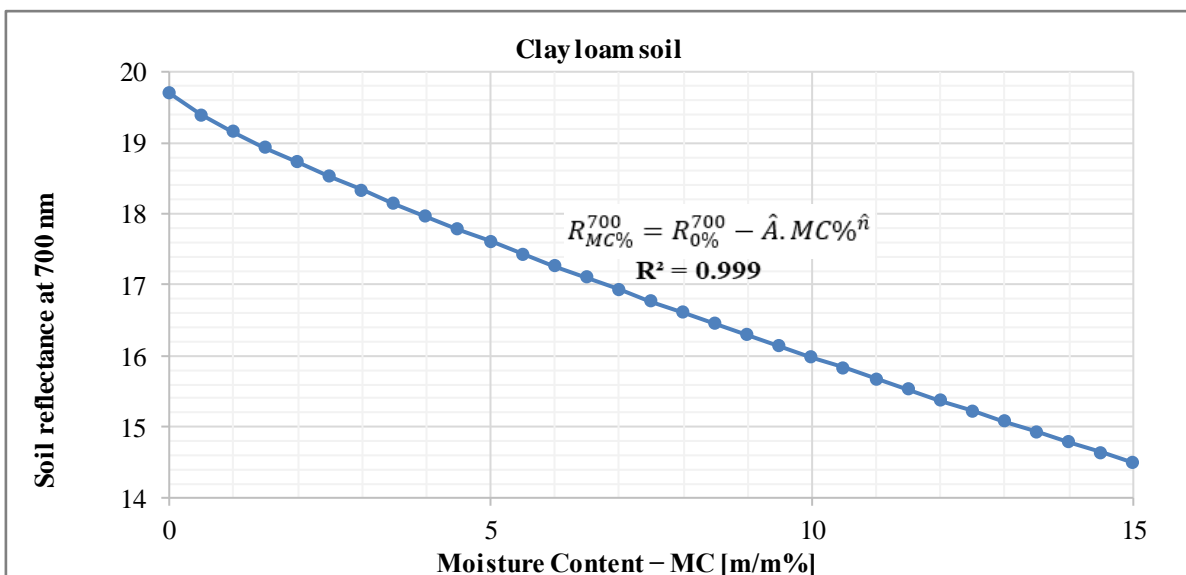


Figure A9.3. Spectral reflectance at 700 nm – soil moisture content relationship for clay loam.

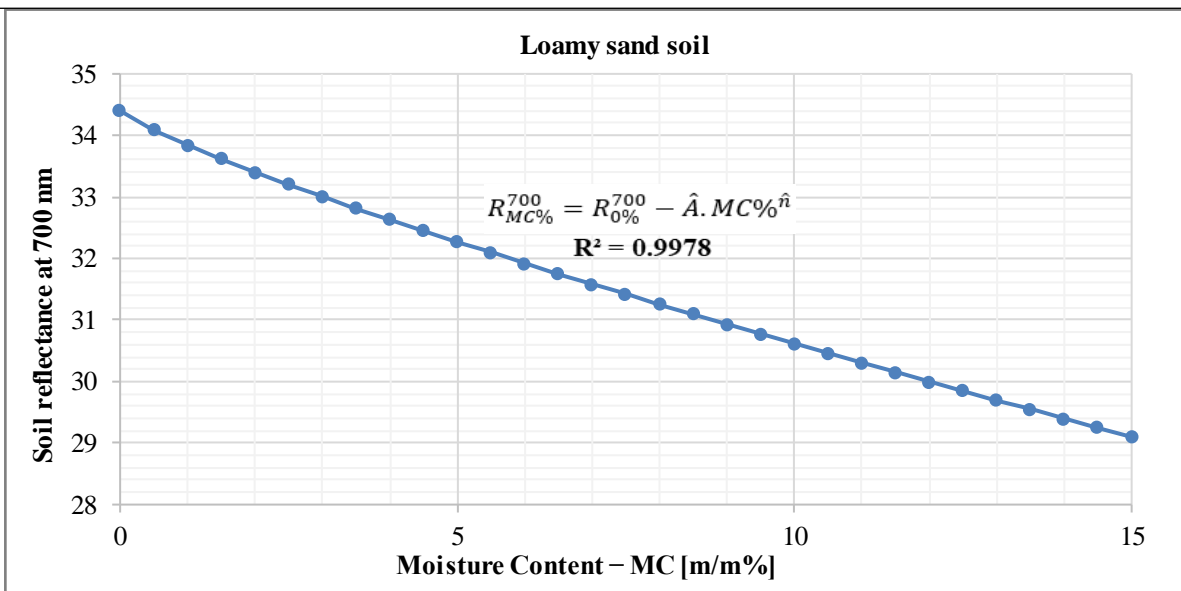


Figure A9.4. Spectral reflectance at 700 nm – soil moisture content relationship for loam.

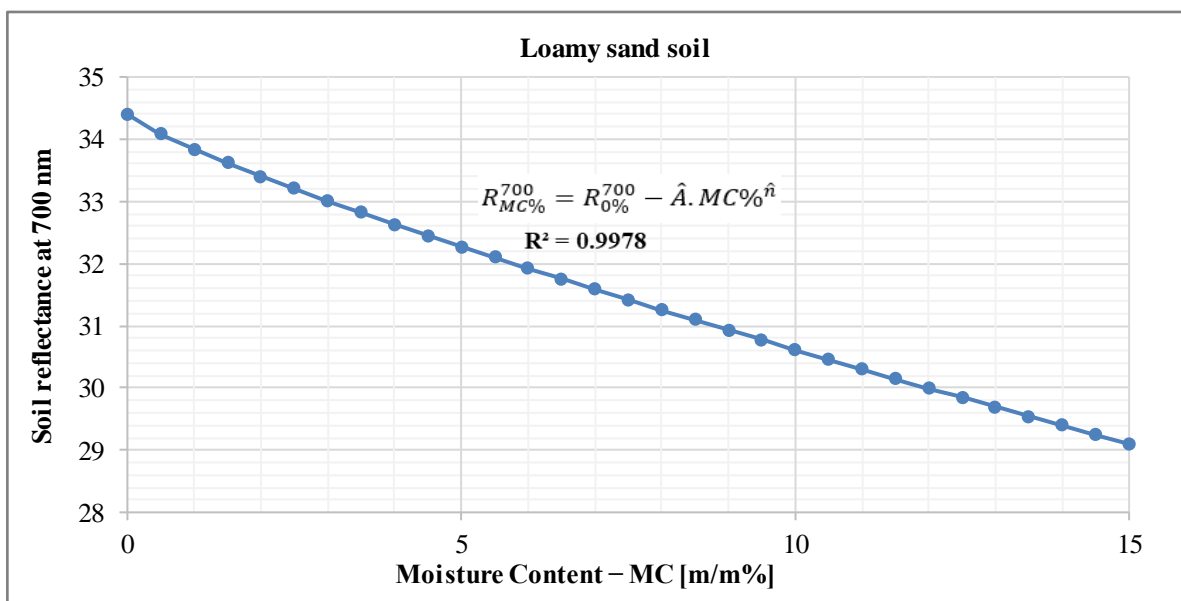


Figure A9.5. Spectral reflectance at 700 nm – soil moisture content relationship for loamy sand.

10. ACKNOWLEDGEMENT

I would like to extend my sincere appreciation to those who have played an instrumental role in supporting and guiding me throughout this research project. Their assistance and direction have been critical to its success.

- **Prof. Peter Kiss (Supervisor):** I am extremely grateful to Professor Dr. Peter Kiss for his unwavering support, guidance, and patience throughout my academic journey. I deeply appreciate his trust in my abilities and the opportunity to learn from him. It is an honour to have been his student.
- **Dr. György Pillinger (Co-Supervisor):** I extend my heartfelt gratitude to Dr. György Pillinger, a senior lecturer in the Department of Vehicle Technology, for his support, direction, and profound understanding of the subject. His expertise has been indispensable in unravelling this research's intricacies.
- **Doctoral Schools of Mechanical Engineering:** I express my sincere gratitude to **Professor Dr. Gábor Kalácska**, the Head of the Ph.D. School, and Dr. István Seres, the Secretary of the Ph.D. School, for their kind guidance throughout my academic journey.
- **Ms. Zsuzsanna Tassy and Ms. Edit (International PhD Coordinators):** I express my sincere gratitude to Ms. Zsuzsanna Tassy, the former International PhD Coordinator at DHC, and Miss Edit, the current International PhD. Coordinator at DHC, for your constant kindness and support throughout this challenging journey.
- **Tamás Török (Lab Technician):** I express my sincere gratitude to Tamás Török, a committed laboratory technician within the Department of Vehicle Technology, for his indispensable support in carrying out experiments and facilitating our research endeavours.
- **Anna Makai (Supervisor secretary):** I extend my deepest gratitude to Anna Makai for her kindness and warmth when I visit the office. Her thoughtful care, reminiscent of my mother's presence, and her offering of coffee and conversation make me feel welcomed.
- **Family:** I extend my sincerest gratitude to my family, comprising my father, mother, sisters, brothers, nieces, nephews, aunts, and uncles, for their steadfast support throughout this challenging endeavour.
- **Friends and Mates:** I am grateful to my associates and peers for their support, encouragement, and fellowship during this demanding academic journey.
- **Stipendium Hungaricum Scholarship Program and Sudan:** I extend my heartfelt appreciation to the Stipendium Hungaricum Scholarship Program and my homeland, Sudan, for granting me the privilege of being nominated for this prestigious position and allowing me to undertake my PhD studies in Hungary
- **Research Funding Support:** This project (**Project no. 2022-2.1.1-NL-2022-00012**) has been implemented with the support provided by the Ministry of Culture and Innovation of Hungary from the National Research, Development and Innovation Fund, financed under the 2022-2.1.1-NL funding scheme

This academic endeavour has been enhanced and made feasible owing to the collective support of these individuals and institutions. We extend our gratitude to you for playing an indispensable role in the culmination of this endeavour.

Gödöllő, March 2025

Ahmed Elawad Eltayeb Ahmed